

**Nanostructured Electro-Magnetic Materials from the Guest-
Host Organic- Inorganic Hybrid Ternary System of
Polyaniline- Polyhydroxy iron Cation- Clay Composite:
Preparation, Properties and Applications**

THESIS SUBMITTED TO

THE UNIVERSITY OF KERALA

FOR THE AWARD OF THE DEGREE OF

DOCTOR OF PHILOSOPHY

IN

CHEMISTRY

UNDER THE FACULTY OF SCIENCE

By

REENA V. L.

MATERIALS AND MINERALS DIVISION
NATIONAL INSTITUTE FOR INTERDISCIPLINARY SCIENCE AND TECHNOLOGY
(CSIR)
THIRUVANANTHAPURAM 695012
KERALA, INDIA

2010

*Dedicated to my beloved
family*



DECLARATION

I hereby declare that the Ph. D thesis entitled “**Nanostructured Electro-Magnetic Materials from the Guest-Host Organic- Inorganic Hybrid Ternary System of Polyaniline- Polyhydroxy iron Cation- Clay Composite: Preparation, Properties and Applications**” is an independent work carried out by me at the National Institute for Interdisciplinary Science and Technology (CSIR), Thiruvananthapuram, under the supervision of Dr. J. D. Sudha and Dr C. Pavithran and it has not been submitted anywhere else for any other degree, diploma or title.

Reena V. L.

Thiruvananthapuram

December 2010

राष्ट्रीय अंतर्विषयी विज्ञान तथा प्रौद्योगिकी संस्थान

(वैज्ञानिक एवं प्रौद्योगिकी अनुसंधान परिषद्)
(पहले क्षेत्रीय अनुसंधान प्रयोगशाला)

NATIONAL INSTITUTE FOR INTERDISCIPLINARY SCIENCE AND TECHNOLOGY

(Council of Scientific & Industrial Research)
(formerly Regional Research laboratory)

इन्डस्ट्रियल इस्टेट डाक घर, तिरुवनन्तपुरम 695 019, भारत
Industrial Estate P.O., Thiruvananthapuram 695 019, India



CERTIFICATE

This is to certify that the work embodied in the thesis entitled **“Nanostructured Electro-Magnetic Materials from the Guest-Host Organic-Inorganic Hybrid Ternary System of Polyaniline- Polyhydroxy iron Cation-Clay Composite: Preparation, Properties and Applications”** has been carried out by **Ms. Reena V.L.** under our supervision and guidance at the National Institute for Interdisciplinary Science and Technology (*Formerly Regional Research Laboratory*), Thiruvananthapuram

Dr. C. Pavithran
Deputy Director & Scientist G
National Institute for Interdisciplinary
Science and Technology (CSIR),
Thiruvananthapuram

Dr. J. D. Sudha
Sr. Technical Officer
National Institute for Interdisciplinary
Science and Technology (CSIR),
Thiruvananthapuram

Acknowledgements

First and foremost I owe to ALMIGHTY for making this happen.

I would like to record my deepest gratitude to my research supervisor Dr J. D. Sudha. It has been a rare honour and exclusive privilege to be her first Ph.D. student. Over the years of our association, she has taught me, how good experimental chemistry is done. I appreciate all her contributions of guidance, support and ideas to make my Ph.D. experience productive and stimulating. I am also thankful for the excellent example she has provided as a successful woman chemist and a teacher.

I was extraordinarily fortunate in having, Dr. C. Pavithran as my research supervisor. I am indebted for his advice, guidance, support and encouragement with which I am immensely benefited.

My sincere thanks go to Dr. Suresh Das, Prof. T. K. Chandrasekhar and Dr. B. C. Pai, present and former Directors of NIIST, for providing me an opportunity to carry out my research work in NIIST and for allowing me to avail all the facilities here.

I owe special note of gratitude to Dr C. P. Reghunadhan Nair (Head, PSC, VSSC), Dr. Aloysius (NPL), Dr. Prabhakar Rao, Dr. T. Emilia Abraham, Dr. K. G. K. Warriar, Dr. A. Ajayaghosh, Dr. C. H. Suresh, Dr. D. Ramaiah, Dr. M. L. P. Reddy and Dr. A. Bhoje Gowde, for their valuable suggestions at various stages of my research.

I remain thankful to Dr. A. R. R. Menon, Mr. M. Brahmakumar and Dr. T. P. D. Rajan, MMD, NIIST, for their encouragement. I would also like to put on record my thanks to all my teachers who have directed me to the present position.

The characterization studies discussed in this dissertation would not have been possible without the aid of Mr. M. C. Chandran, Mr. P. Guruswamy, Mr. Robert Philip, Dr. Ramaswamy, Ms. Viji, Mr. Veluswamy, Mr. Mirash, Mr. Jathish, Dr. Roy and Mr. Willy Paul.

My time at National Institute for Interdisciplinary Science and Technology was made enjoyable in large part due to the many friends that became a part of my life. The members of my group have contributed immensely to my personal and academic time at NIIST. The group has been also a source of good advice and

collaboration. My groupmates, Ms. Sivakala, Mr. Ramakrishnan, Dr. Prasanth, Ms. Jisha, Ms. Anija, Ms. Nisha and Mr. Jithin are acknowledged for every help that has been rendered to me, especially Ms. Sivakala and Mr. Ramakrishnan for their detailed review, constructive criticism and excellent advice during the preparation of this thesis. Mr. K. V. Ratheesh is acknowledged for his valuable suggestions during the printing stage of this thesis. Other past and present NIIST mates with whom I have had the pleasure to associate with are my great friends, Dr. Bindu, Ms. Chameswary, Ms. Sasikala, Mr. Binu, Ms. Manju, Ms. Reshmi, Ms. Shiny, Ms. Viola, Ms. Sonia, Mr. Jinish, Dr. Smitha, Dr. Deepa, Dr. Jancy, Dr. Amrutha, Ms. Rekha, Dr. Deepak, Dr. Anil, Mr. Balamurugan, Ms. Reshmi, Ms. Deepa, Ms. Lekshmi, Ms. Annu and Mr. Anto.

Where would I be without my family? My parents deserve special mention for their inseparable support and prayers. My Father in the first place is the person who put the fundament of my learning character, showing me the joy of intellectual pursuit ever since I was a child. My Mother is the one who sincerely raised me with her caring and gently love. Leena and Rejoy, thanks for being so supportive and caring siblings. My uncles, aunts and cousins are also acknowledged. Words fail me to express my appreciation to my husband Mr. Prem whose dedication, love and support has taken the load off my shoulders. I owe him for being unselfishly let his intelligence, passions, and ambitions collide with mine. Thoughtful support from my mother-in-law, brothers-in law and sisters- in law are also deeply acknowledged. To my family, I dedicate this thesis.

Financial assistance from Council for Scientific and Industrial Research is gratefully acknowledged.

Finally, I would like to extend my warmest thanks to everybody who was important to the successful realization of thesis, as well as expressing my apology that I could not mention personally one by one.

Reena V. L.

CONTENTS

	Page
Declaration	i
Certificate	ii
Acknowledgements	iii
List of Tables	x
List of Figures	xi
Abbreviation	xvi
Preface	xix
Chapter 1: Nanostructured Electro-Magnetic Polymer-Inorganic Hybrid Composites	
1.1. Abstract	1
1.2. Introduction	1
1.3. Intrinsically Conducting Polymers	4
1.4. Doping Process	6
1.4.1. Electrical conduction mechanism in conducting polymers	8
1.4.2. Band theory in conducting polymers	9
1.5. Polyaniline (PANI)	10
1.6. Nanostructured conducting polymer	13
1.6.1. Template synthesis	14
1.6.1.1. Hard template synthesis	15
1.6.1.2. Soft template synthesis	16
1.7. Conducting polymer -inorganic hybrid nanocomposites	18
1.7.1. Polyaniline- clay nanocomposites	19
1.7.2. Multifunctional conducting polymer- metal nanoparticle	

hybrid composites	24
1.7.2.1. Electro-magnetic polymer –inorganic hybrid composites (EMPCs)	27
1.8. Scope and Objective of the work	36
Chapter 2: Role of Amphiphilic Dopants on the Shape and Properties of Electrically Conducting Polyaniline-Clay Nanocomposite	
2.1. Abstract	41
2.2. Introduction	41
2.3. Results and Discussion	43
2.3.1.1. Preparation of 4- hydroxy-2-pentadecyl benzene sulphonic acid	43
2.3.1.2. Preparation and characterization of PANIs and PANICNs	45
2.3.2. Structural characterization	47
2.3.2.1. UV-vis spectroscopy	47
2.3.2.2. FT-IR spectroscopy	49
2.3.2.3. X- ray diffraction (XRD)	50
2.3.3. Morphology	55
2.3.4. Electrical conductivity	59
2.3.5. Thermal properties	61
2.4. Conclusion	63
2.5. Experimental	64
2.5.1. Materials	64
2.5.2.1. Preparation of 4- hydroxy-2-pentadecyl benzene sulphonic acid	64
2.5.2.2. Preparation of PANI-DBSA and PANICN-DBSA	65
2.5.3. Description of experimental techniques	65

**Chapter 3: Nanostructured Multifunctional Electro-Magnetic Materials
From Polyaniline-Clay-Polyhydroxy Iron Composite:
Preparation and Properties**

3.1.	Abstract	68
3.2.	Introduction	68
3.3.	Results and Discussion	72
3.3.1.1.	Preparation of polyhydroxy iron cation (PIC)	72
3.3.1.2.	Preparation of PIC intercalated clay (PHIC)	74
3.3.1.3.	Preparation of electromagnetic polyaniline-polyhydroxy iron – clay composite (PPIC)	74
3.3.1.4.	Preparation of water dispersible electro-magnetic polyaniline- polyhydroxy iron - clay composite (PPICSA)	76
3.3.2.	Particle size measurements	79
3.3.3.	Structural characterization	80
3.3.3.1.	UV- vis spectroscopy	80
3.3.3.2.	FT-IR spectroscopy	82
3.3.4.	X-ray diffraction studies	83
3.3.5.	Morphology	86
3.3.6.	Conductivity measurements	89
3.3.7.	Magnetic property	91
3.3.8.	Thermal stability	95
3.4.	Conclusions	96
3.5.	Experimental section	97
3.5.1.	Materials	97
3.5.2.	Synthesis procedure	97
3.5.2.1.	Determination of critical micelle concentration of PDPSA	97

3.5.2.2.	Preparation of polyhydroxy iron cation (PIC)	98
3.5.2.3.	Preparation of PIC intercalated clay (PHIC)	99
3.5.2.4.	Preparation of polyaniline- polyhydroxy iron clay composite (PPIC)	99
3.5.2.5.	Preparation of PPIC- PDPSA (PPICSA)	100
3.5.3.	Description of experimental techniques	100

Chapter 4: Development of Amperometric Sensor Based on Nanostructured Polyaniline-Polyhydroxy Iron Cation – Clay Composite Modified Pt Electrode for Ascorbic Acid

4.1.	Abstract	103
4.2.	Introduction	103
4.3.	Results and Discussion	107
4.3.1.	Preparation and properties of PPICSA	107
4.3.2.	Electrochemical characteristics of PPICSA modified Pt electrode	107
4.3.3.	Estimation of AA	109
4.3.4.	Operational stability and shelf life	113
4.3.5.	Effect of interference on the determination of AA	115
4.4.	Conclusions	116
4.5.	Experimental section	117
4.5.1.	Materials and methods	117
4.5.2.	Preparation of PPICSA modified Pt electrode	117

Chapter 5: Preparation of Electro-Magnetic Blends of Polyaniline-Polyhydroxy Iron Cation- Clay with Polycarbonate and its Property Evaluation

5.1.	Abstract	120
5.2.	Introduction	120
5.3.	Results and Discussion	122

5.3.1.	FT-IR spectroscopy	123
5.3.2.	Electrical conductivity and conduction mechanism	124
5.3.3.	Morphology of PPPC	127
5.3.4.	Rheological Properties	129
5.3.5.	Thermal stability	130
5.3.6.	Mechanical testing	132
5.3.7.	EMI shielding	133
5.4.	Conclusions	134
5.5.	Experimental section	135
5.5.1.	Materials and methods	135
5.5.2.	Preparation of electro-magnetic blends of PPICSA/PC (PPPC)	135
5.5.3.	Description of experimental techniques	135
	Summary, Conclusion and Future Perspective	138
	List of Publications	144
	References and Bibliography	148

List of Tables

	Page
1) Table 1.1. Chemical structure of commonly used smectite clays	19
2) Table 2.1. Experimental details of PANIs and PANICNs	46
3) Table 2.2. Studies on the solubility of PANIs and PANICNs	47
4) Table 2.3. Details of the XRD and morphology of PANIs and PANICNs	56
5) Table 3.1. Details of elemental analysis	78
6) Table 3.2. Details of XRD studies	85
7) Table 3.3. Details of electrical properties of PPIC	90
8) Table 3.4. Details of electrical properties of PPICSA	91
9) Table 3.5. Details of magnetic properties of PPIC	93
10) Table 4.1. Recovery of AA in the presence of some possible interference at PPICSA/Pt electrode	116
11) Table 5.1. Electrical conductivity and mechanical property of PPPC blends	133
12) Table 5.2. EMI SE details of PPPC blends	134

List of Figures

	Page
1) Scheme 1.1. Doping mechanism in conjugated polymers	6
2) Scheme 1.2. Doping in polyacetylene	6
3) Scheme 1.3. Electronic band structure of metals, inorganic semi-conductor, conducting polymer and insulator	10
4) Scheme 1.4. Chemical oxidative polymerization of aniline	11
5) Scheme 1.5. Mechanism for polymerization of aniline	12
6) Scheme 1.6. Different oxidation states of polyaniline	12
7) Scheme 1.7. Chemical synthesis of PANI-MMT	21
8) Figure 1.1. Applications of electro-magnetic polymer nanocomposites	3
9) Figure 1. 2. Structure of polyacetylene	4
10) Figure 1.3. Common electrically conducting polymers	5
11) Figure 1.4. Common applications of ICPs	5
12) Figure 1.5. Common amphiphilic organic dopants	7
13) Figure 1.6. Structure of polyaniline	11
14) Figure 1.7. The annual number of publications on the subject of 'PANI' and 'PANI+ nano', as provided by the search engine of SCIFINDER scholar	14
15) Figure 1.8. Template synthesis	15
16) Figure 1.9. Schematic representation for hard template polymerization	16
17) Figure 1.10. Schematic representation for soft template polymerization	17
18) Figure 1.11. Structure of Montmorillonite clay	20
19) Figure 1.12. Intercalated and exfoliated polymer clay nanocomposites	22
20) Figure 1.13. XRD of clay, intercalated and exfoliated polymer-clay nanocomposites	23

21)	Figure 1.14. Schematic representation for the preparation of PEDOT/MnO ₂ nanocomposites	24
22)	Figure 1.15. Schematic representation for the preparation of gold/PANI nanocomposites	25
23)	Figure 1.16. Core- shell Au- PANI composite	26
24)	Figure 1.17. The scheme of the visible light photocatalysis process over PANI-CdS composite	26
25)	Figure 1.18. Scheme for the preparation of Fe ₃ O ₄ / PANI nanocomposite	28
26)	Figure 1.19. Schematic illustration for the synthesis process of Fe ₃ O ₄ @PANI core/shell composite	29
27)	Figure 1.20. Polymerization procedure for PANI/ Zn _{0.6} Cu _{0.4} Cr _{0.5} Fe _{1.5-x} La _x O ₄ Composites	30
28)	Figure 1.21. Bonding mechanism in the PANI/ iron oxide nanocomposites	31
29)	Figure 1.22. Schematic illustration of the synthesis process of PANI/magnetite nanorod composites	34
30)	Figure 1.23. Schematic diagram illustrates the formation mechanism for the core- shell Fe ₃ O ₄ /PANI-CSA or Fe ₃ O ₄ /PANI-TSA composite particles by self-assembly of Fe ₃ O ₄ nanoparticles, aniline and CSA or TSA	35
31)	Scheme 2.1. Preparation of PDPSA	44
32)	Scheme 2.2. Preparation of polyaniline clay nanocomposites	48
33)	Scheme 2.3. Formation of self- assembled micro/nanofibers of PANI-DBSA and PANICN-DBSA	54
34)	Scheme 2.4. Formation of self- assembled micro/nanostructured PANI-PDPSA and PANICN-PDPSA	59
35)	Figure 2.1. FT-IR spectrum of PDPSA	44

36)	Figure 2.2. UV-vis spectra of (A) PANIDBSA, (B) PANICN-PDPSA , (C) PANICN-DBSA, (D) PANICN-NSA, (E) PANICN-pTSA , (F) PANICN-SA and (F) PANICN-CSA48	
37)	Figure 2.3. FT-IR spectra of (A) clay, (B) PANI- DBSA and (C) PANICN-DBSA	49
38)	Figure 2.4. XRD pattern of (A) Na ⁺ Cloisite, (B) PANICN-CSA, (C) PANICN-SA, (D) PANICN-pTSA, (E) PANICN-NSA and (F) PANICN-DBSA	51
39)	Figure 2.5. Energy minimized structure of (A) PANI-DBSA (B) PANI-NSA (C) PANI-pTSA (D) PANI-SA and (E) PANI- CSA	52
40)	Figure 2.6. XRD of (A) Clay, (B) PANI-PDPSA, (C) PANICN- PDPSA1, (D) PANICN-PDPSA2, (E) PANICN- PDPSA3 and (F) PANICN- PDPSA4	54
41)	Figure 2.7. SEM picture of (A) PANI- DBSA (B) PANI- NSA(C) PANI- pTSA (D) PANI- SA (E) PANI- CSA (F) PANI- PDPSA, (G) PANICN- DBSA (H)PANICN-NSA(I) PANICN- pTSA (J)PANICN- SA(K)PANICN- CSA and (L) PANICN-PDPSA	55
42)	Figure 2.8. TGA curves of (A) PANI-DBSA (B) PANICN-DBSA	61
43)	Figure 2.9. DSC curves of (A) PANICN-DBSA (B) PANI-DBSA	62
44)	Scheme 3.1. Preparation of PIC	72
45)	Scheme 3.2. Preparation of PPIC	74
46)	Scheme 3.3. Redox Property of Fe ²⁺ /Fe ³⁺ exploited for the polymerization of aniline	75
47)	Scheme 3.4. Preparation of water dispersible PPIC using PDPSA	77
48)	Figure 3.1. DLS plot of (A) PIC and (B) PIC- PDPSA	73
49)	Figure 3.2. PLM picture of polyhydroxy iron cation	73
50)	Figure 3.3. MALDI -TOF spectra of PPIC1	76
51)	Figure 3.4. EDS spectrum of (A) PPIC and (B) PPICSA	79
52)	Figure 3.5. DLS histograms showing the size distribution of (A) PPICSA (B) PPIC	79
53)	Figure 3.6. Molecular weight determination of PPICSA using MALDI-TOF	80
54)	Figure 3.7. UV- vis spectra of (A) PANI (B) PANICN (C) PPIC and (D) PPICSA	81

55)	Figure 3.8. FTIR Spectra of (A) PPICSA, (B) PPIC, (C) PHIC, (D) PANI and (E) Na ⁺ Cloisite.	82
56)	Figure 3.9. XRD diffractogram of (A) Na ⁺ Cloisite (B) PHIC (C) PPIC and (D) PPICSA	84
57)	Figure 3.10. PLM images of (A) PPIC (B) PPICSA	86
58)	Figure 3.11. SEM images of (A, B) PPC (C) PPIC (D) PPICSA	86
59)	Figure 3.12. TEM images of electro-magnetic composite synthesized with inset showing its aq dispersion(A,B) PPIC and (C,D) PPICSA	88
60)	Figure 3.13. Typical M-H curve of PPIC4	93
61)	Figure 3. 14. M-H curves of PPIC and PPICSA with varying concentration of PDPSA at 300 K (A) PANI (B) PPICSA1 (C) PPICSA2(D) PPICSA3 (E) PPICSA4 (F) PPICSA5 (G) PPIC	94
62)	Figure 3.15. TG plot of (A) PANI (B) PPIC (C) PPICSA and (D) Clay	95
63)	Figure 3.16. Intensity of scattered light against concentration for CMC determination	97
64)	Scheme 4.1. Sequence of events that occur in PPICSA mediated AA sensor	109
65)	Figure 4.1. A typical cyclic voltammogram of PPICSA at Pt electrode	107
66)	Figure 4.2. Cyclic voltammogram of PPICSA as a function of scan rate at Pt electrode	108
67)	Figure 4.3. Linear relation of square root of scan rate with current	111
68)	Figure 4.4. Logarithm of scan rate as a function of ΔE_p showing a straight line	112
69)	Figure 4.5. Variation in current intensity as a function of concentration of AA (1 mM) at PPICSA/Pt electrode	113
70)	Figure 4.6. Electrochemical study of AA at PPICSA/Pt electrode for 50 cycles showing its reasonably good operational stability	114

71)	Figure 4.7. Cyclic voltammogram of PPICSA demonstrating its excellent storage stability	114
72)	Figure 4.8. Effect of various possible interference for the estimation of AA	115
73)	Scheme 5.1. Schematic representation of hydrogen bonding between PC and PPICSA	124
74)	Figure 5.1. Clear transparent green film of PPPC blend	123
75)	Figure 5.2. FT-IR spectra of PC and PPPC	124
76)	Figure 5.3. Temperature dependant conductivity of PPPC6 blend	126
77)	Figure 5.4. 3D VRH curve of PPPC6 blend	127
78)	Figure 5.5. Polarized light micrographs of PPPC blends with (A) 5 wt% PPICSA, (B) 10 wt% PPICSA and (C) 15 wt% PPICSA	128
79)	Figure 5.6. SEM and AFM figures of PPPC blend at percolation threshold concentration	129
80)	Figure 5.7. Plot of storage modulus and loss modulus vs. angular frequency	130
81)	Figure 5.8. TG plots of PC and PPPC blends	131
82)	Figure 5.9. DSC plots of PC and PPPC blends	132

Abbreviation

AA- Ascorbic acid

AAS- Atomic absorption spectroscopy

AFM- Atomic force microscopy

APS- Ammonium persulphate

APTES- Aminopropyl triethoxy silane

BET- Brunauer- Emmett- Teller

CB- Conduction band

CdS- Cadmium Sulphide

CEC- Cation exchange capacity

CHCl₃-Chloroform

CMC- Critical micelle concentration

CP- Conducting polymers

CSA- Camphor sulphonic acid

CV- Cyclic voltammetry

DBSA- Dodecyl benzene sulphonic acid

DLS- Dynamic light scattering

DMF- Dimethyl formamide

DMAc- Dimethyl acetamide

DSC- Differential scanning calorimetry

EB- Emeraldine base

ES- Emeraldine salt

EMI- Electromagnetic Interference

EMPC- Electro-magnetic polymer –inorganic hybrid composites

FT-IR- Fourier transform infrared spectroscopy

ICP- Intrinsically conducting polymers

LEB- Leucoemeraldine base

MALDI- TOF - Matrix assisted laser desorption ionization –Time of flight

M_s - Saturation magnetization

NMP- N-methyl pyrrolidone

NMR- Nuclear magnetic resonance

nm- Nanometer

NSA- Naphthalene sulphonic acid

PANI- Polyaniline

PANICN- Polyaniline-clay nanocomposite

PC- Polycarbonate

PDPSA- 4 hydroxy-2-pentadecyl benzene sulphonic acid

3-PDP- 3- Pentadecyl phenol

PDPPA - 3-Pentadecyl phenyl phosphonate

PEDOT- Polyethylenedioxy thiophene

PHIC- Polyhydroxy iron cation intercalated clay

PIC- Polyhydroxy iron cation

PLM- Polarized light microscopy

PNB- Pernigraniline base

PPIC- Polyaniline- polyhydroxy iron cation- clay composite

PPICSA- 4- hydroxy-2-pentadecyl benzene sulphonic acid doped polyaniline- polyhydroxy iron cation- clay composite

ppm- parts per million

PPPC- Electro-magnetic blends of PPICSA/PC

PPy- Polypyrrole

pTSA- Para toluene sulphonic acid

PVP- Polyvinyl pyrrolidone

SA- Stearic acid

SEM- Scanning electron microscopy

VB- Valence band

V₂O₅ -Vanadium pentoxide

TEM- Transmission electron microscopy

T_g – Glass transition temperature

TGA- Thermogravimetric analysis

WXR- Wide angle X-ray diffraction

PREFACE

Nanostructured electro-magnetic polymer composites comprising of conducting polymers hosting magnetic nanoparticles have gained attraction among the researchers as they exhibit dual functionalities like electrical conductivity and magnetic property in a unique system. Apart from electro-magnetic properties, high thermo-mechanical properties are also expected for materials for high technological applications. In this context, preparation of a polyaniline-polyhydroxy iron-clay composite (PPIC) is receiving interest since it is a novel guest-host system consisting of exfoliated nanoclay layers dispersed in nanomagnets engulfed by conducting polyaniline. Thus, the resulting system is expected to provide materials having electro-magnetic properties endowed with excellent mechanical strength, thermal stability and good processability. Also the $\text{Fe}^{2+}/\text{Fe}^{3+}$ redox couple present in PPIC can be exploited for its chemical sensor activity.

The first chapter of the thesis describes the recent developments in the field of nanostructured conducting polymers, polyaniline clay nanocomposites and electro-magnetic polyaniline nanocomposites.

Synthesis of polyaniline clay nanocomposite is interesting since polyaniline can exhibit high conductivity in the constrained environment of clay with low loading of polyaniline. It has been reported that amphiphilic dopants can play multiple roles of intercalating agent, dopant and structure directing agent. In the second chapter we describe the effect of rigidity and functionality of the amphiphilic dopant on the morphology and electrical conductivity of the polyaniline clay nanocomposite and a plausible mechanism for the formation of different morphology with the change in the functionality of the dopant is suggested. (J. Appl. Polym. Sci. 113, 2009, 4066–76, J. Polym. Sci. Part B. Polym. Phys., 45, 2007, 2664-73).

In the third chapter, we present the development of water dispersible electromagnetic polyaniline- polyhydroxy iron cation- clay composites (PPICSA). PPICSA was prepared by polymerization of aniline in the aqueous dispersion of

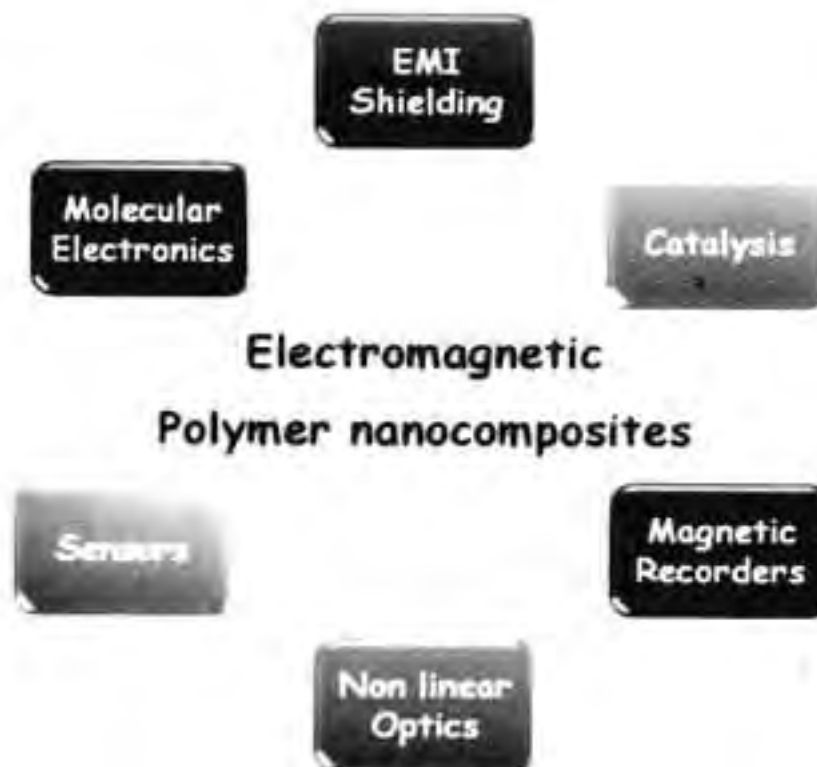
polyhydroxy iron intercalated clay in presence of amphiphilic dopant- 4 hydroxy-2-pentadecyl benzene sulphonic acid (derived from cashew nut shell liquid) at room temperature. Effect of compositional variation of clay, dopant and aniline on the electrical and magnetic property of PPIC is investigated. Studies showed that these electro-magnetic nanocomposites exhibited nanotape like morphology. They showed excellent electrical conductivity and ferromagnetic property with thermal stability up to 350 °C. All these noteworthy features make them a prospectable candidate for high technological applications (J. Phys. Chem. B. 114, 2010, 2578–85).

In the fourth chapter, we describe the performance characteristic of PPICSA modified Pt electrode as an amperometric sensor for ascorbic acid. The performance characteristics of the electrode were studied with respect to response time, sensitivity, operational stability and storage life. Common possible interferences of the sample matrices were tested and the results revealed that the present electrode exhibited high selectivity towards ascorbic acid. Moreover, this unique low cost and user friendly sensor can be used for the analysis of ascorbic acid present in food, beverages and pharmaceuticals.

In the fifth and final chapter, we describe the development and property evaluation of electromagnetic interference shielding materials based on PPICSA and polycarbonate. The onset of percolation threshold has been manifested from the morphological studies in combination with electrical conductivity measurements. EMI shielding efficiency, mechanical properties and thermal stability suggested that these transparent composite films can be used for the fabrication of EMI shielding/ electrostatic dissipation material for the encapsulation of electronic devices for high technological applications.

Chapter - 1

Introduction



1.1. Abstract

Development of nanostructured electro-magnetic polymer composites are receiving considerable attention for their potential applications in various fields such as electro-magnetic interference shielding, antistatic coatings, chemical sensors, photo-electric devices and so forth. Nanocomposites comprising conducting polymers hosting magnetic particles have gained attraction among researchers as they exhibit dual functionalities like electrical conductivity and magnetic property in a unique system. Apart from electro-magnetic properties, high thermo-mechanical properties are also expected for these materials for high technological applications. In this respect, development of conducting polymer-clay- magnetic nanocomposite is receiving interest since it is a novel guest host system comprising nanoclay layers containing magnetic nanoparticles engulfed by conducting polymers. It is also reported that certain amphiphilic organic acid molecules can play multiple role of intercalating agent, structure directing agent, dopant, template and capping agent during the preparation of conducting polymer-clay nanocomposites and conducting polymer-metal nanoparticle composite. In this chapter, an overview of the recent developments in conducting polymers with special emphasis on polyaniline, polyaniline- clay nanocomposite, preparation and properties of electro-magnetic polymer composites etc are described. Finally, scope and objective of the thesis is presented.

1.2. Introduction

Development of nanostructured electro-magnetic polymer-inorganic hybrid composites is receiving a lot of attention since they combine the

synergetic properties of inorganic particles with the conducting polymeric counterparts. The interpenetration of the two phases on nanoscale can yield composite materials whose collective performance is greatly enhanced compared to either of the constituent phases. Conducting polymers, however, arouse a great interest among researchers because of their curious electronic and optical properties. It has been reported that a number of metal and metal oxide nanoparticles like Pt, Pd, TiO₂, SnO₂, MnO₂, SiO₂, Fe₂O₃, Fe₃O₄ etc. can be encapsulated into the core of conducting polymers to give multifunctional composites (Qi *et al.*, 1998, Huang *et al.*, 1998, Neoh *et al.*, 1999, Drelinkiewicz *et al.*, 1998, Hable *et al.*, 1991, Esteban *et al.*, 1989, Armes *et al.*, 1991, Torsi *et al.*, 1998, Partch *et al.*, 1991, Huang *et al.*, 1995, Gangopadhyay *et al.*, 1999, Wan *et al.*, 1998, Somani *et al.*, 1999, Somani *et al.*, 1999). Among which, the integration of magnetic nanoparticles have become an area of particular interest for applications in various fields as they combine both electric and magnetic property in a unique material system. Among magnetic nanoparticles, iron oxides such as magnetite (Fe₃O₄) and maghemite (Fe₂O₃) have attracted much technological importance. A layer of conducting polymer on the surface of magnetic nanoparticles protects the nanoparticles from leaching and improves compatibility with other organic polymers. Conductive polymers confined inside layered silicate have attracted great interest both in industry and academia, since the constrained environment of the layered silicate is expected to lead to a high degree of polymer ordering and thereby exhibit excellent optical, electronic, thermo-mechanical and other related functional properties of the original material. Barrier properties that may undergo substantial improvements include

decreased permeability to gases, water and hydrocarbons and chemical resistance when compared with virgin polymer. The properties of these nanocomposite materials depend not only on the properties of their individual components but also on their morphology and interfacial characteristics.

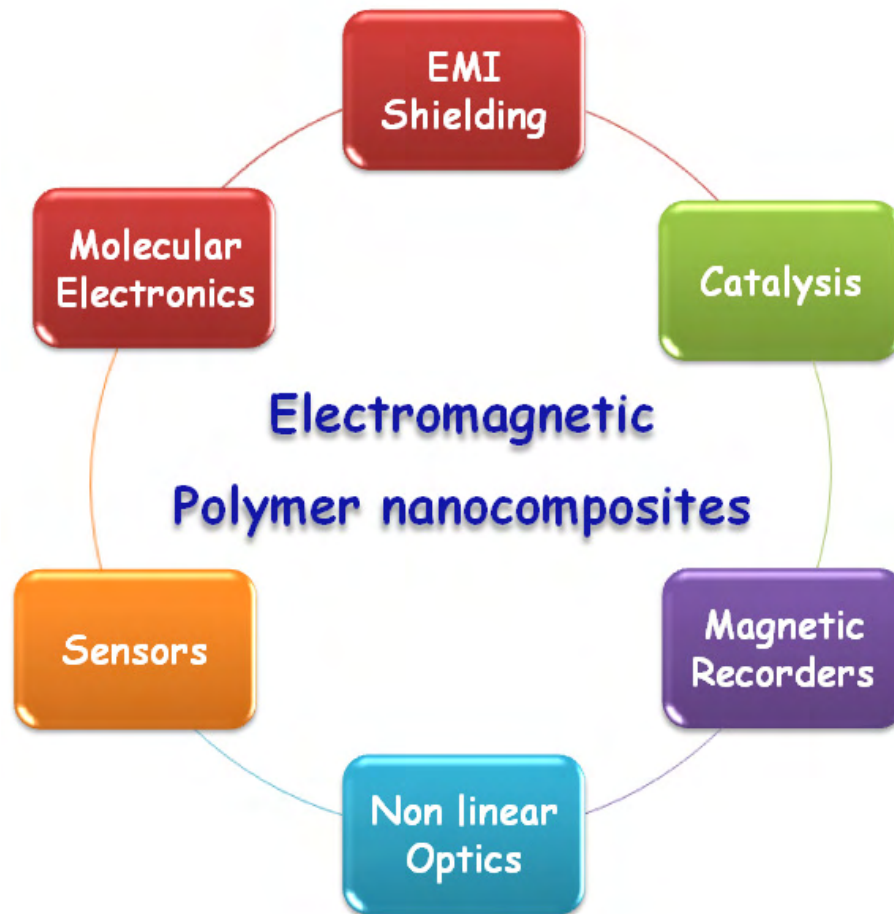


Figure 1.1. Applications of electro-magnetic polymer nanocomposites

All these superior properties make them a promising candidate in many high innovative technological applications like electro-magnetic shielding, magnetic recorders, nonlinear optics, batteries, catalysis, sensors, and so forth (Nazar et al., 1992, Cao et al., 1992, Vassilion et al., 1990, Beecroft et al., 1999) (Figure 1.1.).

1.3. Intrinsically conducting polymers

Intrinsically conducting polymers (ICPs) are planar organic molecules that have got an extended conjugated π - orbital through which the electron can move from one part of the polymer chain to the other. The ground breaking discovery of conducting polyacetylene (Figure 1.2.) in 1977 by Hideki Shirakawa, Alan Mac Diarmid and Alan Heeger initiated an extensive and systematic research devoted to various aspects of the chemistry and physics of conducting polymers both in their insulative and conductive states. As a result, they were crowned the prestigious Nobel prize in chemistry in the year of 2000 (Heeger, 2001, Mac Diarmid, 2001, Shirakawa, 2001).

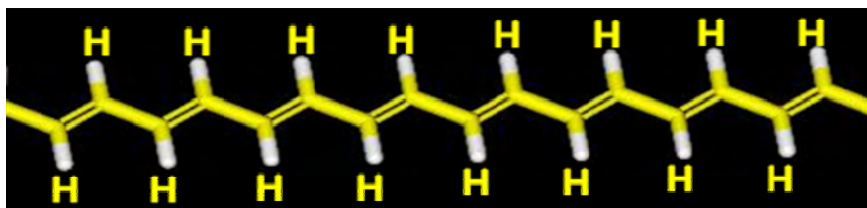


Figure 1. 2. Structure of polyacetylene, the first discovered conducting polymer

After this serendipitic discovery, the research towards ICPs has continued to accelerate at an unexpectedly rapid rate and attracted the attention of scientists, which led to the discovery of various other ICPs and their derivatives (Heeger, 2001, Mac Diarmid, 2001, Shirakawa, 2003). According to the search engine of SCIFINDER scholar, over 45,000 scientific articles relating to ICPs were published since 1977. Figure 1.3. represents the molecular structures of common ICPs. ICPs are endowed with broad range of tunable properties derived from its structural flexibility and find applications in many high technological areas.

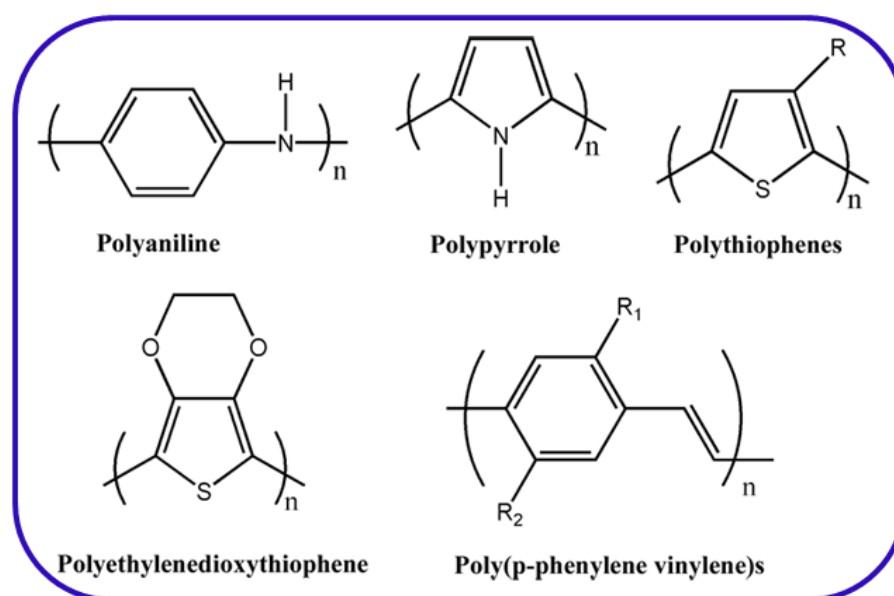


Figure 1.3. Common electrically conducting polymers

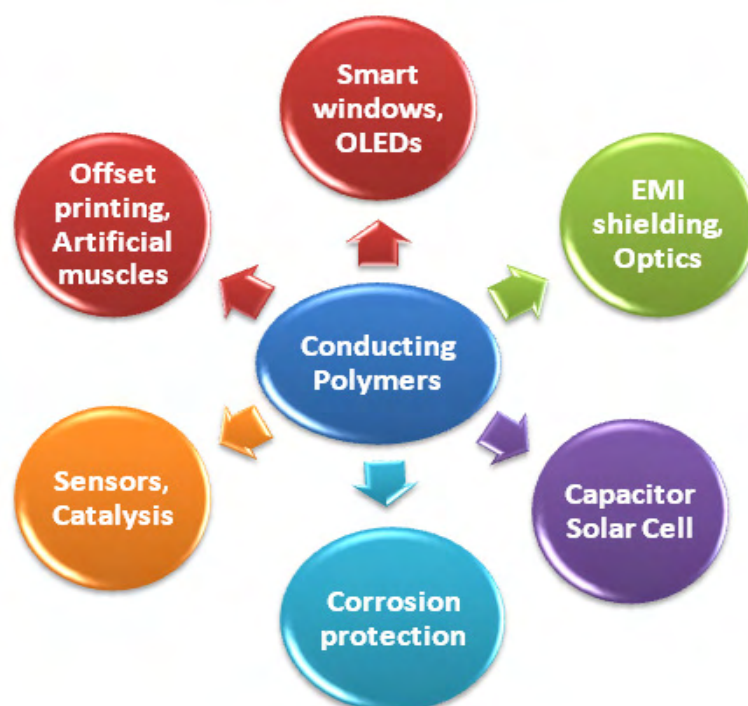


Figure 1.4. Common applications of ICPs

The applications are based on two main properties of ICPs: conductivity and electro activity. The extended π -systems of conjugated polymer are highly

susceptible to chemical or electrochemical oxidation and reduction. These reactions alter the electrical and optical properties of the polymers. Based on these properties, its application can be classified as represented in the Figure 1.4.

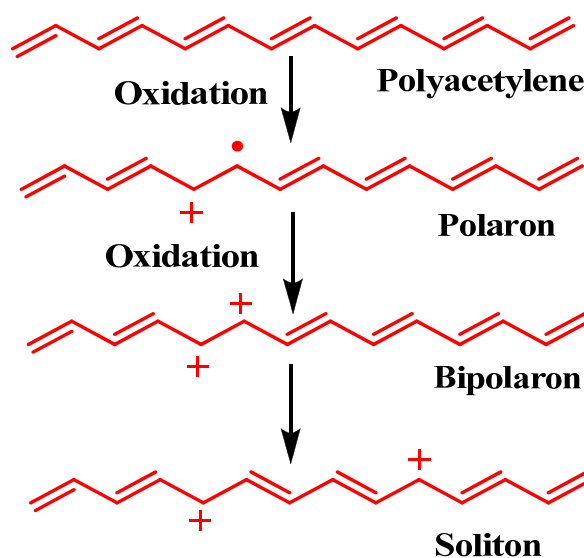
1.4. Doping process

Intrinsically conducting polymers are normally insulative materials. They can be made into conducting by the process known as doping.



Scheme 1.1. Doping mechanism in conjugated polymers

Doping is a process of either addition (n-doping) or removal of electron (p-doping) to form charge carriers. Both n-type (electron donating- e.g., Na, K, Li, Ca, tetrabutylammonium) and p-type (electron accepting-e.g., I₂, PF₆, BF₆, Cl₂ AsF₆) dopants have been reported to tune insulative to conductive transition in ICPs (scheme 1.1) (Huang *et al.*, 1986).



Scheme 1.2. Doping in polyacetylene

During doping, the first step is the formation of a cation radical, which is called a polaron. This is followed by a second electron transfer with the formation of a dication known as a bipolaron. These charges separate along the polymer chain to form solitons (Epstein *et al.*, 1994). The generation of polarons, bipolarons and solitons in polyacetylene is shown in scheme 1.2. Mineral acids such as HCl, H₂SO₄ etc are low cost and easily available dopants for the protonation of ICPs. But the disadvantages with these inorganic acid doped ICPs are their insolubility, infusibility and intractability. The ideal remedy is to use amphiphilic organic acid dopants like sulphonic acids, phosphonic acids and phosphoric acids. Amphiphilic dopant molecules are those which contains hydrophilic and hydrophobic group in the same molecule.

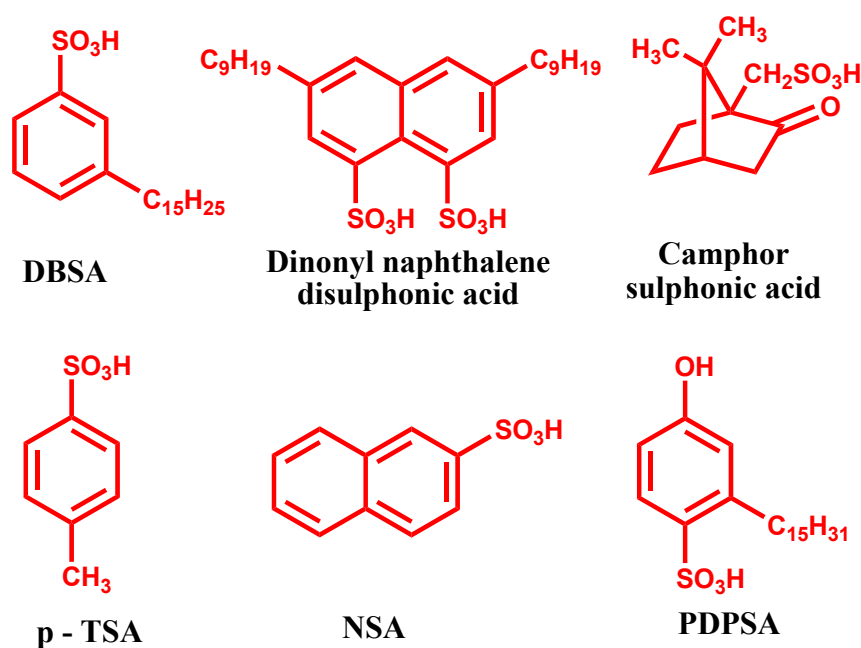


Figure 1.5. Common amphiphilic organic dopants

Because of their special structural features, they can play dual role of doping and plasticization which will enhance the processability of these ICP as well as their

composites. Another advantage of these amphiphilic acids is their micelle formation through self-assembly which will act as template/structure-directing agent during the formation of nanostructured ICPs. The structure of common amphiphilic dopants are depicted in Figure 1.5. Electrical conductivity of the doped ICPs depends upon the concentration and nature of the dopant and also on the doping techniques. Electrical conductivity (σ) for ICPs can be obtained from the product of the number of charge carriers (n), the charge associated with each carrier (e) and the mobility of the carriers (μ)

$$\sigma = en\mu \quad (1)$$

1.4.1. Electrical conduction mechanism in conducting polymers

Different mechanisms are suggested for the electrical conduction in ICPs. ICPs are highly disordered, containing a mixture of crystalline and amorphous regions. It is necessary to consider the transport of charge carriers along and between the polymer chains and also along complex boundaries established by the multiple number of phases. This has been studied by examining the temperature dependent conductivity. If the conductivity of ICPs shows a positive variation with increase in temperature, it is said to follow the semiconductor behavior. Various models have been proposed for the electrical conduction mechanism in ICP. For the temperature dependent conductivity, the most reliable model proposed is variable range hopping (VRH) (Wang *et al.*, 1992, Lee *et al.*, 1997). Variable range hopping model is based on Mott's law (Shklovskii *et al.*, 1979). Accordingly, the resistivity of localized polaron at low temperature follows the equation (2)

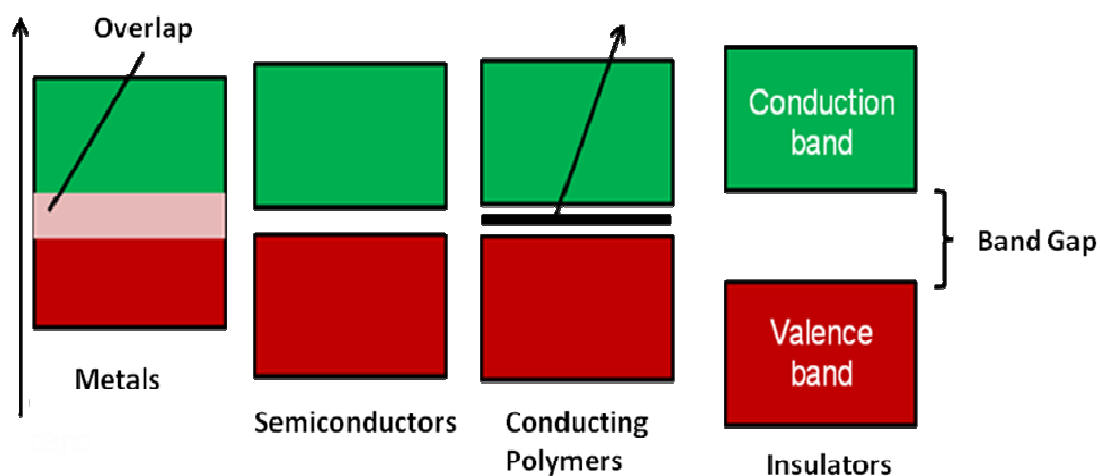
$$\rho(T) = \rho_0 \exp(T_0/T)^m \quad (2)$$

Where ρ_0 is the pre-exponential factor and T_0 , the Mott characteristic temperature. The value of the exponent 'm' depends critically on the nature of hopping process and can have values $m = 1/2$, $1/3$ and $1/4$ for one-dimensional variable range hopping (1D VRH) (Wang *et al.*, 1992, Lee *et al.*, 1997), 2D VRH (Shklovskii *et al.*, 1985, Campos *et al.*, 1997) and 3D VRH (Li *et al.*, 2004), respectively.

1.4.2. Band theory in conducting polymers

The nature of electrical conduction in materials can be classified based on the band theory. According to band theory, the atomic orbitals overlap to form the molecular orbital. The lowest fully occupied band is called the valence band (VB) and the highest unoccupied band is called the conduction band (CB). When electrons are excited from VB to the CB, current flows in these materials. The energy gap between VB and CB is called the forbidden band gap. For a conductor, the highest energy level of the VB and the lowest energy level of CB overlap each other, meaning that the forbidden band gap does not exist and electrons pass easily into the CB. For an insulator, the separation between the two bands is too large and promotion of an electron to the CB is practically not possible. With semiconductors, the forbidden gap is moderate and limited conduction occurs. Conjugated polymers with a degenerate ground state have a slightly different mechanism. They produce polarons and bipolarons on doping. However, the charged cations are not bound to each other by a higher energy bonding configuration and can freely separate along the chain. Their formation results in

the creation of new localized electronic states that appear in the middle of the energy gap. At high doping levels, the charged polarons interact with each other to form a polaron band which is placed between the VB and the CB as shown in the scheme 1.3. and can almost merge with the band edges to create true metallic conductivity.



Scheme 1.3. Electronic band structure of metals, inorganic semiconductor, conducting polymer and insulator

1.5. Polyaniline (PANI)

Among the various ICPs, PANI (Figure 1.6.) stands out because of its low cost, broad range of tunable properties derived from its structural flexibility and advantages like good environmental stability, ease of preparation, performance stability, tunable conductivity by appropriate doping/dedoping process and unique optical and electrical properties (Genies *et al.*, 1990). Conductivity of PANI salts was reported for the first time by Green and Woodhead in 1910. The interest shown in PANI as a synthetic ICP has continued to grow in recent years

and is now commercially available under the trade name Ormecon™, Versicon® and so forth.

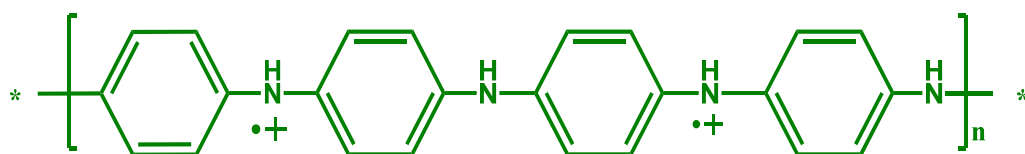
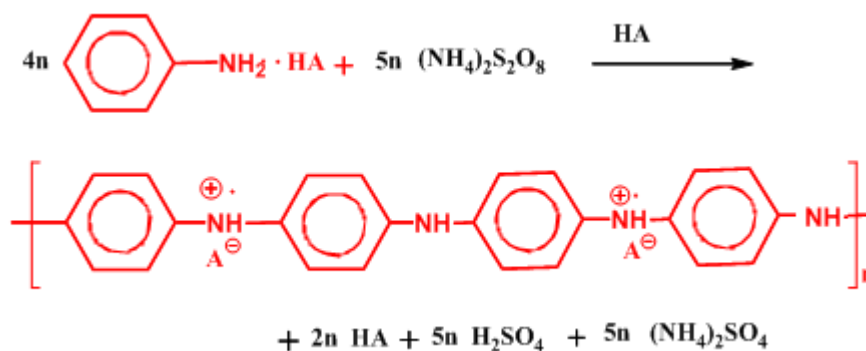


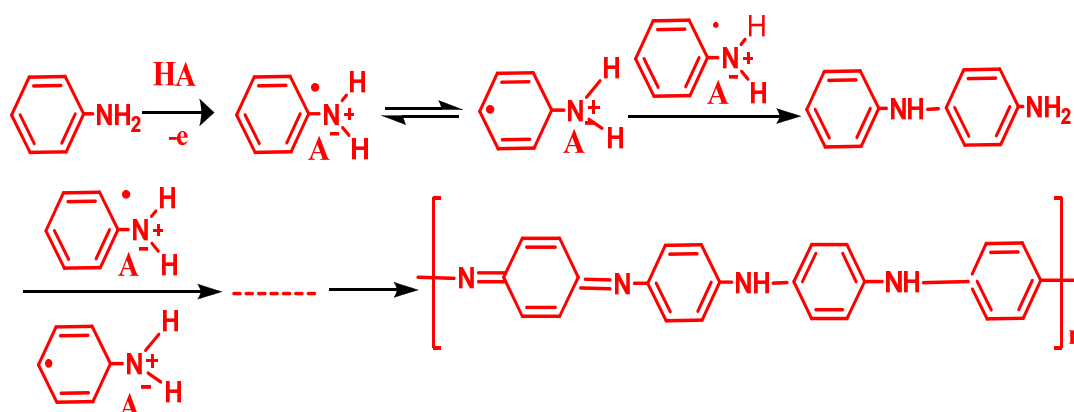
Figure 1.6. Structure of polyaniline

Usually, conducting PANI can be synthesized from monomer aniline by either oxidative polymerization or electrochemical polymerization at ambient temperature (Diaz *et al.*, 1980). The chemical oxidation of aniline is the most feasible route for the large scale synthesis of PANI. Chemical synthesis of PANI is carried out by direct oxidation of aniline using an appropriate chemical oxidative radical initiator such as hydrogen peroxide, ammonium persulfate etc. at a pH below 2 (scheme 1.4.).



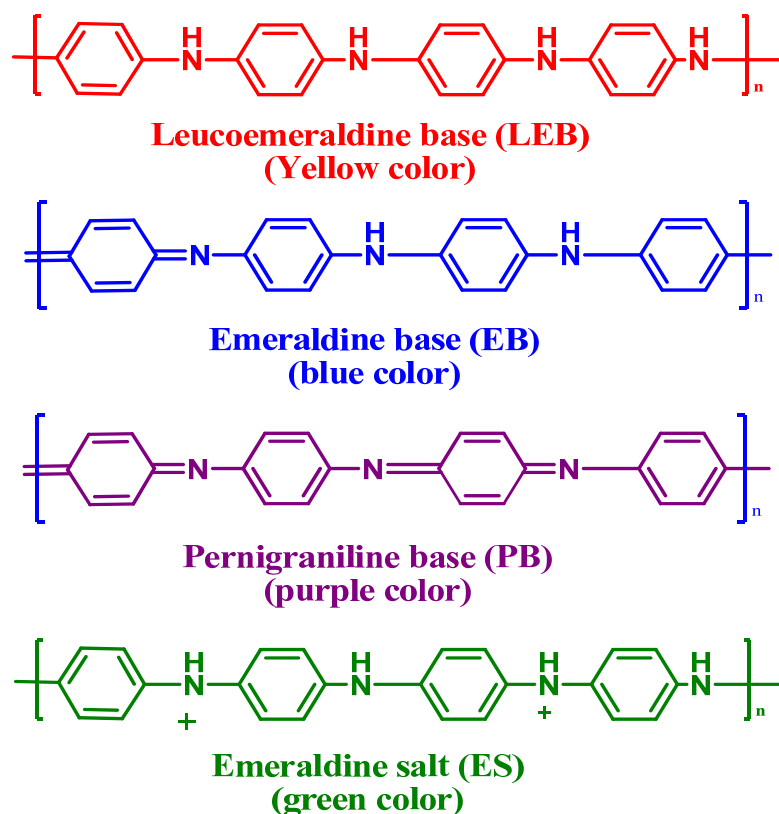
Scheme 1.4. Chemical oxidative polymerization of aniline

Scheme 1.5. represents the free radical mechanism for the formation of conducting PANI by the polymerization of aniline using the oxidative radical initiator, ammonium persulfate (APS).



Scheme 1.5. Mechanism for polymerization of aniline

Depending on the oxidation level, PANI can be synthesized in the fully reduced leucoemeraldine base (LEB), half-oxidized emeraldine base (EB), fully oxidized pernigraniline base (PNB), and conductive emeraldine salt (ES) (Scheme 1.6.).



Scheme 1.6. Different oxidation states of polyaniline

Of these four forms, EB and ES is the most stable and widely investigated ones. EB differs substantially from LEB and PNB in the sense that its conductivity can be tuned via doping from 10^{-10} to 100 S cm^{-1} , whereas LEB and PNB form cannot be made conducting. The conducting ES is achieved by doping EB with aqueous protonic or functionalized acids where protons are added to the $-N=$ sites.

1.6. Nanostructured conducting polymer

The beauty of ICPs is hampered by the serious disadvantages like intractability, insolubility and infusibility and hence low processability for various applications (Cho *et al.*, 2004, Rao *et al.*, 2003). Also they exhibited inferior thermo-mechanical properties compared to conventional polymers. A promising strategy for getting the maximum property of ICPs is to confine them in nanometer regime. During its nanofabrication, a paradigm shift can be expected from its bulk counter parts.

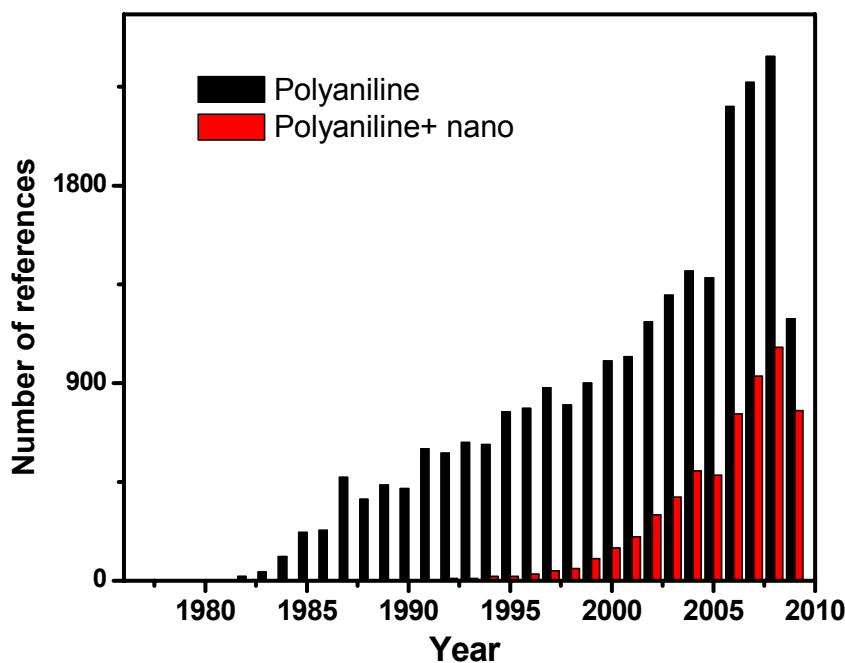


Figure 1.7. The annual number of publications on the subject of 'PANI' and 'PANI+ nano', as provided by the search engine of SCIFINDER scholar

Synthesis of nanostructured ICPs is receiving much importance due to its uniqueness and high performance arising from their nanosize, large surface area and better dispersibility. As these nanomaterials have higher electroactive surface area, the charge transfer and mass transport improves significantly and hence enhances their performance characteristics in various devices (Huang *et al.*, 2003, Liu *et al.*, 2003). Regardless of the practical applications eventually developed, these nanostructured materials certainly will challenge researchers in the years to come with new and unexpected phenomena. Synthesizing nanostructures of ICP has attracted growing research attention as evident from Figure 1.7. which provides the annual number of publications on the subject of 'PANI' and 'PANI+ nano', as provided by the search engine of SCIFINDER scholar.

There are several principle synthetic strategies for the preparation of nanostructured ICPs. They include mechanical stretching, electro-spinning, electrochemical, template, templateless, enzymatic, plasma, photo induced, seed-mediated etc (Xiong *et al.*, 2004, Delvaux *et al.*, 2000, Genies *et al.*, 1985, Genies *et al.*, 1985, Mativetsky *et al.*, 2002, Choi *et al.*, 2003, Sauer *et al.*, 2002, Huang *et al.*, 2004, Kobayashi *et al.*, 2001, Arias *et al.*, 1996, Mejias *et al.*, 2002, Nastase *et al.*, 2005, Nastase *et al.*, 2006, Barros *et al.*, 2003, Khanna *et al.*, 2005).

1.6.1. Template synthesis

Template can be considered as a nanoreactor which provides a local environment where pH and charge density near the template molecules controls the shape of the resulting ICPs. Template synthesis is divided into hard template (physical template) and soft template (chemical template) (Figure 1.8.) route.

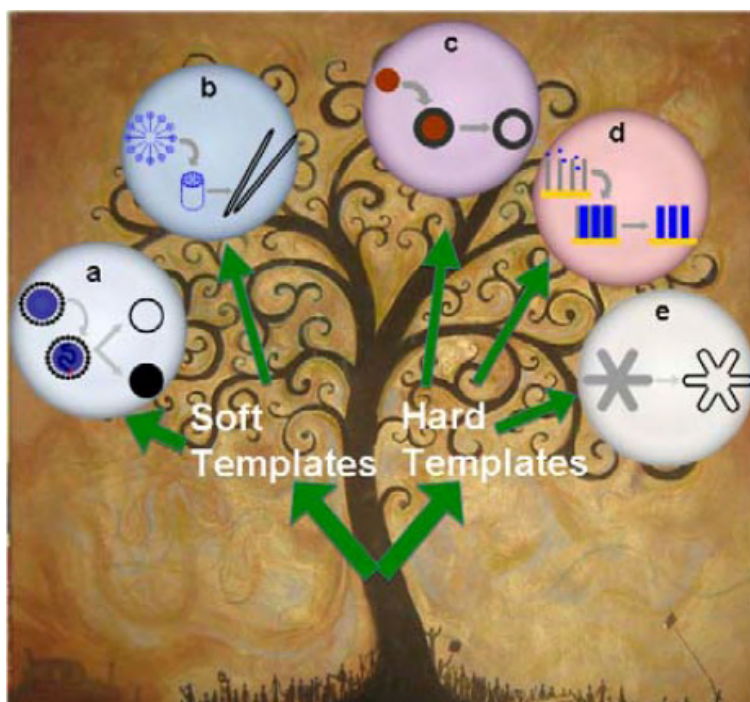


Figure 1.8. Template synthesis

1.6.1.1. Hard template

Hard template route is one of the most effective and simple technique for the preparation of nanostructured ICPs (Liu *et al.*, 2010). It was first proposed by Martin (Martin *et al.*, 1994, Hulteen *et al.*, 1997, Martin *et al.*, 1998) and it involves the synthesis of ICP within the pores or channels of membranes like track-etched polycarbonate, anodic aluminium oxide (Jackowska *et al.*, 2008) or solid porous materials such as zeolites (Treuba *et al.*, 2004), silica-based mesoporous molecular sieves (Cho *et al.*, 2004), oxides (Dauginet *et al.*, 2005, Zhang *et al.*, 2005), graphite composites (Wang *et al.*, 2006, Wang *et al.*, 2006), polyoxometallates (Kulesza *et al.*, 2002) etc. In this method, the desired material with the required shape is synthesized within the pores of the template. Template is then removed, leaving the ICP in nanometer regime. This method has

been used both for chemical and electrochemical polymerization (Xiong *et al.*, 2004, Demoustier *et al.*, 1999, Delvaux *et al.*, 2000, Mativetsky *et al.*, 2002). However, the disadvantages of the method are: (i) tedious post synthesis etching procedure which is required for the removal of the template, and (ii) during this post synthesis process, the soft polymeric structures may be damaged and would aggregate into micro dimension. An example for the preparation of nanostructured conducting PEDOT using gold sputtered electrode as hard template is shown in Figure 1.9. (Liu *et al.*, 2008).

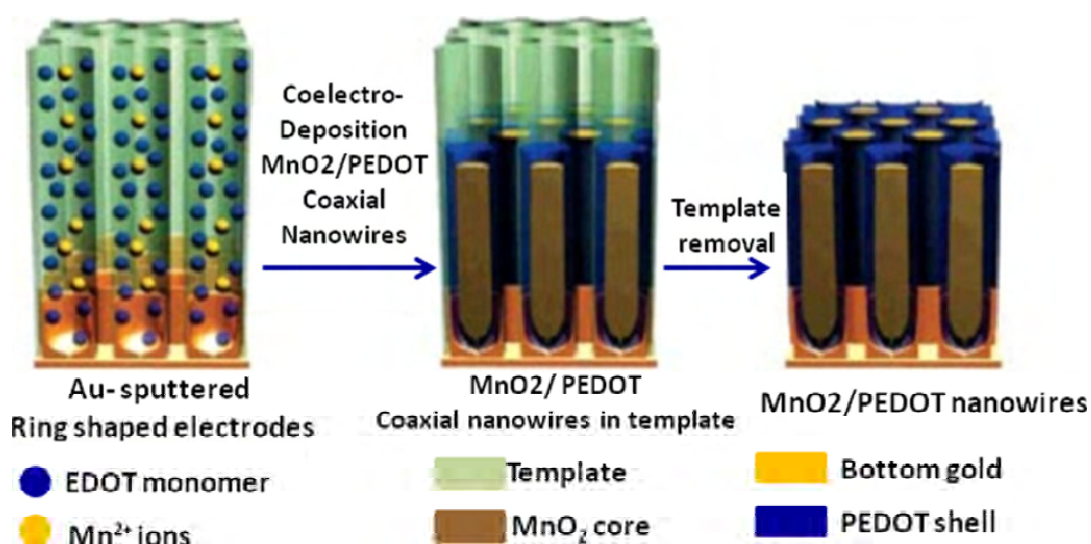


Figure 1.9. Schematic representation for hard template polymerization

1.6.1.2. Soft template

Soft template polymerization is simpler and less expensive when compared to hard template method since it eliminates the use of any solid template and the postsynthesis etching procedure. It includes functional molecules like surfactants (Vijay *et al.*, 2002, Carswell *et al.*, 2003, Yang *et al.*, 2005, Sarno *et al.*, 2005, Wang *et al.*, 2005), liquid crystals (Huang *et al.*, 2002), polyelectrolytes (Shao *et al.*,

2002, Zhu *et al.*, 2006) or block copolymers (Bates *et al.*, 1999). It is believed that these functional molecules can promote the formation of nanostructured soft condensed phase materials (e.g., micelles and emulsions) which can serve as “soft templates” during the formation of ICP (Figure 1.10.) (Carswell *et al.*, 2003).

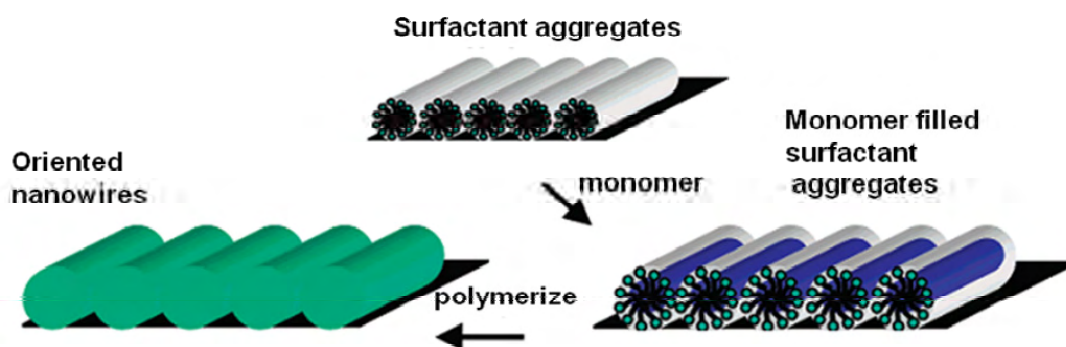


Figure 1.10. Schematic representation for soft template polymerization

The formation of the nano-structured ICP depends on the reaction conditions such as the concentration of monomer, the molar ratio of monomer to oxidant and the functionality of the molecule.

Amphiphilic acids are the most used “soft template” molecules for the preparation of nanostructured PANI. Wan’s group studied the effect of organic sulfonic acids such as methane sulfonic acid, p-methylbenzene sulfonic acid, β -naphthalene sulfonic acid etc. on the morphologies of the products (Huang *et al.*, 1999). Many other sulfonic acids such as azobenzene sulfonic acid, D-10-camphorsulfonic acid were also used as soft templates for the preparation of PANI nanotubes (Huang *et al.*, 2002, Huang *et al.*, 2003, Wan *et al.*, 2003, Zhang *et al.*, 2002, Zhang *et al.*, 2005). Soft template routes are more scalable but

they rely on the nature of the functional molecules which forms the soft templates.

1.7. Conducting polymer -inorganic hybrid nanocomposites

Conducting polymer-inorganic hybrid composites exhibits synergetic properties arising from the molecular level mixing of both inorganic and organic species. A nanocomposite is a material with nanometric domains of two coexisting phases without mutual solubility. Here the organic and inorganic components are held together either by weak forces, such as vander Waals or hydrogen bonding interactions or by strong covalent bonds. Conducting polymer-inorganic hybrid nanocomposites improve the electrical conductivity, ionic conductivity, thermo-mechanical and other related functional properties of the original material. There are several principle synthetic strategies for the preparation of polymer-inorganic hybrid nanocomposites depending on the type of host structure which includes three dimensional (3D) framework system such as zeolites, mesoporous materials, two dimensional (2D) layered materials such as clay, metal phosphates, dichalcogenides (MoS_2 , WSe_2 and NbS_2), one dimensional (1D) and zero dimensional materials such as metal clusters (Schollhorn, 1996). The confinement of organic polymer inside 2D layered inorganic hosts involves either the direct insertion of extended polymer chains or intercalation of monomer followed by polymerization. Among the inorganic hosts, layered clay has gained interest due to their exceptional mechanical strength and thermal stability.

1.7.1. Polyaniline- clay nanocomposites (PANICN)

PANICN represents a new class of molecular composites with diverse electrical, optical, mechanical and thermal properties (Porter *et al.*, 1997, Huguenin *et al.*, 2004, Rong *et al.*, 2001, Lim *et al.*, 2002). They consist of sandwiched multilayers in which PANI chains are confined between nanoclay layers. Smectite clays used in the synthesis of nanocomposites can be natural or synthetic. Table 1.1 summarizes chemical formula of the commonly used smectite clays for the preparation of nanocomposite materials among which the montmorillonite is the most widely used one because of its wide expandibility, chemical resistance, cation exchangeability and well understood intercalation chemistry.

Table 1.1. Chemical formula of commonly used smectite clays.

Group	Species	Octahedral Occupancy	Formula (Ideal)
Smectite	Montmorillonite	Diocahedral	$\text{Ca}_{0.25}\text{Si}_4^{(\text{IV})}(\text{Al}_{1.5}\text{Mg}_{0.5})^{(\text{VI})}\text{O}_{10}(\text{OH})_2$
Smectite	Beidellite	Diocahedral	$\text{Ca}_{0.25}(\text{Si}_{3.5}\text{Al}_{0.5})^{(\text{IV})}\text{Al}_2^{(\text{VI})}\text{O}_{10}(\text{OH})_2$
Smectite	Saponite	Triocahedral	$\text{Ca}_{0.25}(\text{Si}_{3.5}\text{Al}_{0.5})^{(\text{IV})}\text{Mg}_3^{(\text{VI})}\text{O}_{10}(\text{OH})_2$
Smectite	Hectorite	Triocahedral	$\text{Ca}_{0.25}\text{Si}_4^{(\text{IV})}(\text{Mg}_{2.5}\text{Li}_{0.5})^{(\text{VI})}\text{O}_{10}(\text{OH})_2$
Smectite	Laponite	Diocahedral	$[(\text{Si}_8(\text{Mg}_{5.34}\text{Li}_{0.66})\text{O}_{20}(\text{OH})_4)] \cdot \text{Na}_{0.66}$

Moreover they are abundant naturally occurring material and are easily available (Vaia *et al.*, 1993, Mehrotra *et al.*, 1990). They are having high aspect

ratio and each layer have dimension of 1 nm thickness and $\sim 500\text{-}1000$ nm length. Their basic building blocks are aluminium silicate containing octahedral sheets of aluminium surrounded by eight oxygen atoms sandwiched between tetrahedral sheets of silicon surrounded by four oxygen atoms. These layers organize themselves in a parallel fashion to form stacks with a regular vander Waals gap in between them called interlayer spacing or gallery. Substituting ions of lower charge for higher charge (e.g., Mg^{2+} replacing Al^{3+}) in the octahedral sheets produces negatively charged layers which is counter balanced by the presence of alkali and alkaline earth metal cations in the clay gallery (Figure 1.11.) (Purnell, 1990).

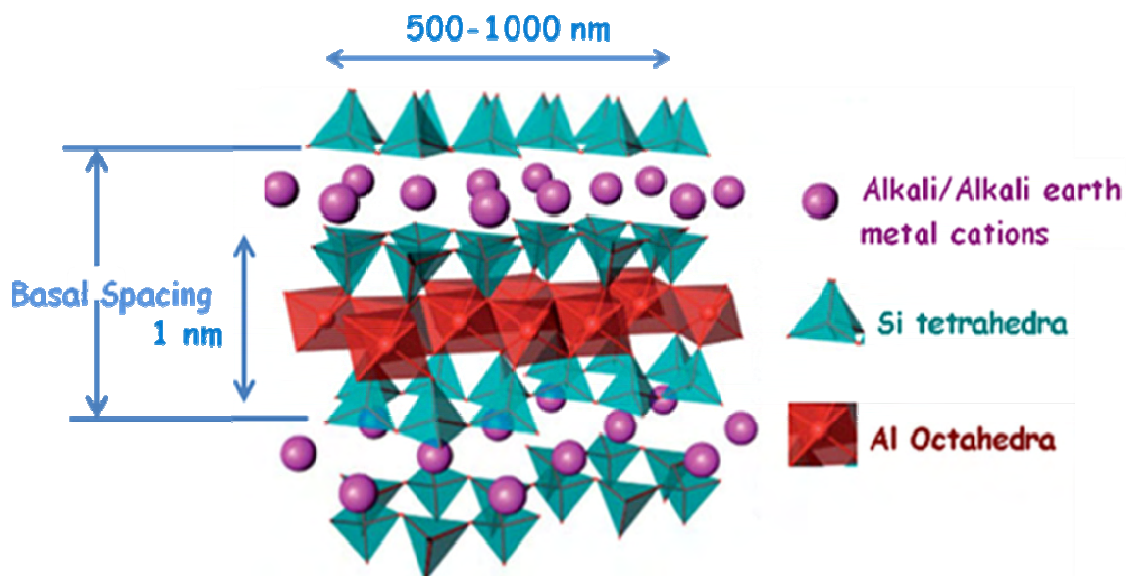
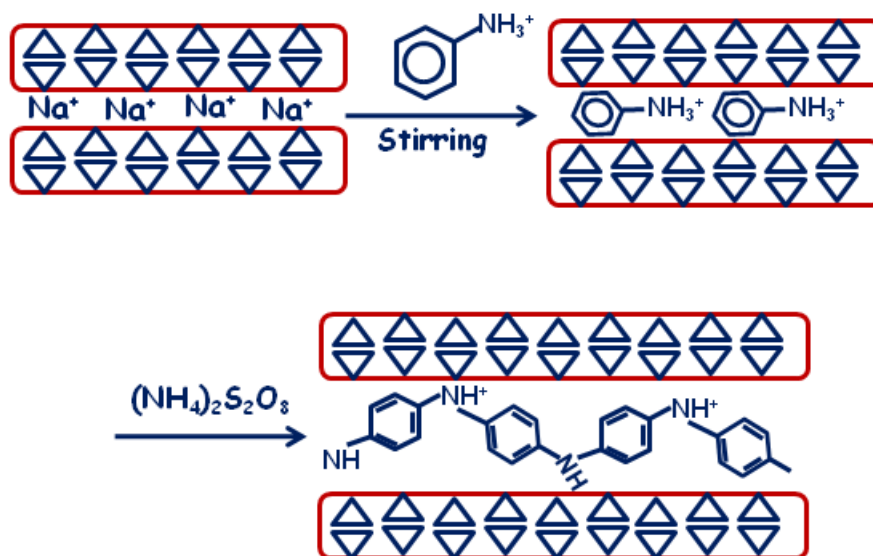


Figure 1.11. Structure of Montmorillonite clay

This charge is not locally constant, but varies from layer to layer, and must be considered as an average value over the whole crystal. The variability of the c-axis dimension permits the intercalation of a large variety of inorganic and

organic interlayer cations through the cation exchange process and thereby desirable physical properties can be engineered into this material.

PANICNs can be synthesized by chemical oxidation of aniline inside the clay layers as represented in the scheme 1.7.



Scheme 1.7. Chemical Synthesis of PANI-MMT

Recently, several reports have been published on chemical methods of synthesis of PANICNs (Nazzal *et al.*, 1985, Yeh *et al.*, 2001, Kim *et al.*, 2002, Sun *et al.*, 1995, Kim *et al.*, 2003, Chang *et al.*, 1992, Wu *et al.*, 2000, Lee *et al.*, 2000), where PANI-clay nanocomposites have been prepared from the mixture of aniline and clay in aqueous solution using APS as the oxidative radical initiator at acidic pH. Taking into account the difficulties of intercalating polymers into clay having narrow interlayer distance, efforts have been made to organically modify the clay by insertion of amphiphilic surfactant molecules. These amphiphilic molecules due to the presence of both hydrophobic and hydrophilic group can reduce the interlayer interaction of the clay and can promote the confinement of anilinium

ion inside the clay gallery. After intercalation of the anilinium ion, the extrinsic initiator, APS can enter and initiate polymerization for getting protonated PANI chain confined PANICNs. The functionalized amphiphilic molecules can also play the role of dopants during the formation of conducting PANICNs.

Wu and coworkers (Wu *et al.*, 1996) have synthesized nanocomposites of PANI- MMT using dodecylbenzene sulphonic acid (DBSA) as an emulsifier. Kim and coworkers (Kim *et al.*, 2003) and Yang and coworkers (Yang *et al.*, 2002) have also reported the preparation of nanocomposites of PANI with organically modified clay which exhibited good electrical conductivity and thermo-mechanical property due to the effective intercalation. PANICN synthesized can be classified into two types depending upon the crystallographic organization of nanoclay layers in the polyaniline matrix (Ray *et al.*, 2003) (Figure 1.12.)

1. Intercalated nanocomposites: Polymer layers are confined inside the clay galleries which are organized in a crystallographically regular fashion.
2. Exfoliated nanocomposites: The individual clay layers are dispersed in a continuous polymer matrix in a random fashion by an average distances that depends on the clay loading.

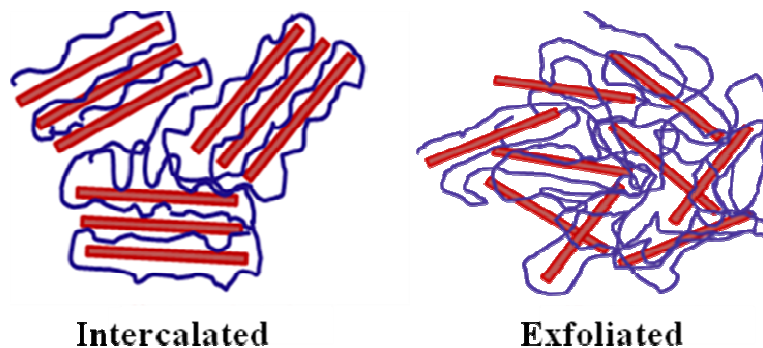


Figure 1.12. Intercalated and exfoliated polymer- clay nanocomposites

These two types of arrangement can be differentiated using WXR D technique (Figure 1.13.) and TEM observation. Due to the easiness and availability, WXR D is most commonly used to probe the nanocomposite structure (Pavlidou *et al.*, 2008, Beyer *et al.*, 2002, Alexandre *et al.*, 2000, Ray *et al.*, 2003, Porter *et al.*, 2000). For intercalated nanocomposite, in the XRD pattern, the characteristic reflection corresponding to the d_{001} plane of clay, exhibit a shift in the position towards lower diffraction angle which would correspond to the dimension of the confined polymer chains. On the other hand, in an exfoliated nanocomposite, the delamination of the nanoclay layers in the polymer matrix results with the disappearance of any coherent X-ray diffraction peak corresponding to the d_{001} plane.

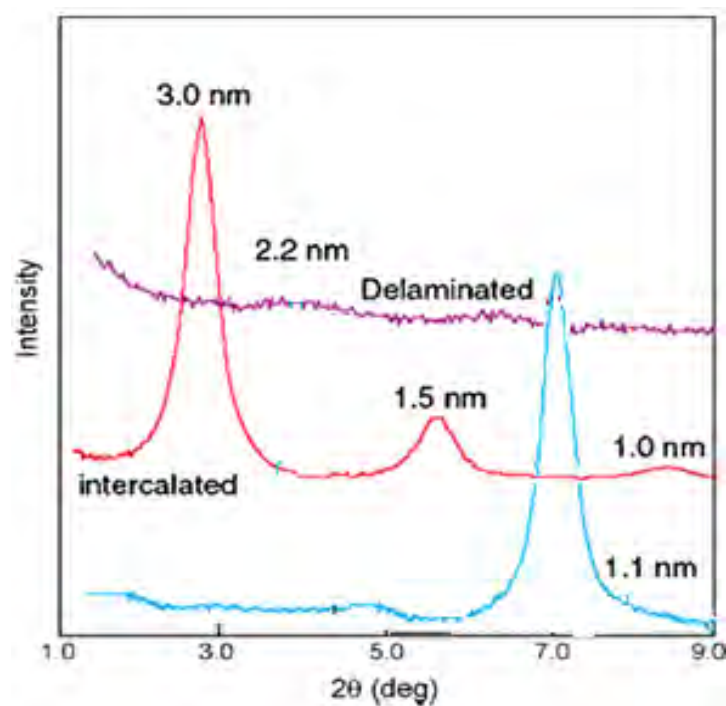


Figure 1.13. XRD of clay, intercalated and exfoliated polymer-clay nanocomposites

1.7.2. Nanostructured multifunctional conducting polymer-metal hybrid composites.

Multicomponent polymer systems comprising nanoparticles of metals or metal oxides like Au, Ag, Pd, TiO₂, ferrites, Ni, V₂O₅ etc are receiving considerable research attention for their various potential applications, since they can be tailored to exhibit novel electrical, magnetic and optical properties along with good film forming property. (Qi *et al.*, 1998, Huang *et al.*, 1998, Neoh *et al.*, 1999, Drelinkiewicz *et al.*, 1998, Hable *et al.*, 1991, Esteban *et al.*, 1989, Armes *et al.*, 1991, Torsi *et al.*, 1998, Partch *et al.*, 1991, Huang *et al.*, 1995, Gangopadhyay *et al.*, 1999, Wan *et al.*, 1998, Somani *et al.*, 1999, Somani *et al.*, 1999).

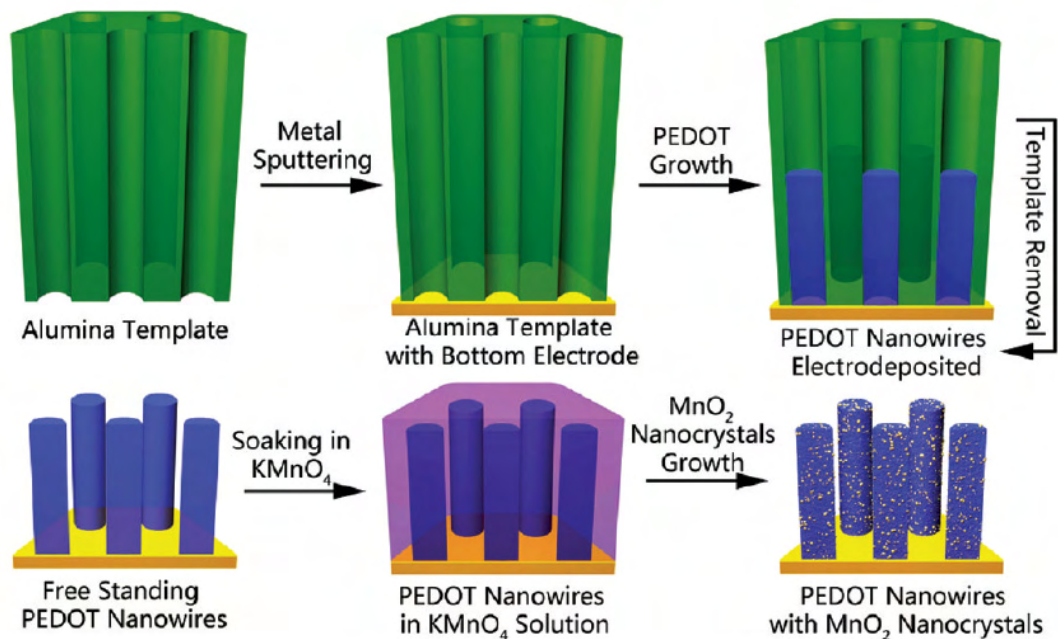


Figure 1.14. Schematic representation for the preparation of PEDOT/MnO₂ nanocomposites

Liu and co workers (Liu *et al.*, 2010) electrochemically synthesized MnO₂ nanoparticle enriched PEDOT nanowires by initially preparing PEDOT

nanowires by hard template route followed by removal of the template and then soaking these PEDOT nanowires in potassium permanganate solution as represented in the Figure 1.14. The composites exhibited very high specific capacitance due to the high surface area of the MnO₂ nanoparticle enriched PEDOT nanowires and can therefore be used as the supercapacitor electrode materials for lithium ion batteries.

Han and coworkers (Han *et al.*, 2010) described a versatile two step method for the preparation of gold/PANI core/shell nanocomposites with the aid of a non-ionic surfactant as represented in the Figure 1.15.

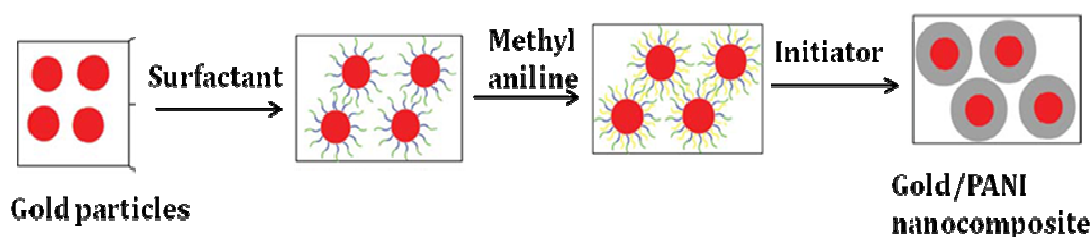


Figure 1.15. Schematic representation for the preparation of gold/PANI nanocomposites

Initially, the surfactant and monomer were introduced to gold colloids followed by the addition of oxidant to initiate the polymerization to create a PANI shell around each gold nanoparticle. These composites are becoming the research focus not only from fundamental scientific interest but also from practical applications like in plastic digital memory.

Whitesides and coworkers (Lahav *et al.*, 2006) have electrochemically synthesized composites of Au and PANI using anodized aluminum oxide membranes as hard template. The composite exhibited nanotubular morphology having ~200 nm width and several micrometers length where PANI forms the

core and Au, the shell (Figure 1.16.). They have illustrated its suitability in incorporating into solar-cell and OLED devices.

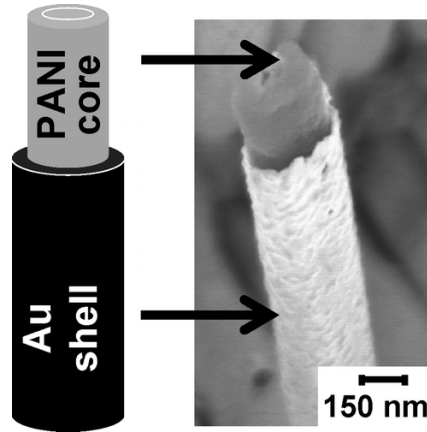


Figure 1.16. Core- shell Au- PANI composite

Zhang and coworkers (Zhang et al., 2010) reported a novel process for the synthesis of PANI - CdS composites by polymerization of aniline in presence of CdS nanoparticles.

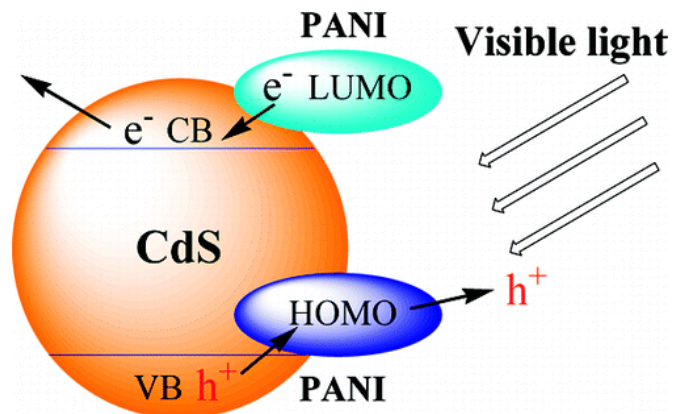


Figure 1.17. The scheme of the visible light photocatalysis process over PANI-CdS composite

These functional nanocomposites exhibited enhanced visible light photocatalytic activity and excellent antiphotocorrosion performance of CdS (Figure 1.17). This novel CdS based photocatalysts invoke tremendous hope in solving the serious environmental and energy challenges.

1.7.2.1. Electro-magnetic polymer –inorganic hybrid composites (EMPCs).

Electro-magnetic polymer composites comprising ICPs hosting magnetic nanoparticles have attracted a great deal of attention as they exhibit dual functionalities like electrical conductivity and magnetic property endowed with processability in a unique material system. It is known that the conducting material can shield effectively the electric component of an electro-magnetic wave, whereas, only magnetic materials can effectively shield the magnetic component of an electro-magnetic wave. Thus, if the materials having both magnetic and electric components are used as electromagnetic interference shielding materials, good shielding effectiveness can be achieved. Also they find potential applications in various fields such as antistatic coatings, biological applications, chemical sensors, transducers, rechargeable battery and corrosion protection coatings (Li *et al.*, 2006, Wang *et al.*, 2005, Xu *et al.*, 2008, Ding *et al.*, 2008, Li *et al.*, 2009, Vossmeier *et al.*, 2002).

Till date, many electro-magnetic functionalized composites of the ICPs have been successfully synthesized via chemical or electrochemical methods (Kim *et al.*, 2002, Long *et al.*, 2005, Yoon *et al.*, 2004, Gangopandhyay *et al.*, 2000) by integrating ICPs with various metal and metal oxides like Ni, V₂O₅, Pt, ferrites etc (Xu *et al.*, 2008, Karatchevtseva *et al.*, 2006, Gangopandhyay *et al.*, 2000 Caruso *et al.*, 2001 Rajeswar *et al.*, 2001). Among which, the iron oxides are unique because of their high saturation magnetization and relative stability in atmospheric conditions.

There are several methodologies suggested for the preparation of EMPCs. Wan and coworkers (Wan *et al.*, 1996) synthesized EMPC of PANI containing

nanometer sized iron oxide by a chemical method and envisaged the pH dependent electro-magnetic properties. These EMPCs exhibited superparamagnetic behavior with a saturation magnetization of 6 emu g^{-1} (10 wt % Fe loading) and conductivity of $10^{-1} \text{ S cm}^{-1}$. Javed and coworkers (Javed *et al.*, 2007) developed EMPCs by *in-situ* polymerization of aniline using ferrofluid as shown in Figure 1.18. Effect of the ferrite concentration on the conductivity and magnetic properties of EMPCs were investigated.

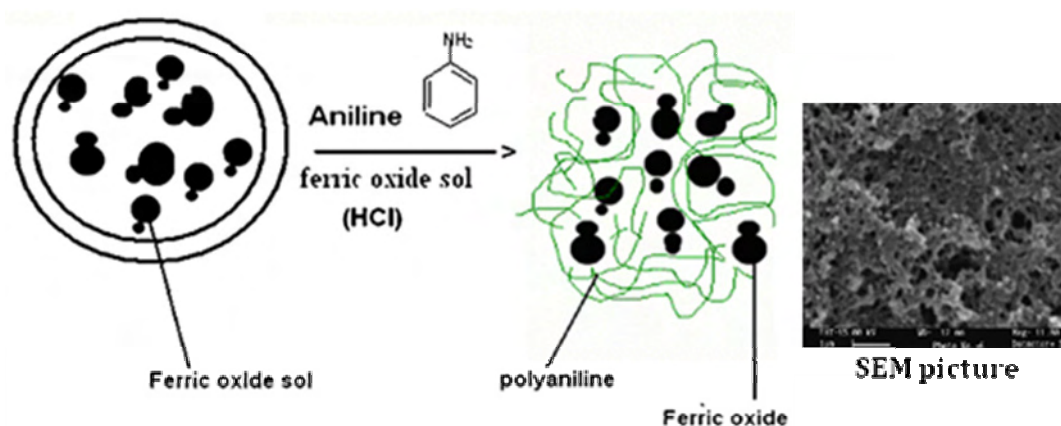


Figure 1.18. Scheme for the preparation of $\text{Fe}_3\text{O}_4/\text{PANI}$ nanocomposite

Conductivity of the EMPC was found to be in the range of $10^{-3} \text{ S cm}^{-1}$ and saturation magnetization, 3.2 emu g^{-1} with no coercivity revealing super paramagnetic behavior (8 wt% Fe_3O_4 loading). SEM picture of this EMPC showed a homogeneous nanoporous structure with uniform distribution of particles where the PANI as well as iron oxide phase form a network like structure as shown in Figure 1.18.

Xuan and coworkers (Xuan *et al.*, 2008) reported a novel synthetic strategy for the preparation of EMPC with core shell microspheres via a simple *in-situ* surface polymerization method as shown in the Figure 1.19. Here, the

Fe_3O_4 is surface modified with 3-aminopropyltriethoxysilane and further micellised in presence of polyvinyl pyrrolidone (PVP) and subjected to *in-situ* surface polymerization of aniline using APS as the oxidative radical initiator. These EMPC showed well-defined blackberry like morphology under SEM and exhibited saturation magnetization of 45 emu g^{-1} (30 wt% Fe_3O_4). Results suggested that it can serve as an ideal candidate for biomedical applications such as nucleic acid extraction, cancer diagnosis, biosensors and drug delivery. They proposed that the present method can be extended to other magnetic core materials (Fe, $\gamma\text{-Fe}_2\text{O}_3$, Co and Ni) and to a range of other conductive shell polymers such as Ppy, polythiophene, etc.

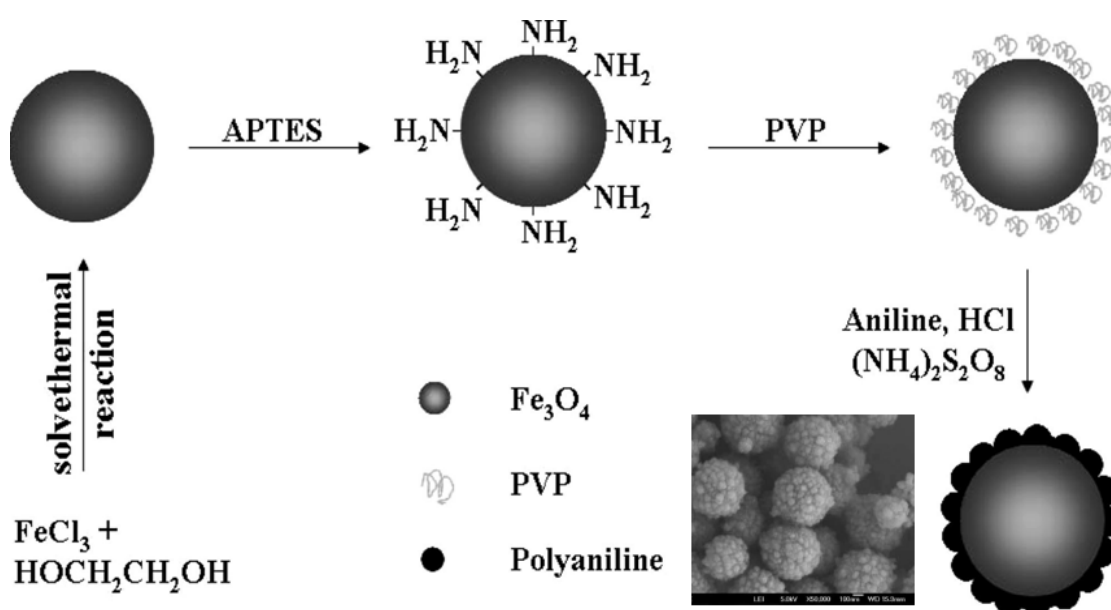


Figure 1.19. Schematic illustration for the synthesis process of Fe_3O_4 @PANI core/shell composite

Literature showed that the electrical and magnetic properties of EMPCs can be tailored by controlling the type and amount of metal ion substitution in ferrites. Li and co-workers (Li *et al.*, 2008) synthesized PANI-

$\text{Zn}_{0.6}\text{Cu}_{0.4}\text{Cr}_{0.5}\text{Fe}_{1.5}\text{O}_4$ (20 wt% ferrite loading) EMPC by *in-situ* polymerization of aniline in the presence of $\text{Zn}_{0.6}\text{Cu}_{0.4}\text{Cr}_{0.5}\text{Fe}_{1.5}\text{O}_4$ nanoparticles. SEM and TEM images showed core-shell morphology with magnetic ferrite as core and conducting PANI as shell. These nanocomposites under applied magnetic field exhibited hysteresis loops with saturation magnetisation (M_s) of 10 emu g^{-1} . In another report, they had synthesized EMPC from $\text{Zn}_{0.6}\text{Cu}_{0.4}\text{Cr}_{0.5}\text{Fe}_{1.5-x}\text{La}_x\text{O}_4$ ($x = 0 \sim 0.06$) ferrites doped with La by a rheological phase reaction method as represented in the Figure 1.20 (Li *et al.*, 2008). These EMPC exhibited ferromagnetic nature with saturation magnetization of 3 emu g^{-1} and coercivity of 18 Oe (25 wt% Fe_3O_4).



Figure 1.20. Polymerization procedure for PANI/ $\text{Zn}_{0.6}\text{Cu}_{0.4}\text{Cr}_{0.5}\text{Fe}_{1.5-x}\text{La}_x\text{O}_4$ composites (inset showing the TEM image of core shell PANI composite)

The formed electromagnetic composite is stabilised by different type of interaction between PANI and metal particles. They (Li *et al.*, 2006) suggested

three bonding models to explain the interaction between PANI and ferrites which is illustrated in Figure 1.21.

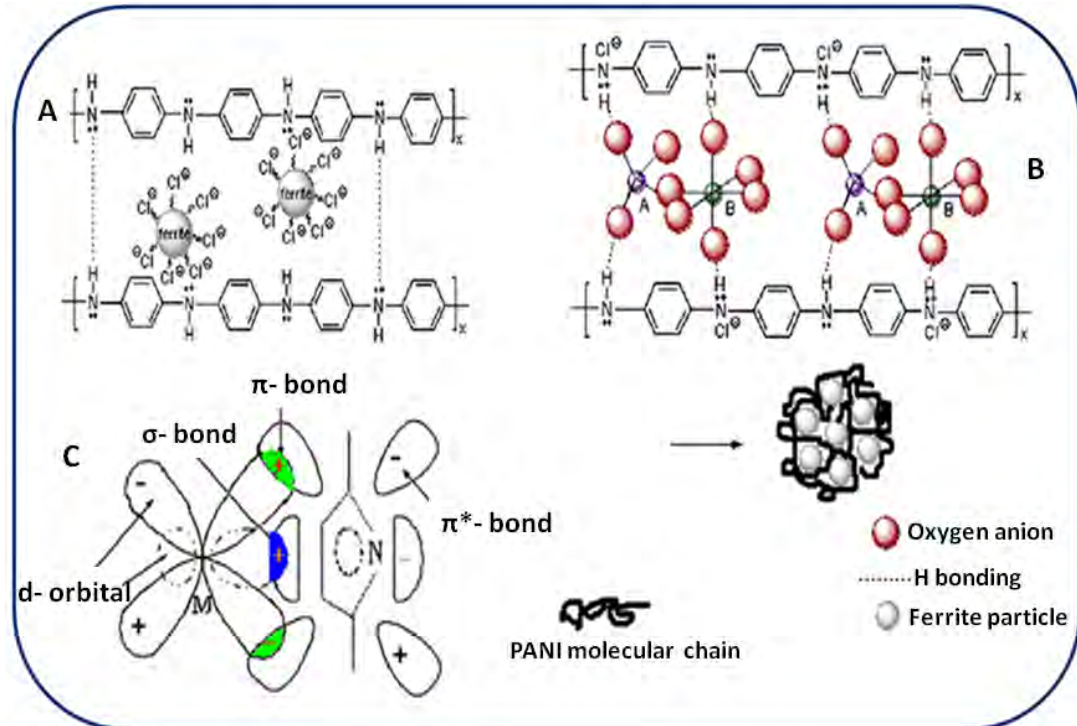


Figure 1.21. Bonding mechanism in the PANI/ iron oxide nanocomposites

The charge compensation model (Figure 1.21. A) reveals that there is charge compensation effect between ferrites and PANI chains in the composites. The surface of the ferrite is positively charged due to the polymerization of aniline in acidic conditions. Therefore, adsorption of anion, say chloride (Cl^-) may compensate the positive charges on the ferrite surface. Beside these charge compensation process, extra adsorption of the Cl^- on the ferrite surface would work as the charge compensator for positively charged PANI chains in the formation of PANI-ferrite composites. Figure 1.21. (B) represents the H- bonding model in PANI-ferrite EMPC systems. The hydrogen bonding interaction between PANI chains make them twist to form network structure. In addition, the

hydrogen bonding interaction between the PANI chains and the oxygen atoms on the ferrite surface make ferrite particles embedded into the network of PANI. The third model (Figure 1.21. C) suggest that there is σ - π interaction between metal oxide and PANI in EMPCs, which includes (1) overlapping of π molecular orbital of PANI with the empty d-orbital of iron to form the σ -bond and (2) overlapping of π^* molecular orbital of PANI with the d-orbital of metal ions to form the π -bond.

EMPC of PANI-CoFe₂O₄ with cage like morphology was reported by Ding and coworkers (Ding *et al.*, 2008) in which the self-assembled PANI nanofibers (~15 nm in diameter) entwines around the octahedral CoFe₂O₄ magnet which is acting as the nucleation site or template. The cage like composites exhibited high conductivity of $\sim 5 \text{ S cm}^{-1}$ and ferromagnetic function with a high coercive force (H_c)=1000 Oe and saturation magnetization (M_s)= 40 emu g⁻¹ (25 wt % ferrite loading).

EMPC prepared through the above mentioned strategies could not exhibit excellent conductivity, sufficient stability and definite shape. Also they suffered from the disadvantage of leaching out of iron oxide nanoparticles from the composite due to the presence of strong mineral acids (Xu *et al.*, 2004, Xue *et al.*, 2006). Literature showed that EMPC can exhibit novel magnetic properties when the metal nanoparticles are in the isolated state. A critical obstacle during assembling and maintaining nanoscale magnetic material is its agglomeration, which is a deterrent to its applications (Y.K. Gunko *et al.*, 2001). Moreover, several applications require consolidation and sintering of these nanomaterials

into solid blocks or thin films. These processing routes often lead to unavoidable agglomerations and larger grains of these magnetic particles that effectively prevent them from attaining full potential in terms of the magnetic and electric response (Neamtu *et al.*, 2005).

Encapsulating these magnetic nanoparticles in polymer matrix prevents its grain growth and agglomeration. However, the control over the dispersion of the nanoparticle in a polymer matrix is still in its embryonic stage at the research level. To achieve excellent dispersion, competition between polymer–polymer and polymer–particle interactions have to be balanced to avoid clustering of particles in polymer nanocomposites. Hence, to exploit the full potential of these materials, it is important to address these problems. An ideal remedy is to use surfactant molecules during the polymerization process. Literature showed that surfactant molecules can act as capping agent for controlling the size and shape of the metal nanoparticles apart from inducing plasticization and doping effect for EMPCs.

Ding and coworkers (Ding *et al.*, 2005) have reported a facile one-pot synthetic strategy for the preparation of PANI-magnetite nanocomposites in presence of the amphiphilic molecule, dodecyl benzene sulphonic acid through micelle assisted self-assembly method and is represented in Figure 1.22. Here, the DBSA serves not only as a dopant, but also as a surfactant and could also control the morphology of the formed EMPC. The presence of high concentration of DBSA effectively prevent the formation of larger magnetite particles and these composites exhibited ferromagnetic behavior with saturation magnetization and

coercivity values of $\sim 17.73 \text{ emu g}^{-1}$ and 63.8 Oe , respectively with 10 wt% loading of Fe. Moreover, it is worth noticing that the resulting PANI/magnetite nanocomposites can form stable nanorods with uniform size and high yields. SEM images of these EMPC (inset) showed that the magnetite particles adsorb on the surface of each PANI nanorods and are uniformly dispersed.

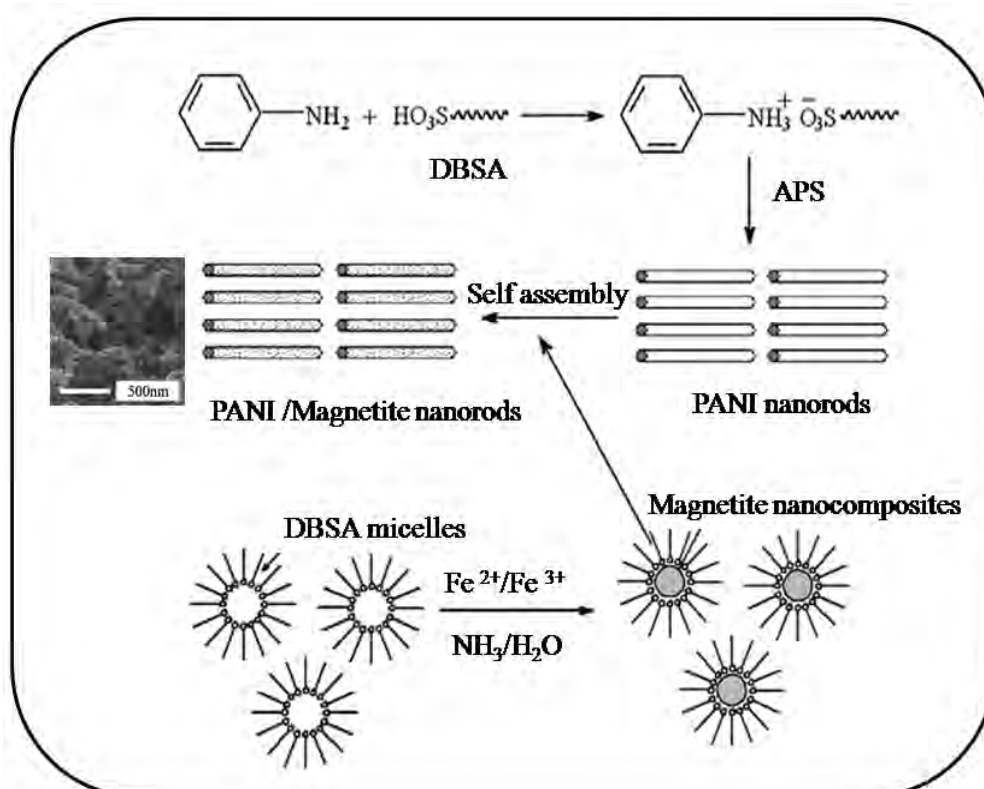


Figure 1.22. Schematic illustration of the synthesis process of PANI/magnetite nanorod composites

A couple of reports have risen from the group of Lee (Reddy *et al.*, 2008, Reddy *et al.*, 2007) where they used CSA and pTSA as surfactant dopants. EMPC of Fe_3O_4 nanoparticles and PANI were prepared via chemical oxidative polymerization in presence of CSA and pTSA. These organic acid molecules form a complex with aniline molecules and will self-assemble to form spherical micelle covering the Fe_3O_4 nanoparticles. During polymerization, it formed EMPC with

core-shell morphology and exhibited electrical conductivity of $\sim 0.1 \text{ S cm}^{-1}$ with superparamagnetism having $M_s \sim 5 \text{ emu g}^{-1}$ (10 wt% ferrite).

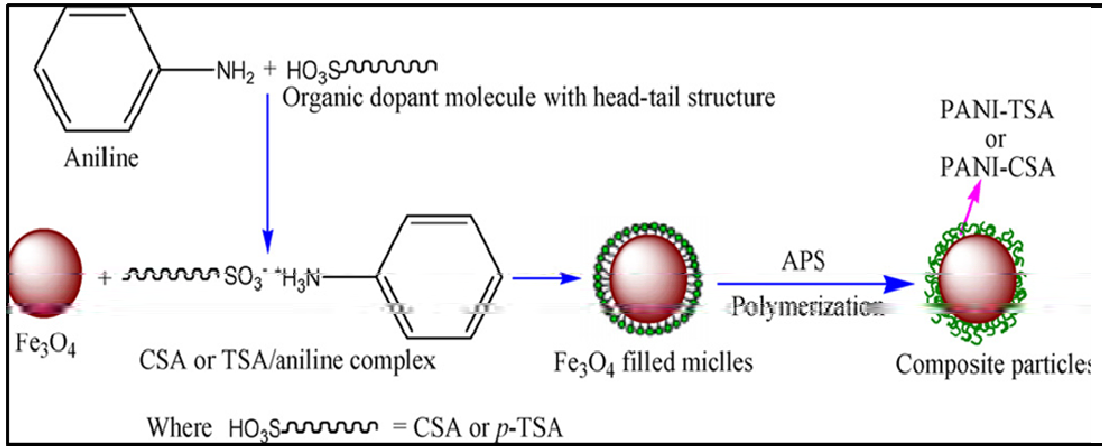


Figure 1.23. Preparation of PANI/Fe₃O₄ EMPC prepared in presence of surfactant molecule

They have also synthesized EMPCs by incorporating magnetite nanoparticles into the matrix of poly(aniline-co-8-amino-2-naphthalenesulfonic acid) through chemical oxidative polymerization of aniline and 8-amino-2-naphthalenesulfonic acid in the presence of magnetite nanoparticles and controlled the particle size to 10-15 nm. Composites exhibited good electrical conductivity (0.45 S cm^{-1}) as well as magnetic property ($M_s = 10 \text{ emu g}^{-1}$) with 10% Fe₃O₄ loading.

Tang and coworkers (Tang *et al.*, 1999) developed a process for the preparation of γ -Fe₂O₃-PANI EMPC films in the presence of surfactants like ω -methoxypoly(ethylene glycol) phosphate, DBSA and CSA and the prepared films which exhibited high electrical conductivity ($82\text{-}237 \text{ S cm}^{-1}$), and superparamagnetism.

In this chapter, we have described briefly an overview of the recent developments in the field of electromagnetic polymer composites with special emphasis on different strategies for the preparation EMPCs and its properties. It is clear from the above discussions that for achieving the full potential of EMPCs, composites are to be made with excellent electrical conductivity and magnetic property with low loading of magnetic nanoparticles. Moreover retaining the stability in size and shape with well segregated magnetic nanoparticles is also challenging for considering it as a prospectable candidate for different applications. Apart from all these factors, thermo-mechanical properties, processability and better dispersibility are also relevant.

1.8. Scope and objective of the work

Development of nanostructured electro-magnetic polymer composites with electric and magnetic properties endowed with high mechanical strength and thermal stability are challenging because of their ease of processability, light weight and so forth. They are receiving considerable attention for potential applications in various fields such as electrochemical display devices, nonlinear optics, sensors, electro-magnetic interference shields, microwave absorbing materials, catalysis, magnetic recorders, rechargeable batteries etc. Several strategies are reported for the preparation of EMPCs which are mainly based on the incorporation of iron oxide based magnetic materials or substituted ferrites with various ICPs like PANI, Ppy, polythiophene etc. But the disadvantage with these systems is that it may require high loading of these magnetic nanoparticles for achieving excellent magnetic property which is deterrent for space vehicles

and also for light weight portable devices. It can also cause poor mechanical strength for the fabricated materials. Other problems associated with these EMPCs are low performance stability, inability to tune the size and shape of the magnetic nanoparticles for enabling them to exhibit excellent magnetic performance. Promising strategy for getting maximum electrical conductivity is by confining the ICP in the nanometer regime. Addressing all these issues is a challenge for the development of high performance EMPC for various technological applications.

Researchers have shown that salts of certain metals like iron, chromium etc. can form polyhydroxy cations like keggin ions in their highest oxidation states via hydrolysis at acidic pH followed by deprotonation and polycondensation. They can form discrete structures (keggin ions) having high electron density and large number of unpaired electrons in high-spin combined with the possibility of forming spin-crossover magnetic molecular materials (Ksenofontov *et al.*, 2004). So they are expected to exhibit high magnetic property with low loading of magnetic nanoparticles. It has been reported that EMPC prepared in presence of surfactant like DBSA, CSA etc could control the size and shape of the magnetic nanoparticles by a capping mechanism followed by self-assembly process. The repulsive forces which are induced by coating of the particles with surfactants prevent them from aggregation and thereby control the size and shape of the formed nanoparticles. However, retaining the stability in size and shape with well segregated magnetic nanoparticles in EMPC is still a challenge.

Apart from all these factors, thermo-mechanical properties are also important for these materials which could be imparted by preparing their clay composites. The presence of nanoclay layers having high aspect ratio is expected to enhance thermo-mechanical property and all other associated barrier properties for these nanocomposites. Moreover, in the confined environment of nanoclay layers, polyaniline takes an extended conformation and charged carriers will be in a highly delocalized state and will exhibit excellent electrical conductivity with low loading. The presence of amphiphilic dopant during the preparation of PANICNs can play the multiple role of dopant, structure directing agent and intercalating agent. Also it can control the morphology of the formed nanostructured conducting PANI through its template action and different nature of aggregation arising from the noncovalent interactions like hydrogen bonding, π - π stacking and electrostatic layer-by-layer assembling among the protonated PANI chains. In this context, development of nanostructured amphiphilic molecule doped electro-magnetic polyaniline- polyhydroxy iron cation- clay nanocomposite is receiving interest since they combine electro-magnetic, thermo-mechanical property and processability in a single system.

One of the objective of this thesis was to develop nanostructured conducting polyaniline and its clay composite using six structurally different amphiphilic dopants having backbone - phenyl, naphthyl, alicyclic, and alkyl groups and studying the role of functionality and rigidity of the amphiphilic dopants on the morphology, electrical property, extent of intercalation/exfoliation and thermal stability.

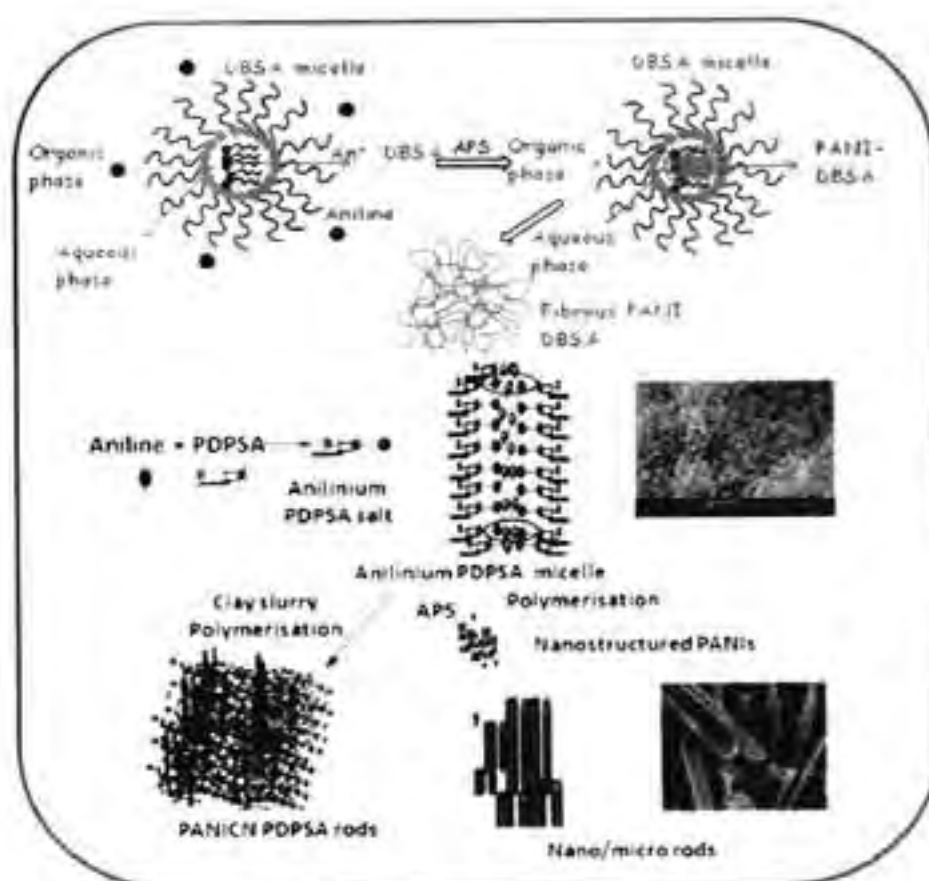
Another approach was to prepare nano/microstructured multifunctional electro-magnetic polyaniline-polyhydroxy iron-clay (PPIC) composite material by emulsion polymerization of aniline in the presence of polyhydroxy iron cation intercalated clay at room temperature. It was further extended for the preparation of water dispersible derivative of PPIC (PPICSA) via template polymerization using an amphiphilic dopant, 4-hydroxy-2-pentadecyl benzene sulphonic acid derived from renewable resource. Discussion of the structure-property correlation and interaction mechanism among the component were further aimed using the results manifested from different analytical techniques like UV-vis and FT-IR spectroscopy, conductivity, magnetic property, TEM, SEM, PLM and so forth.

The next objective was to envisage the application of PPICSA as a novel modifier for platinum electrode in amperometric sensor for ascorbic acid (AA) by studying the performance characteristics of the electrode with respect to response time, sensitivity, operational stability, storage life and selectivity towards AA. Last and final objective was to study the suitability of PPICSA as an EMI shielding material by blending PPICSA with polycarbonate and investigating the properties like percolation threshold concentration, electrical conductivity, thermo-mechanical stability, rheological property, EMI shielding efficiency and so forth.

The present thesis work is a systematic investigation to fulfill the above objectives.

Chapter - 2

Role of Amphiphilic Dopants on the Shape and Properties of Electrically Conducting Polyaniline-Clay Nanocomposite



2.1. Abstract

Novel self-assembled nano/microstructured conducting polyaniline-clay composites were prepared by in-situ intercalative emulsion polymerization of aniline in an aqueous dispersion of clay using structurally different amphiphilic dopants- dodecyl benzene sulphonic acid , p-toluene sulphonic acid, naphthalene sulphonic acid, camphor sulphonic acid and stearic acid. The role of functionality and rigidity of these amphiphilic dopants on the morphology and electrical property of the PANI and PANICNs were studied. Properties were compared with PANIs and PANICNs prepared using a renewable resource based bifunctional amphiphilic dopant, 4-hydroxy-2-pentadecyl benzene sulphonic acid derived from cashew nut shell liquid. XRD, FT-IR and SEM studies showed that the self-assembled nano/microstructured aggregates were formed by the combined non-covalent interactions such as phenyl-phenyl stacking, hydrogen bonding, ion-dipole interaction and electro static layer by layer self-assembling. The structure-directing effect of monofunctional and bifunctional amphiphilic dopants on the nucleation and growth mechanism during the formation of micro/nanostructured PANIs and PANICNs were also discussed. Electrical conductivity and thermal stability were observed to be higher for PANICNs.

2.2. Introduction

Development of polyaniline-clay nanocomposites (PANICN) has been receiving considerable research interest because of their dramatic improvement in electrical conductivity, thermo-mechanical property, environmental stability and so forth (Yeh et al., 2001, Goddard et al., 2003, Kuila et al., 2004). PANICN consists of sandwiched multilayers in which PANI chains are confined in

nanoclay layers. Conducting PANI chains in the interlayer spaces are assumed to take a more expanded conformation than in the bulk form, thus enhancing the conductivity of the composites owing to the free motion of charge carriers. Several strategies were reported for the preparation of PANICNs for potential applications in nano-electronic devices, optical applications, rechargeable batteries, electromagnetic interference shielding and also for mitigating electrical charge build up in light weight structures (Hirao, 2002, Deore *et al.*, 2004, Martin, 1994).

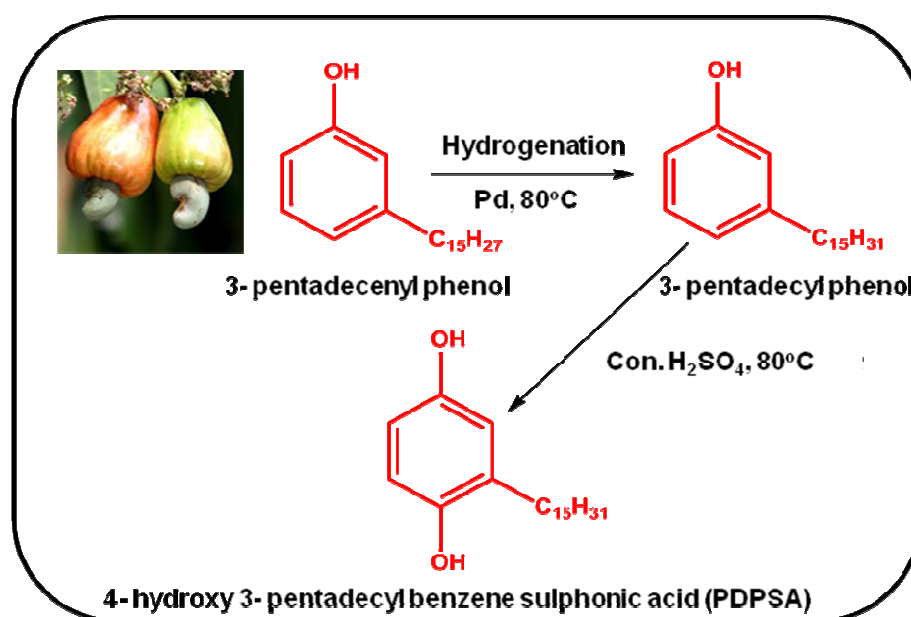
One of the commonly used methods to prepare PANICN is the intercalation of anilinium salt of amphiphilic molecule into the gallery of clay by a cation exchange process followed by *in-situ* intercalative polymerization (Kim *et al.*, 2001). The amphiphilic dopants can function as intercalating agent and can reduce the inter gallery interaction. They can maximize the affinity between hydrophilic host (clay) and hydrophobic guest (aniline) and can also serve as dopant for PANI. A variety of petroleum based amphiphilic dopants which belong to the families of sulphonic acids, phosphonic acids and phosphoric acid esters are reported. Now a days, due to the fast depletion of the petroleum products and also high cost of these dopants, research has been focussed on renewable resource based amphiphilic molecules as they are very attractive because of their wide availability and low cost. It has been noted that few molecular systems based on derivatives of 3- pentadecyl phenol and related structures possess structural feature required for multiple functions of protonation, solubilisation and plasticization. One of the significant feature of these dopants is that they have a flexible n-alkyl (C₁₅H₃₁) substituent in the meta position of the aromatic

ring which makes the doped PANI processable and render high solubility in common solvents (Raji *et al.*, 1999). The presence of both hydrophilic and hydrophobic moiety in the same molecule imparts compatibility for the doped PANI with a wide spectrum of polymers for probing application involving polymer blends. Thus it would be scientifically and technologically rewarding to investigate the effect of such a dopant on the properties of PANI and its clay nanocomposite. It is expected that the size and the functionality of the amphiphilic dopant can influence the extent of intercalation, electrical conductivity and also shape of the formed micro/ nanostructured PANICNs. Here, we present PANIs and PANICNs prepared using petroleum based five structurally different amphiphilic dopants like camphor sulphonic acid (CSA) with alicyclic backbone, dodecyl benzene sulphonic acid (DBSA) and para toluene sulphonic acid (pTSA) with phenyl backbone, stearic acid with alkyl backbone and naphthalene sulphonic acid (NSA) with naphthyl backbone and compare and evaluate their properties like electrical conductivity, extent of intercalation, morphology and thermal stability with PANIs and PANICNs prepared using a low cost renewable resource based amphiphilic dopant, PDPSA.

2.3. Results and Discussion

2.3.1.1. Preparation of 4- hydroxy-2-pentadecyl benzene sulphonic acid (PDPSA)

PDPSA was prepared by the sulphonation of 3-pentadecyl phenol using conc. sulphuric acid as shown in Scheme 2.1. It was purified and structural characterization was done by FT-IR and ¹H NMR spectroscopy.



Scheme 2.1. Preparation of PDPSA

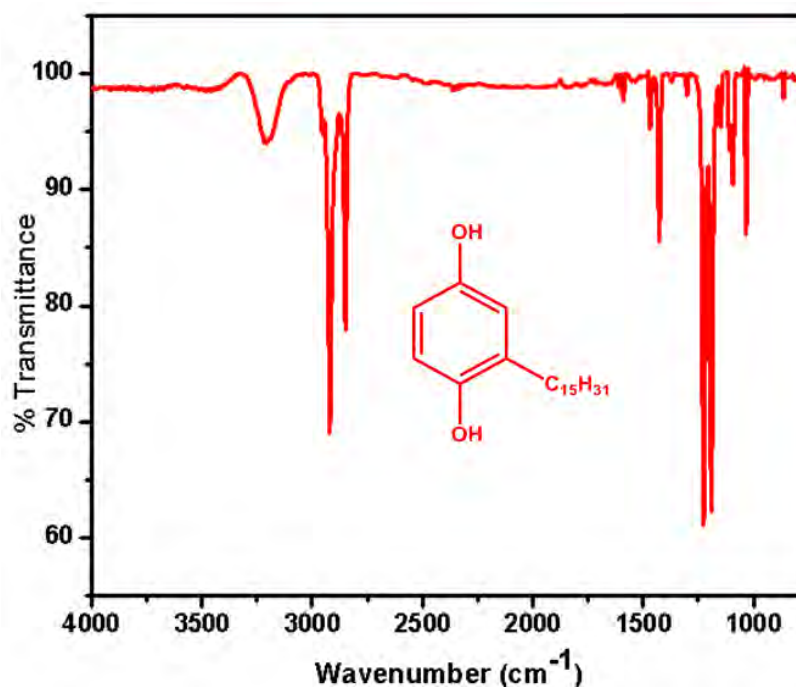


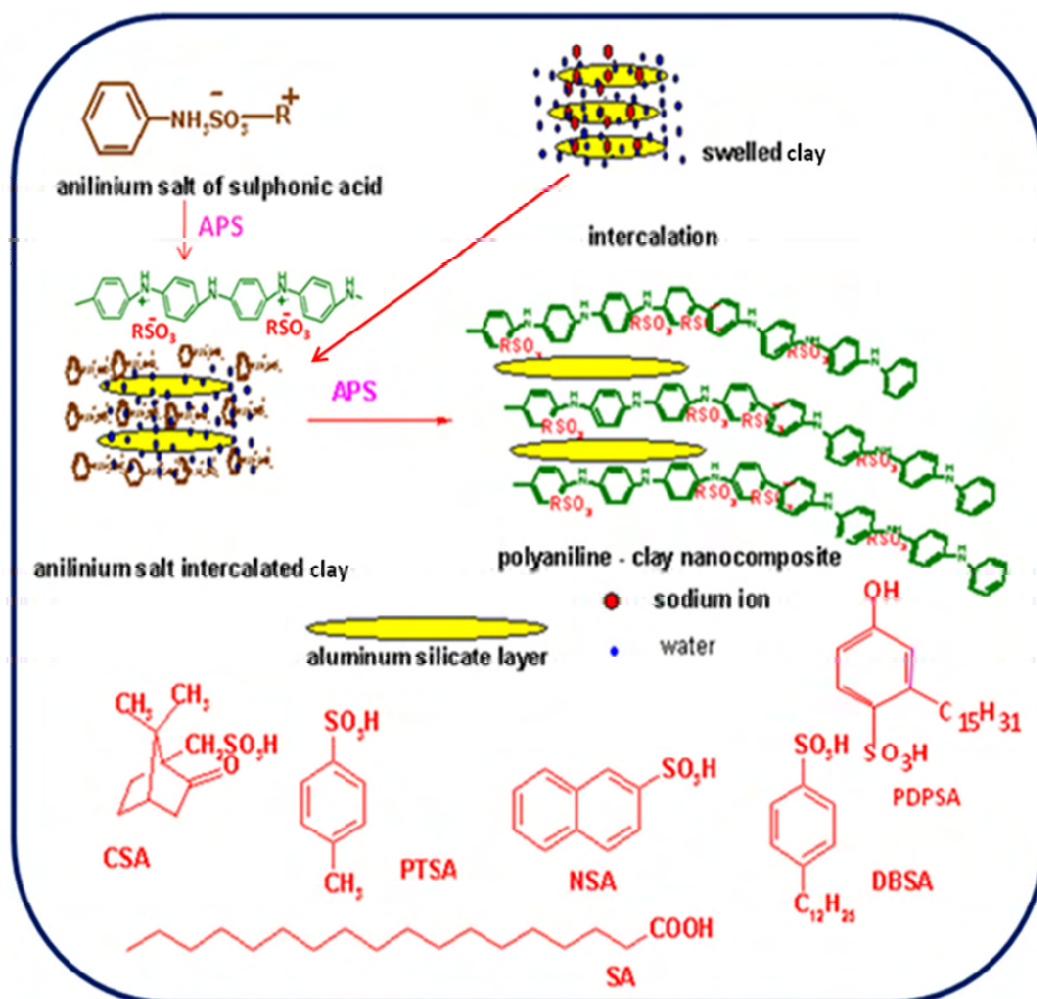
Figure 2.1. FT-IR spectrum of PDPSA

Figure 2.1. shows the FT-IR spectrum of PDPSA. It exhibited peaks with $\nu_{(\max)}$ 2919, 2841, 1469 cm^{-1} ($-\text{CH}_2-$)_n, 1605, 694 cm^{-1} (Ar), 1227 cm^{-1} (CO), 1305, 1195 cm^{-1} (SO) and 1032 cm^{-1} (SO_3). In ^1H NMR (CDCl_3 , ppm), the peaks observed were

at δ 0.8-0.9 (3H, t, CH₂-CH₃), 1.25 [26H, m, (-CH₂-)_n], 2.8 (2H, t, Ph-CH₂-), 5.7 (1H, OH), 6.8-6.9 (3H, m, Ar), 7.0 (1H, d, ArC-5).

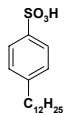
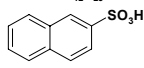
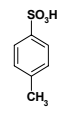
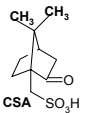
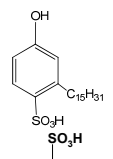
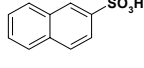
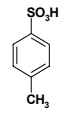
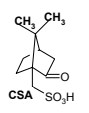
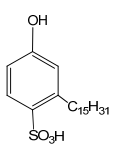
2.3.1.2. Preparation and characterization of PANIs and PANICNs

Nanostructured electrically conducting PANIs and PANICNs were prepared by *in-situ* intercalative emulsion polymerization of anilinium salts of the amphiphilic dopants in aqueous dispersion of clay at 0-5 °C using APS as oxidant initiator (Jia *et al.*, 2002) and the experimental details are illustrated in Table 2.1.



Scheme 2.2. Preparation of polyaniline and polyaniline clay nanocomposites

Table 2.1. Experimental details of PANIs and PANICNs

Sample	Dopant	Aniline: dopant	% wt of clay	% yield	Appearance
PANI-DBSA		1: 0.1	0	60	Emeraldine green powder
PANI-NSA		1: 0.1	0	70	"
PANI-pTSA		1: 0.1	0	76	"
PANI-SA		1: 0.1	0	80	"
PANI-CSA		1: 0.1	0	76	"
PANI-PDPSA		1: 0.1	0	70	"
PANICN-DBSA		1: 0.1	5	77	"
PANICN-NSA		1: 0.1	5	80	"
PANICN-pTSA		1: 0.1	5	80	"
PANICN-SA		1: 0.1	5	80	"
PANICN-CSA		1: 0.1	5	77	"
PANICN-PDPSA		1: 0.1	5	80	"

PANICNs prepared using the dopants DBSA, NSA, pTSA, SA, CSA and PDPSA are designated as PANICN-DBSA, PANICN-NSA, PANICN-pTSA, PANICN-SA, PANICN-

CSA and PANICN- PDPSA, respectively and the corresponding protonated PANIs without clay are indexed as PANI-DBSA, PANI-NSA, PANI-pTSA, PANI-SA, PANI-CSA and PANI-PDPSA. Synthesized PANIs and PANICNs were in the emeraldine green color. Solubility studies of PANIs and PANICNs were performed in various solvents having different polarity. It was observed that doped PANIs were completely soluble in m-cresol and partially soluble in solvents like chloroform and toluene while PANICNs were only partially soluble in m-cresol and DMF and were insoluble in chloroform and toluene. Details of the solubility studies are given in Table 2.2.

Table 2.2. Studies on the solubility of PANIs and PANICNs

Sample	m- Cresol	DMF	Chloroform	Toluene
PANI-DBSA	CS	CS	PS	PS
PANI-NSA	CS	CS	PS	PS
PANI-pTSA	CS	CS	PS	PS
PANI-SA	CS	CS	PS	PS
PANI-CSA	CS	CS	PS	PS
PANI-PDPSA	CS	CS	PS	PS
PANICN-DBSA	PS	PS	PS	IS
PANICN-NSA	PS	PS	IS	IS
PANICN-pTSA	PS	PS	IS	IS
PANICN-SA	PS	PS	IS	IS
PANICN-CSA	PS	IS	PS	IS
PANICN-PDPSA	PS	PS	PS	IS

CS- completely soluble, PS- partially soluble, IS- insoluble

2.3.2. Structural Characterisation

2.3.2.1. UV-vis spectroscopy

UV- vis spectroscopy is a very sensitive tool for studying the electronic structure and nature of protonation in conducting polymers. UV-vis spectra of

PANI-DBSA, PANICN-DBSA, PANICN-NSA, PANICN-pTSA, PANICN-SA PANICN-PDPSA, and PANICN-CSA are shown in Figure 2.2.

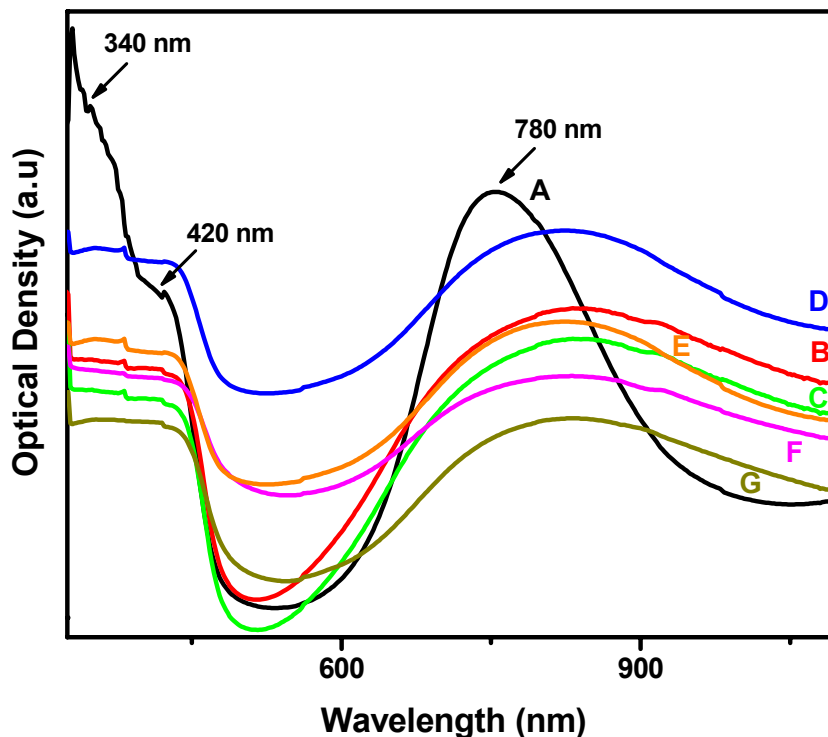


Figure 2.2. UV-vis spectra of (A) PANI-DBSA, (B) PANICN-PDPSA, (C) PANICN-DBSA, (D) PANICN-NSA, (E) PANICN-pTSA, (F) PANICN-SA and (F) PANICN-CSA

Generally all PANIs exhibited three absorption peaks and the UV- vis spectra of PANI with a representative dopant, DBSA is shown. The absorption peaks observed were at (i) ~ 340 nm (π - π^* transition) (ii) ~ 420 nm (polaron band to π^* transition)(Xia et al., 1995) and (iii) ~ 780 nm (π -polaron band transition) (Ruokolainen *et al.*, 2000, Lv *et al.*,2005). In PANICNs, a red shift is observed for the peak at ~ 780 nm with a broad absorption band (called “free carrier tail”) in the near infra red region. Also the peak at 340 and 420 nm overlaps to form a broad band. This is due to the delocalization of electrons in the polaron band promoted by an extended conformation of the PANI chains inside the clay galleries. The twist defects between the aromatic rings of PANIs intercalated

between the clay layers are removed and the interaction between adjacent isolated polarons therefore becomes stronger and the polaron band becomes more dispersed in energy (more delocalised). These observations were further strengthened during the conductivity measurements.

2.3.2.2. FT-IR spectroscopy

FT-IR spectroscopy is an effective technique for studying the interactions between the dopant anion and the PANI chains and also between the PANI chains and clay surface. FT-IR spectra of clay, PANI and PANICN prepared with a representative dopant, DBSA are given in Figure 2.3.

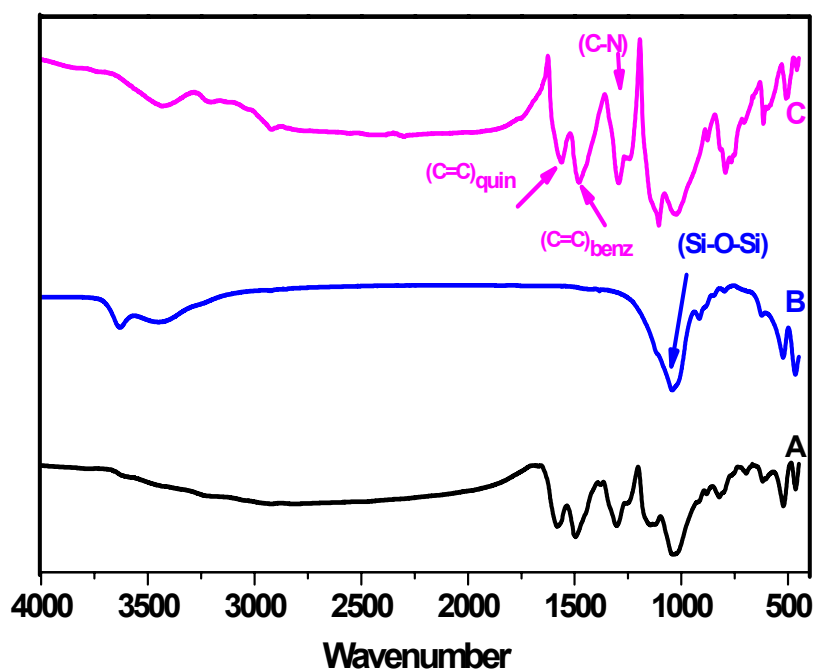


Figure 2.3. FT-IR spectra of (A) PANI- DBSA, (B) clay and (C) PANICN-DBSA

The characteristic bands corresponding to pristine clay appeared at 1030 [$\nu(\text{Si-O})$], 911 [$\nu(\text{Al-OH})$] and 525 cm^{-1} [$\nu(\text{Si-O-Al})$] (Stubican *et al.*, 1961, Liu *et al.*, 1993). The absorption peak around 1574 and 1490 cm^{-1} observed in PANI are attributed to the $(\text{C}=\text{C})_{\text{str}}$ of quinoid and benzenoid, respectively (Chen *et al.*, 1995). In PANICNs, the $(\text{C}=\text{C})_{\text{str}}$ of the quinoid is shifted from 1590 cm^{-1} to

1572 cm^{-1} and that of the benzenoid from 1502 to 1485 cm^{-1} , indicating the longer effective conjugation length for PANI chains confined in PANICN (Li *et al.*, 2006). However, from a closer look at the spectra, it was observed that the band at 1295 cm^{-1} , assigned as the stretching vibration of C-N in PANI is significantly shifted to 1302 cm^{-1} in PANICNs and the peak at 1030 cm^{-1} of clay shifted to 1027 cm^{-1} in PANICN. This frequency shifts are believed to be caused by the hydrogen bonding interaction between PANI and the basal surface of clay (i.e. NH...O hydrogen bonding). The bands at 1040 and 506 cm^{-1} can be assigned due to the sulphite anion present in PANI and PANICN.

2.3.2.3. X-ray Diffraction (XRD)

XRD is an efficient analytical tool to probe the extent of intercalation/exfoliation and the dimension of the self-assembled stacked layers in both PANIs and PANICNs. During intercalation, the PANI- dopant chains get confined in between the clay layers and the distance between the clay layers is increased depending on the dimension of the doped PANI chains, layer charge density and the functionality of the intercalating chains. XRD patterns of clay, PANICN-CSA, PANICN-SA, PANICN-pTSA, PANICN-NSA, PANICN-DBSA are shown in Figure 2.4. The d_{001} plane of clay exhibited peak at $2\theta = 7.26^\circ$ corresponding to the interlayer spacing of 12.1 Å. PANICN- DBSA showed reflections at $2\theta = 2.59^\circ$ (34 Å) and 5.96° (14.8 Å). The d-spacing of 34 Å can be ascribed to the thickness of the modified self-assembled PANI-DBSA (Jia *et al.*, 2002) and 14.8 Å to the displaced d_{001} plane of the clay layer. The enhancement in the interlayer spacing (~ 5.2 Å) observed is very close to the dimension of PANI-DBSA layer lying parallel to the plane of the clay surface (Kim *et al.*, 2001). This value is calculated

based on the thickness of the corresponding anhydrous aluminum silicate framework (9.6 Å). This result is reminiscent with the observation made by other researchers using layered materials like V_2O_5 (Nakajima *et al.*, 1995) and FeOCl (Kanatzidis *et al.*, 1993).

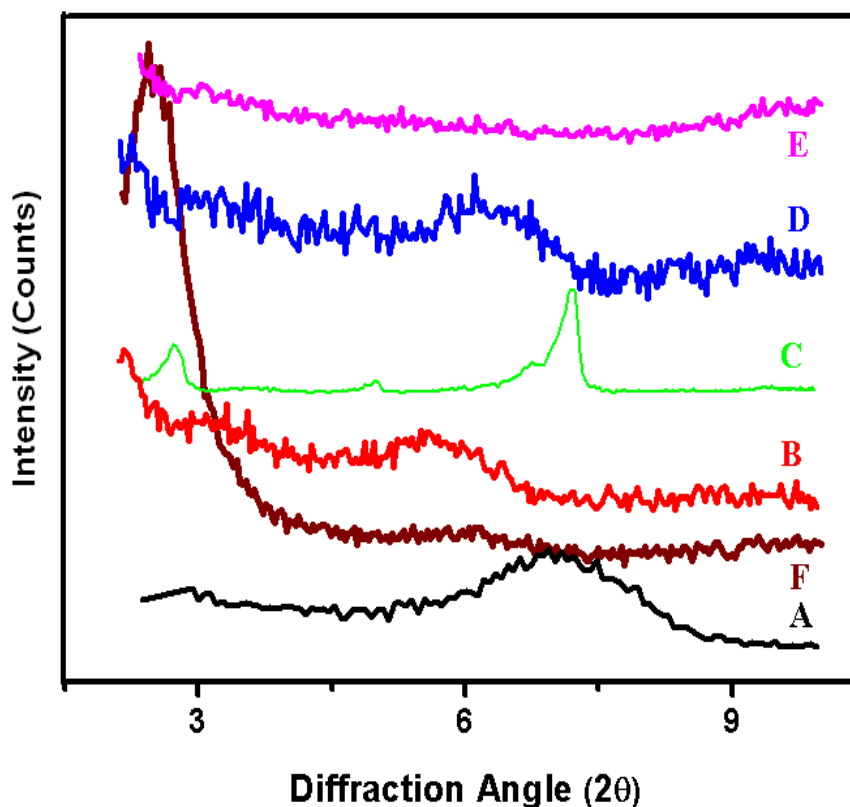


Figure 2.4. XRD pattern of (A) Na^+ Cloisite, (B) PANICN-CSA, (C) PANICN-SA, (D) PANICN-pTSA, (E) PANICN-NSA and (F) PANICN-DBSA

In PANICN-pTSA, the reflection is observed at $2\theta = 6.25^\circ$ (14.1 Å) which corresponds to the dimension of the protonated PANI-pTSA. PANICN-SA exhibited diffraction peaks at 2.4° (36.7 Å), 3.3° (26.6 Å) and 4.77° (18.5 Å). The initial reflection corresponds to the dimension of the electrostatically self-assembled PANI-SA over the nano clay layers while that at 4.77° corresponds to the dimension of PANI-SA (14.4 Å) in PANICN-SA. The diffractogram of PANICN-NSA did not exhibit any peak corresponding to the d_{001} plane of clay, revealing

fully exfoliated clay layers in PANICN-NSA. PANICN-CSA exhibited reflection around $2\theta = 5.45^\circ$ (16.18 Å) corresponding to the dimension of the confined PANI-CSA in PANICN-CSA. Diffractogram of PANI-DBSA showed peak at 29.3 Å corresponding to the thickness of the aggregates formed by the electrostatic layer-by-layer self-assembled structure as reported by Taka and co-workers (Taka *et al.*, 1994). The diffractogram of PANI-NSA and PANI-CSA exhibited silent peak revealing the formation of non-oriented structures. PANI-pTSA showed peak at 10.89 Å. The diffractogram of PANI-SA exhibited reflection at 36.9 Å, 18.7 Å, 13.6 Å, 12.6 Å and 9.6 Å which corresponds to the self-assembled aggregates of PANI-SA. Similar XRD results were reported for stearic acid (ICDD pattern 381923) with d_{001} peak of 39.62 Å positioned approximately at $2\theta = 2.2^\circ$. The energy minimised structures of PANI-DBSA, PANI-NSA, PANI-pTSA, PANI-SA and PANI-CSA were calculated using MMX programme and are shown in Figure 2.5.

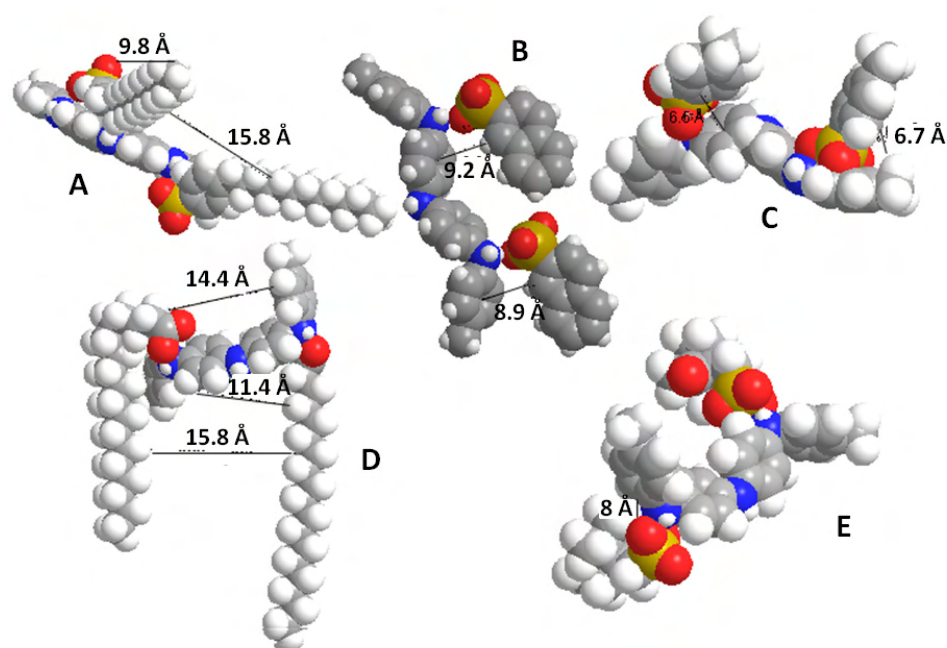


Figure 2.5. Energy minimized structure of (A) PANI-DBSA, (B) PANI-NSA, (C) PANI-pTSA, (D) PANI-SA and (E) PANI-CSA

The dimensions of the doped PANIs confined in PANICNs were correlated with the dimension calculated using energy minimization MMX programme (Gajewski *et al.*, 1990) and are depicted in Table 2.3. The difference in the XRD value from the calculated values is due to the difference in the conformational changes in the doped PANIs during the confinement of the PANI chains in the constrained environment. Moreover, the shape and orientation of the doped PANIs are affected by the combination of the various non-covalent interactions during the formation of self-assembled aggregates. Similar studies on the interaction of alkyl chain having polar head group of the organic molecule with the clay surface which form self-assembled structure on the clay surface was reported earlier by Brindley (Brindley *et al.*, 1965).

Effect of dopant concentration on the extent of intercalation was studied by performing XRD studies with doped PANICN-PDPSA prepared with different concentration of PDPSA. PANICN-PDPSA1, PANICN-PDPSA2, PANICN-PDPSA3 and PANICN-PDPSA4 have molar ratio of aniline: dopant 1:0.5, 1:1, 1:1.5 & 1:2, respectively. Figure 2.6. shows the XRD pattern of clay, PANI-PDPSA, PANICN-PDPSA1, PANICN-PDPSA2, PANICN-PDPSA3 and PANICN-PDPSA4. The diffraction pattern of PANI-PDPSA exhibited two sharp diffraction peaks at 3.1° (28.4 \AA) and 7.9° (11.2 \AA) corresponding to the ordered self-assembled protonated PANI-PDPSA layers. The sharper and oriented diffractogram observed can be attributed to the crystallinity induced by the hydrogen bonding interaction between PANI layers and PDPSA. These results were further strengthened by the observations made by Ruokolainen and coworkers (Ruokolainen *et al.*, 2000). The XRD pattern of PANICN-PDPSA1 showed two

peaks at $2\theta = 2.51^\circ$, 4.75° with d-spacing of 35.19, 18.58 Å. Here, the d_{001} plane of clay is completely shifted to 18.58 Å. The enhancement in the interlayer spacing of ~ 9 Å is very close to the dimension of PANI-PDPSA lying perpendicular to the plane of the clay surface. The second peak observed in the lower angle corresponds to the dimension of the layer thickness of self-assembled PANI-PDPSA.

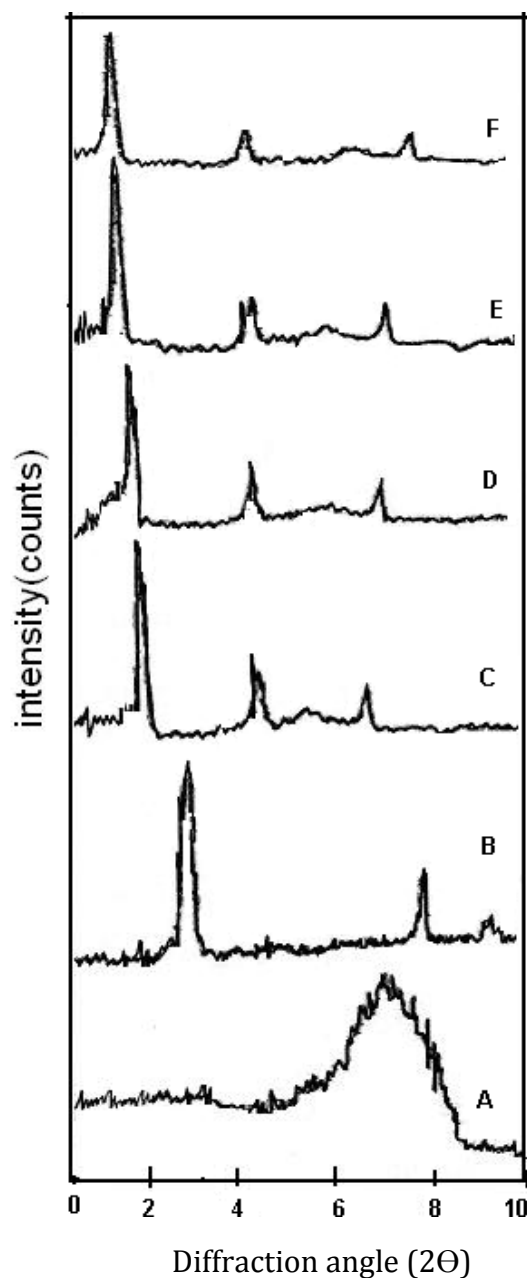


Figure 2.6. XRD of A- Clay, B- PANI-PDPSA, C- PANICN- PDPSA1, D- PANICN- PDPSA2, E- PANICN- PDPSA3 and F- PANICN- PDPSA4

The thickness of the self-assembled PANIs increases with the amount of the dopant loading. PANICN-PDPSA1, PANICN-PDPSA2, PANICN-PDPSA3 and PANICN-PDPSA4 exhibited self-assembled layer thickness of 35 Å, 37 Å, 45 Å & 46.5Å, respectively. In the case of PANICN, the interlayer expansion generally varies in the range of 4 to 9 Å and hence confirmed the confinement of PANI layer inside the nanoclay. The intensity of the peak corresponding to the d_{001} plane of clay was observed to be decreasing with increasing amount of dopant concentration, which can be ascribed due to the increase in the population of exfoliated clay layers.

2.3.3. Morphology

Morphology of PANIs and PANICNs were studied using scanning electron microscopy (Figure 2.7.) and the details of the observed morphology are tabulated in Table 2.3.

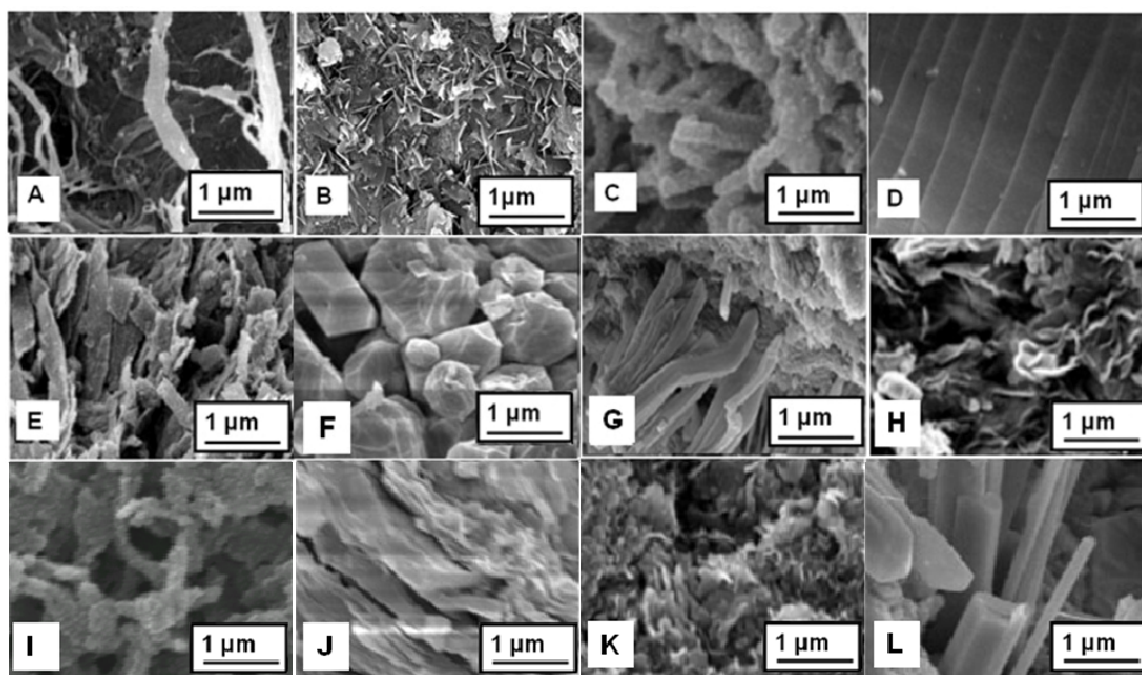


Figure 2.7. SEM picture of (A) PANI- DBSA (B) PANI- NSA (C) PANI- pTSA (D) PANI- SA (E) PANI- CSA (F) PANI- PDPSA, (G) PANICN- DBSA (H) PANICN- NSA (I) PANICN- pTSA (J) PANICN- SA (K) PANICN- CSA and (L) PANICN- PDPSA

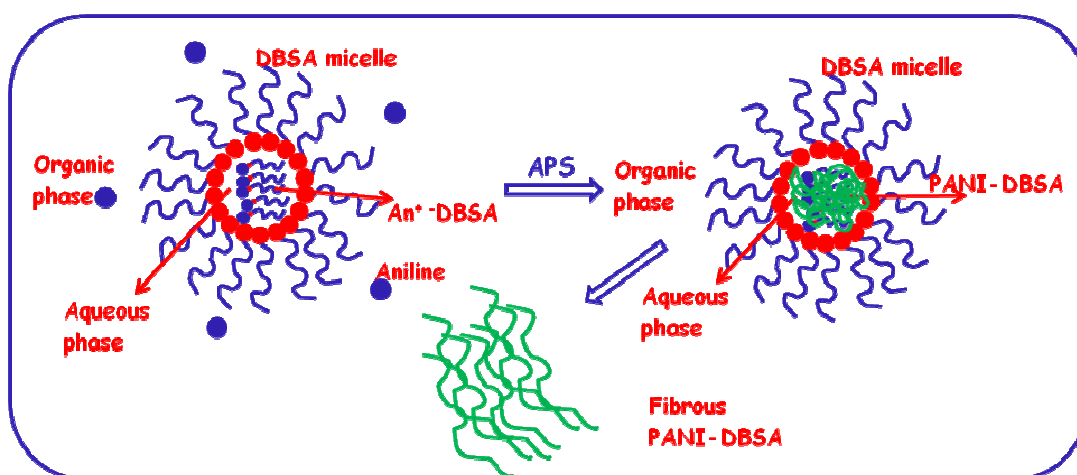
Table 2.3. Details of the XRD and morphology of PANIs and PANICNs

Sample	XRD studies d-spacings (Å)	Dimension of the doped PANI from MMX calculation (Å)	Morphology
PANI-DBSA	29.33, 15	9.8	Nano/micro wires
PANI-NSA	10	8.9	Needle
PANI-pTSA	10.89	6.7	Spongy corel
PANI-SA	36.86, 18.74	11.4	Layered Structure
PANI-CSA	9	8.9	Flakes
PANI-PDPSA	28	-	Hexagonal/ tetragonal structures
PANICN-DBSA	34.05, 14.8,	-	Nano/micro wires
PANICN-NSA	No peak	-	Pleated sheets
PANICN-pTSA	14.11, 10.59	-	Spongy corel
PANICN-SA	36.7, 26.6, 18.5	-	Layered Structure
PANICN-CSA	16.18 Å	-	Rice grain
PANICN- PDPSA	28, 19	-	Rigid rods

PANI-DBSA showed nano/micro wires with diameter less than 250 nm. Needle like structures with thickness of 200 nm is observed for PANI-NSA. PANI-SA showed layered structures with thickness less than 100 nm. PANI-CSA exhibited flake like structures with thickness ~250 nm. Morphology of PANI-pTSA was observed to be spongy coral like structures. PANI- PDPSA exhibited highly oriented regular hexagonal/ tetragonal crystallites with sharp edges.

PANICNs exhibited slight changes in the overall morphology from PANI, which is due to the presence of clays. PANICN-DBSA exhibited aggregated wires having diameter of ~ 300 nm, while PANICN-NSA was observed to be pleated sheets having 100 nm thickness. The micrographs of PANICN-pTSA exhibited spongy coral like morphology having thickness of ~ 200 nm. PANICN-SA showed layered structures with thickness of ~ 150 nm. The micrographs of PANICN-CSA exhibited rice-grain structures with ~ 150 nm size. PANICN- PDPSA exhibited highly oriented nano/micro structured rods with thickness ~ 200 nm. The various morphology observed in protonated PANIs and PANICNs can be ascribed due to the formation of various modes of self-assembling arising from the combined effect of non-covalent interaction among the PANI chains, dopant-PANI interaction and also different extent of ion-dipole interactions between the clay and protonated PANIs. The formation of different morphology in doped PANIs can also be explained on the basis of functionality of the amphiphilic dopant which forms different shapes of micelle that serves as template during the polymerisation. Considering DBSA as the representative monofunctional dopant, having structure quite analogous to PDPSA which is a bifunctional dopant having an additional hydroxyl group, the micro/nano structured fibers or ribbons for PANI-DBSA observed can be suggested through heterogeneous nucleation followed by isotropic growth mechanism as shown in scheme 2.3. Mechanism can be explained as: when aniline is mixed with DBSA, anilinium - DBSA salt is formed by an acid-base reaction which further forms self- assembled spherical micelles through electrostatic layer by layer assembling. Polymerization of aniline starts with the formation of nucleation centre inside

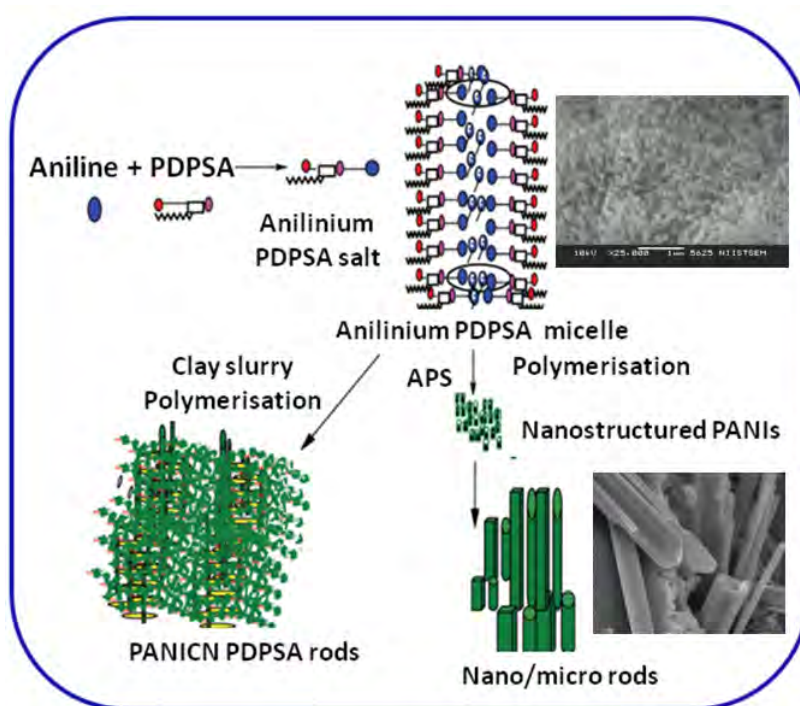
the micelle when it comes in contact with APS. The population of nucleation centre increases as the reaction proceeds. Once the density of nucleation center becomes high, the interfacial energy between them may be minimized (Hassan *et al.*, 2004) and rapid precipitation occurs followed by isotropic growth yielding irregular fibrillar shaped protonated PANIs.



Scheme 2.3. Formation of self-assembled micro/nanofibers of PANI-DBSA and PANICN-DBSA

The micro/nano-rods or cylinders observed in PANI-PDPSA and PANICN-PDPSA can be suggested through a “rod like micelle” guided template polymerization as shown in scheme 2.4. PDPSA contains two hydrophilic groups (-SO₃H and -OH) on the aromatic ring along with long alkyl chain in the meta position to -OH group and para to the -SO₃H. When aniline is mixed with PDPSA, anilinium-PDPSA salt is formed by an acid-base reaction. Because the surface is composed of -SO₃H, NH, OH groups, phenyl rings and partial polarized long alkyl chain of anions, they organize to form rod like micelles and will provide a wide variety of active sites for nucleation (Wei *et al.*, 2002, Langer *et al.*, 1999). The free aniline can diffuse into the center of the micelles to form core. This was

aided through stirring of the aniline- PDPSA for 4-5 h before APS was added. After the addition of APS, the diffusion of excess aniline into the hydrophilic micelle core enables polymerization and PANI nanoparticles would aggregate inside the micelle through interaction including hydrogen bonding, π - π interactions and electrostatic layer by layer self assembling (Ikkala, 2004). These nucleated nanoparticles (homogeneous nucleation) undergo end-on attachment resulting in linear growth of the nanostructure to form nanometer sized cylinders which further aggregate to form micro cylindrical structures both for PANI-PDPSA and PANICN-PDPSA.



Scheme 2.4. Formation of self- assembled micro/nanostructured PANI-PDPSA and PANICN-PDPSA

2.3.4. Electrical Conductivity

Electrical conductivity (σ_{dc}) measurements of the prepared PANIs and PANICNs were measured using a four probe conductivity meter. Electrical conductivity values of PANIs was found to follow the order, PANI-PDPSA ($6.0 \times$

$10^{-2} \text{ S cm}^{-1}$) > PANI-pTSA ($2.1 \times 10^{-2} \text{ S cm}^{-1}$) > PANI-NSA ($1.9 \times 10^{-2} \text{ S cm}^{-1}$) > PANI-CSA ($1.6 \times 10^{-2} \text{ S cm}^{-1}$) > PANI-DBSA ($1.5 \times 10^{-3} \text{ S cm}^{-1}$) > PANI-SA ($8.2 \times 10^{-4} \text{ S cm}^{-1}$). PANICNs also showed the same trends with conductivity values- PANICN-PDPSA ($1 \times 10^{-1} \text{ S cm}^{-1}$) > PANICN-pTSA ($7.5 \times 10^{-2} \text{ S cm}^{-1}$) > PANICN-NSA ($5.3 \times 10^{-2} \text{ S cm}^{-1}$) > PANICN-CSA ($1.92 \times 10^{-2} \text{ S cm}^{-1}$) > PANICN-DBSA ($1.76 \times 10^{-2} \text{ S cm}^{-1}$) > PANICN-SA ($2.8 \times 10^{-3} \text{ S cm}^{-1}$). Measurement showed that conductivity varies with the change in the functionality of the dopants. The higher conductivity exhibited by PANI-PDPSA when compared to other doped PANIs is due to the extended confirmation of the doped PANI-PDPSA arising from its high ordering and charge delocalisation. Conductivity is given by the equation $\sigma = ne\mu$, where n is the number of charge carriers, e is the electronic charge and μ is the mobility of the charge carrier. With the changes in the size of the dopant, the charge mobility varies and thereby exhibited difference in conductivity. Conductivity values are measured to be greater for PANICNs, since the clay layers disrupts the three dimensional organization of PANI chains and will therefore lead to an expanded conformation for PANI chains in the confined environment. The polarons will be in the delocalised state and hence exhibited higher conductivity. These observations further strengthen the studies made by UV-vis spectroscopy.

Effect of the dopant concentration on the conductivity of PANICNs was studied. For, PANICN-PDPSA, when the [aniline]:[PDPSA] molar ratio was varied from 1:0.5, 1:1, 1:1.5 and 1:2, the conductivity values were found to be 5×10^{-2} , 1×10^{-1} , 2.3×10^{-1} and $2.4 \times 10^{-1} \text{ S cm}^{-1}$, respectively. As the concentration of dopant increases, the extent of protonation increases, the number of polarons increases and thereby shows a hike in conductivity. These results are

reminiscent with the observations made by other researchers (Wei et al., 2002, Langer et al., 1999). Thus the electrical conductivity is influenced by the size, functionality and amount of the doped PANI chains present in the system.

2.3.5. Thermal properties

Thermal stability of PANIs and PANICNs were studied by thermogravimetric analysis in nitrogen atmosphere at a heating rate of 10 °C/min. Thermograms of doped PANI and PANICN with the representative dopant, DBSA are shown in Figure 2.8. PANI and PANICN exhibited two-stage decomposition pattern. The weight loss observed below 100 °C can be attributed to the removal of absorbed moisture and low molecular weight volatile compounds present in the protonated PANIs. The second stage weight loss can be due to evolution of the amphiphilic dopant molecule and the decomposition of the PANI backbone. The TG curve of PANICN exhibited a char content of approximately 5 wt% at 800 °C, which was in agreement with the % clay loading in the PANICN.

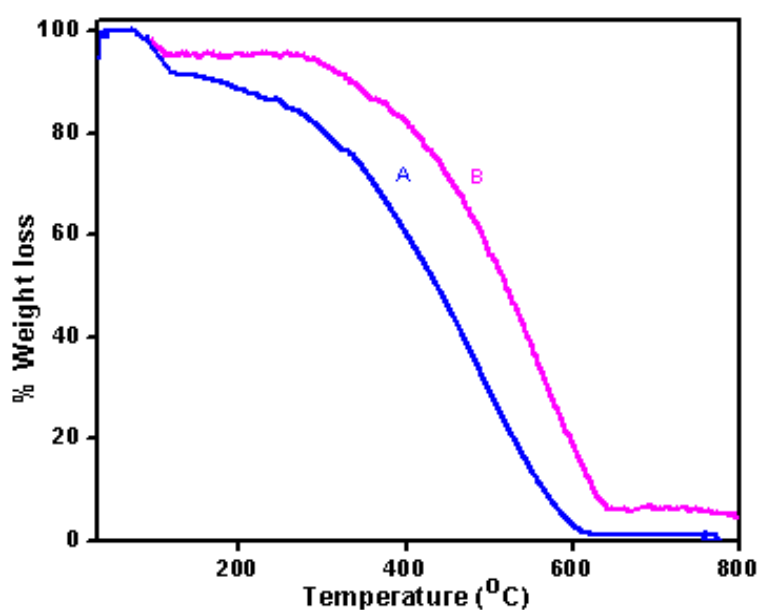


Figure 2.8. TGA curves of (A) PANI-DBSA and (B) PANICN-DBSA

Thermal stability of PANIs is in the order PANI-PDPSA > PANI-pTSA > PANI-NSA > PANI-CSA > PANI-DBSA > PANI-SA. It can be observed that PANICN exhibited higher maximum decomposition temperature (T_m) than their corresponding PANIs. The higher thermal stability observed for PANICNs, compared to PANIs is due to the presence of insulative nanoclay layers. Thermal phase transition temperature of PANIs and PANICNs were studied by DSC at a heating rate of 10°C /min in nitrogen atmosphere. Representative DSC plot of PANI and PANICN (DBSA as the dopant) is shown in Figure 2.9.

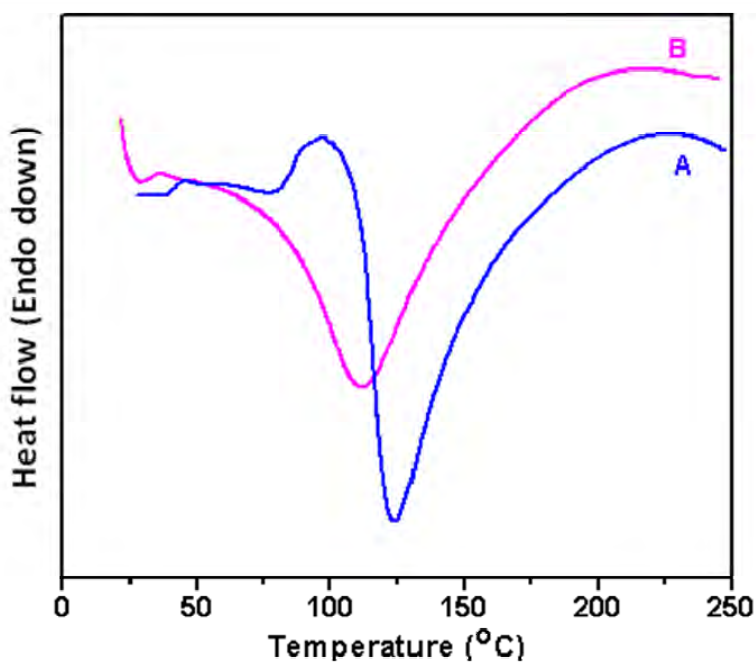


Figure 2.9. DSC curves of (A) PANICN-DBSA and (B) PANI-DBSA

On heating, PANICN exhibited two endothermic transition peaks at 88 °C and 125 °C which can be attributed from two factors. First transition is arising from the conformational change of doped PANI chains in PANICN due to the loss of intermolecular hydrogen-bonded interaction (Vaia *et al.*, 1994). The second phase transition corresponding to the energy change arising from the loss of guest-host interaction between protonated PANI chains and the clay layer. Phase

transition temperature of PANIs was observed to be in the order PANI-SA (56 °C) < PANI-DBSA (109 °C) ~ PANI-pTSA (109 °C) < PANI-NSA (110 °C) < PANI-CSA (122 °C) < PANI-PDPSA (120 °C) and for PANICNs, the order was PANICN-NSA (119 °C) < PANICN-DBSA (120 °C) < PANICN-pTSA (122 °C) < PANICN-SA (136.53 °C) < PANICN-CSA (138.2 °C) < PANICN-PDPSA (150 °C). Generally a higher phase transition temperature was observed for PANICNs when compared to PANIs which is due to the presence of nano clay layers.

2.4. Conclusion

We could successfully synthesize electrically conductive micro/nanostructured PANIs and PANICNs using six structurally different amphiphilic dopants by *in-situ* intercalative emulsion polymerization at room temperature. Studies revealed that the rigidity and functionality of the dopant has got profound influence on the electrical conductivity, morphology, thermal stability and phase transition temperature of PANIs and PANICNs. The variations in the morphology of PANIs and PANICNs are due to the change in the modes of self-assembling arising from the combination of various non-covalent interactions like inter-molecular hydrogen bonding, ion-dipole interaction, electrostatic layer by layer stacking and inter-plane phenyl-phenyl stacking among the PANI chains, PANI- dopant and PANI -clay surfaces. Thermal stability of PANICN was observed to be higher than doped PANIs due to presence of insulative nanoclay layers in the former. In conclusion, PDPSA derived from renewable resource is a low cost intercalating agent cum dopant which can be successfully used as structure directing agent for the preparation of micro/nanostructured PANICN with controlled morphology. The prospects for

the direct application of these nanocomposites were found to be developing electrically conductive composites by blending with other conventional polymers for mitigation of electric charge/EMI shielding materials.

2.5. Experimental

2.5.1. Materials

Aniline (99.5% pure, Ranbaxy chemicals Ltd, Bombay) was distilled under reduced pressure before use. APS, methyl alcohol, pTSA and SA were purchased from Sd. fine Chemicals Limited, Bombay, India. Na⁺ Cloisite clay with cation exchange capacity of 92.6 meq/100g and a mean chemical formula of [(Na,Ca)_{0.33}(Al_{1.67}Mg_{0.33})Si₄O₁₀(OH)₂.nH₂O] was purchased from Loba Chemie, Bombay, India. DBSA (85% in isopropanol), CSA and NSA (~99.5%) purchased from Aldrich were used without further purification. 4-hydroxy-2-pentadecyl benzene sulphonic acid (PDPSA) was prepared from 3-pentadecyl phenol (3-PDP) as reported earlier (Sudha *et al.*, 2007).

2.5.2.1. Preparation of 4-hydroxy-2-pentadecyl benzene sulphonic acid (PDPSA).

10 g of 3-PDP was mixed with 5 ml conc. H₂SO₄ in a 100 ml round bottomed flask using magnetic stirring at 80 °C for 2 h and 110 °C for 1 h. It was then dissolved in ice-cold water and washed with n- butanol and adjusted the pH to 7. Filtered, washed and then acidified to get the PDPSA. Further it was dried in a vacuum oven at 80 °C. Color and appearance – Colorless powder. Yield - 80%. Chemical structure of the PDPSA was characterized by elemental analysis, FT-IR and ¹H NMR. Mol. formula C₂₁H₃₉SO₄. Elem. anal (observed C- 64.9 %, H- 10%, S 8.3%) calculated (C- 65.1% H- 10.07 %, S 8.2%).

2.5.2.2. Preparation of PANI-DBSA and PANICN-DBSA

0.3 g of Na⁺ cloisite in 200 mL deionised water was refluxed in a three-necked round bottomed flask by heating and stirring at 80 °C for 3 h. An aqueous solution of 3 g of aniline (0.032 moles) containing 1.05 g (0.0032 moles) DBSA was added drop wise to the clay dispersion. Heating and stirring continued for 2 - 6 h. It was then cooled down to room temperature and pH was adjusted to 2 - 3 using 11 N HCl. APS (0.035 mole) dissolved in 50 ml water was then added drop wise to initiate the polymerization. Reaction was continued for 3 - 4 h. PANICN formed was precipitated with methanol. The product was isolated by filtration, washed with deionised water several times, finally with methanol and then dried overnight in a vacuum oven at 60 °C. Yield 77 %, Color and appearance: emeraldine green powder. PANIs and PANICNs were also prepared in presence of NSA, pTSA, SA, CSA and PDPSA. Prepared PANICNs with different aniline: PDPSA mole ratio (1:0.5, 1:1, 1:1.5, 1:2) and were designated as PANICN-PDPSA1, PANICN-PDPSA2, PANICN-PDPSA3 and PANICN-PDPSA4, respectively.

2.5.3. Description of experimental techniques

For UV-vis spectral studies, sample were dispersed in deionised water and recorded the spectra using UV-vis spectrophotometer [Shimadzu model 2100] in the range of 300-1100 nm. FT-IR measurements of PANIs and PANICNs were made with a fully computerized Nicolet impact 400D FT-IR spectrophotometer. Polymers were dispersed in potassium bromide and compressed into pellets before recording. All spectra were corrected for the presence of moisture and carbon dioxide in the optical path. The interlayer distance of the clay layers and the formation of self-assembled structures of

PANIs and PANICNs were measured using powder X-ray diffractometer (Philips X'pert Pro) with $\text{CuK}\alpha$ radiation ($\lambda \sim 0.154$ nm) employing X'celerator detector and monochromator at the diffraction beam side. Powder samples were used employing standard sample holder. Averaged 2θ was used with the 2θ resolution of 0.002 degree from 2 to 10° . For conductivity measurements, the samples were pressed into a 13 mm diameter disk and were measured by a standard Four-probe method using a Keithley 6881 programmable current source and 2128A nanovoltmeter at 30 °C. The resistivity of the samples was measured at three different positions, and at least three pellets were measured for each sample: an average of nine readings was used for conductivity calculations. Morphological studies of powder samples of PANIs and PANICNs were studied using scanning electron microscope (SEM, JEOL make, model JSM 5600 LV) at 15 kV accelerating voltage. DSC scans were performed using Dupont DSC 2010 differential scanning calorimeter attached to Thermal Analyst 2100 data solution under nitrogen atmosphere at a heating rate of 10 °C/min from 30 to 200 °C. Thermal stability measurements were performed at a heating rate of 10 °C/min in nitrogen atmosphere using Shimadzu, DTG-60 equipment from 30 to 800 °C.

3.1. Abstract

Electro-magnetic polyaniline-polyhydroxy iron-clay (PPIC) composite was prepared by the oxidative radical emulsion polymerization of aniline in the presence of polyhydroxy iron cation intercalated clay (PHIC) using APS as the initiator. Characterization of the composite showed the formation of microstructured aggregated fibers having saturation magnetization of 2 emu g⁻¹ and coercivity 600 Oe with electrical conductivity of 0.35 S cm⁻¹ (4 wt % PHIC loading). Role of amphiphilic dopant on the formation of electro-magnetic composites was studied by performing experiments in the presence of an amphiphilic dopant, 4-hydroxy-2-pentadecyl benzene sulphonic acid (PDPSA) which resulted in the formation of water dispersible electro-magnetic nanocomposite (PPICSA) with electrical conductivity of ~1 S cm⁻¹ and saturation magnetization of 2.2 emu g⁻¹ with coercivity of ~50 Oe. Here, PDPSA serves the multifunctional role of dopant, micellar template, capping agent, structure directing agent and intercalating agent which was manifested from the studies made from spectroscopy, electrical conductivity, morphology and particle size. A plausible mechanism for the formation of electro-magnetic nanotapes of PPICSA was suggested. Thermal studies were performed using TG and DSC.

3.2. Introduction

Nanostructured electro-magnetic polymer composites comprising conducting polymer hosting magnetic nanoparticles have attracted a great deal of attention as they exhibit dual functionalities like electrical conductivity and magnetic property in a unique material system. It is known that the conducting material can effectively shield electric component of an electro-magnetic wave

whereas, only magnetic materials can shield effectively the magnetic component of the same. Thus, if the materials having both magnetic and electric components are used for EMI shielding, good shielding effectiveness can be achieved. Also they find potential applications in various fields such as antistatic coatings, biological applications, chemical sensors, transducers, rechargeable battery and corrosion protection coatings (Li et al., 2006, Wang et al., 2005, Xu et al., 2008, Ding et al., 2008, Sudha et al., 2009, Li et al., 2009, Vossmeier et al., 2002).

Several strategies were reported for the preparation of electro-magnetic polymer composites which includes the incorporation of magnetic nanoparticles of iron oxide with various CPs like PANI. But the disadvantage with these electro-magnetic polymer – inorganic hybrid composites (EMPC) is that it may require high loading of these magnetic nanoparticles for achieving excellent magnetic property, which is deterrent for space vehicles and light weight portable devices. This could also cause poor mechanical strength for the fabricated materials. Another problem associated with these EMPCs, is their low performance stability and inability to tune the size and shape of the magnetic nanoparticles for enabling them to exhibit excellent conductivity and magnetic performance. Moreover, the dimension of the CP prepared by these strategies was in macro/micro level. A promising strategy for getting maximum electrical conductivity for CP is confining them in the nanometer regime. Addressing all these issues is challenging for the development of high performance EMPC for various technological applications.

Literature reports that salts of certain metals like iron, chromium etc. can form their polyhydroxy cations in their highest oxidation states via hydrolysis

and deprotonation at acidic pH. They can form discrete structures of definite size and shape belonging to the keggin species having large number of unpaired electrons in high-spin combined with the possibility of forming spin-crossover magnetic molecular materials (Ksenofontov *et al.*, 2004). So they are expected to exhibit high magnetic property with low loading of magnetic nanoparticles. Polyhydroxy iron cation (PIC) is prepared by the hydrolysis of ferric chloride hexahydrate in acidic pH. The PIC is having the general structural formula $[\text{Fe}^{\text{II}}\text{O}_4\text{Fe}^{\text{III}}_{12}(\text{OH})_{24}(\text{H}_2\text{O})_{12}]^{7+}$, where 12 Fe^{3+} of octahedral co-ordination surrounds the Fe^{2+} of tetrahedral co-ordination (Lamer *et al.*, 1950). They are of great importance for magnetic and catalytic applications due to the easily accessible $\text{Fe}^{2+}/\text{Fe}^{3+}$ redox couple. Due to the hydrophobicity and large surface area to volume ratio, these PIC nanoparticles tend to aggregate to form macroscopic particles to reduce their surface energy and hence it is difficult to get stable dispersions (Reddy *et al.*, 2007). Block copolymers and surfactants are reported as stabilizing agents for controlling the size and shape of the nanoparticles through a capping mechanism (Xu *et al.*, 2005). The repulsive forces which are induced by coating the particles with surfactants prevent them from aggregation and thereby control their size and shape. Recently our group has reported the formation of nano/ micro structured PANI and PANI-clay nanocomposite using amphiphilic dopants, 4-hydroxy-2-pentadecyl benzene sulphonic acid (PDPSA) and 3-pentadecyl phenyl phosphonate (3-PDPPA) which can play multiple role of micellar template, structure directing agent, dopant, intercalating agent etc (Sudha *et al.*, 2007, Paul *et al.*, 2000, Sudha *et al.*, 2007) and the details are given in chapter 2.

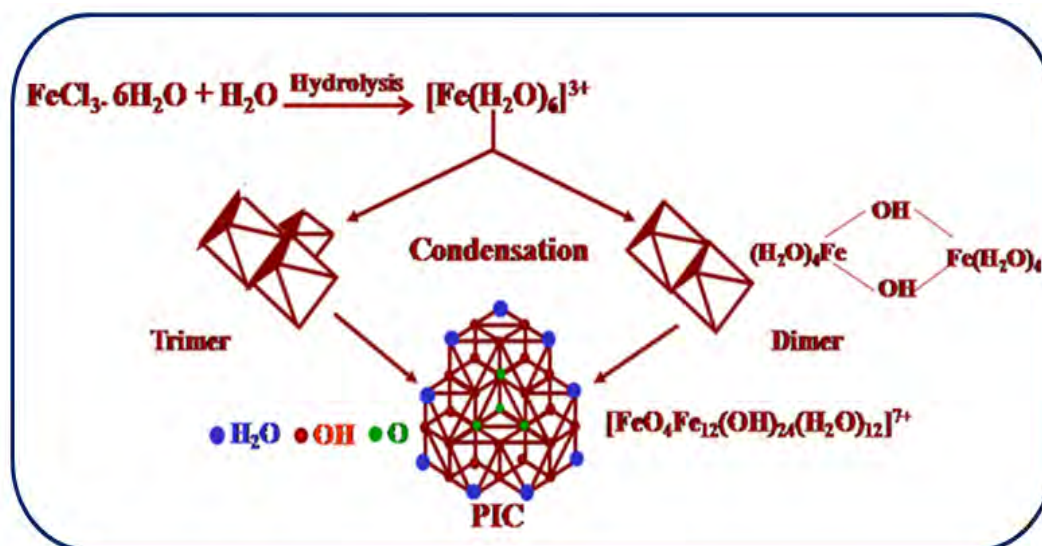
Development of clay containing nanostructured EMPC are receiving attention since it possesses high electrical conductivity and magnetic property along with good thermo-mechanical property and environmental stability with low loading. Smectite clays are interesting inorganic host layered material used to prepare functional materials due to its small particle size, high aspect ratio and capacity to swell and exchange cations for intercalation (Vaia *et al.*, 2001). Details of the structure of clay and its intercalation chemistry are already discussed in chapter 1. In the interlayer region of clay, there exists Na^+ and Ca^{2+} , which can be replaced with polyhydroxy cations of iron (Bradley *et al.*, 1993) and have been studied for their utility as magnetic materials and selective catalysts.

Thus the main challenge was to prepare water dispersible environmentally stable, electro-magnetic materials and to design the structure which will have the greatest effect on the magnetic, conducting and thermo-mechanical properties with processability which are desired for these materials in advanced electro-magnetic applications. Herein, we report the preparation of nano/microstructured multifunctional electro-magnetic polyaniline-polyhydroxy iron - clay composites (PPIC) by emulsion polymerisation of aniline in presence of PIC intercalated clays at room temperature. Then studied the influence of amphiphilic dopant, 4-hydroxy-2-pentadecyl benzene sulphonic acid during the formation of PIC and electro-magnetic PPIC nanocomposite (PPICSA). Then structure-property evaluation of these nanocomposites and also effect of compositional change of aniline, clay, PIC and PDPSA on the electrical conductivity and magnetic property were also discussed.

3.3. Results and Discussion

3.3.1.1. Preparation of polyhydroxy iron cation (PIC)

PIC was prepared by the hydrolysis of ferric chloride at acidic pH of 1.8 as shown in scheme 3.1.



Scheme 3.1. Preparation of PIC

The mechanism involves the formation of a hexa aquo (hydrated) ions, (Cornell *et al.*, 1996), which condense to form dimers and trimers via deprotonation having the structure with Fe octahedra sharing hydroxo and oxo bridges and finally forming Fe_{13} polyhydroxy iron cation (Tomlinson *et al.*, 1998). Particle size of PIC measured using DLS, showed a bimodal distribution curve with particle size of 15 nm and 500 nm (Figure 3.1. A). The formation of larger particles can be due to the aggregation of PIC particles arising from its high surface area and magnetic dipole interactions between the nanoparticles.

PIC was stabilized using PDPSA by performing experiments in presence of PDPSA at a concentration slightly greater than its critical micelle concentration (CMC). The CMC of PDPSA in water was determined by measuring the intensity

of scattered light using dynamic light scattering technique and was found to be 10^{-4} M. DLS measurement of PIC particle prepared in the presence of PDPSA solution (10^{-3} M) exhibited narrow particle size distribution curve with particle size of 8 nm (Figure 3.1. B).

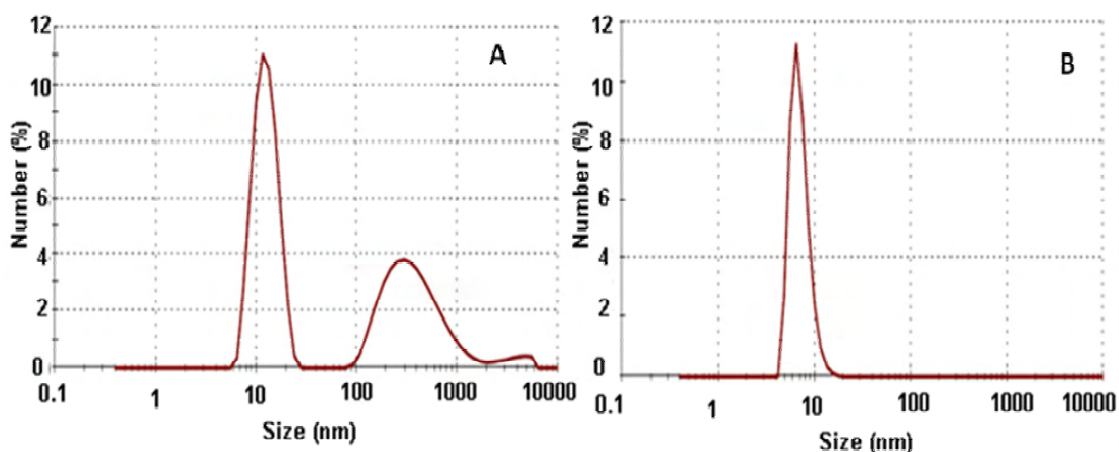


Figure 3.1. DLS plot of (A) PIC and (B) PIC- PDPSA

This can be explained due to the capping mechanism imparted by the surfactant molecules on the surface of charged PIC particles which may induce a repulsive force between the particles. Thus this surfactant can control the size and shape of the formed PIC particle.

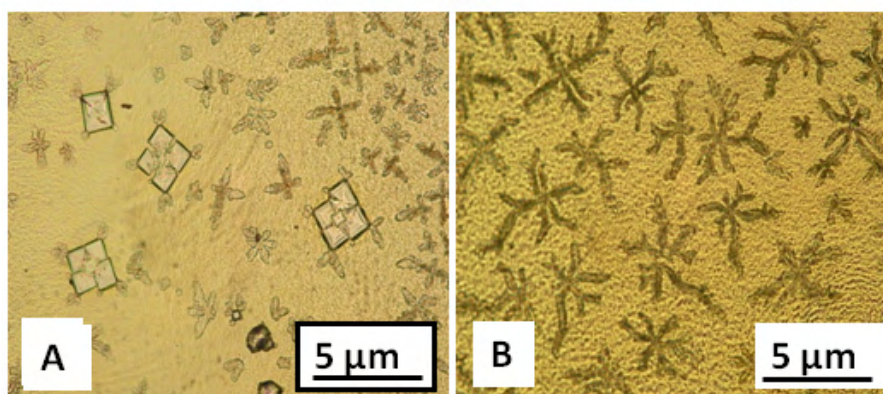


Figure 3.2. PLM picture of polyhydroxy iron cation

The PLM micrograph of PIC is shown in Figure 3.2. It exhibited micropine structure and was observed to be nucleating via a cubic structure that

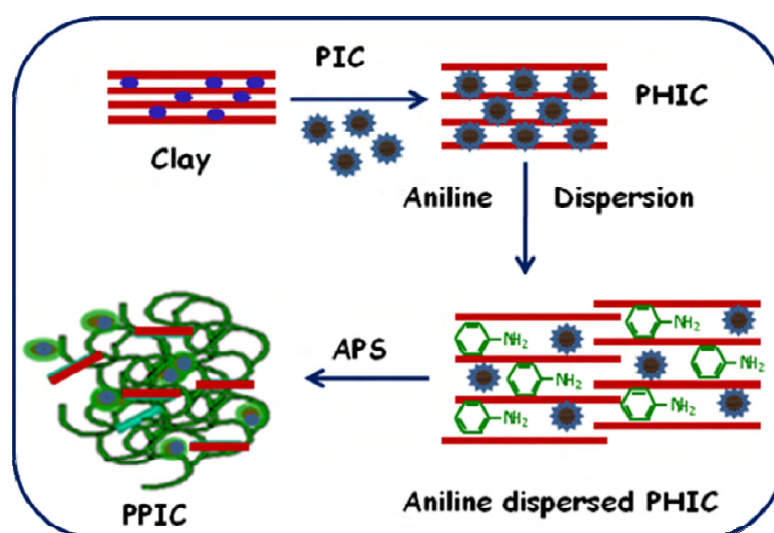
symmetrically cleaves and grows into the micropine structure. A similar micropine structure for $\gamma\text{-Fe}_2\text{O}_3$ was reported earlier by Cao and coworkers (Cao *et al.*, 2005).

3.3.1.2. Preparation of PIC intercalated clay (PHIC)

Intercalation of PIC in clay was conducted by the drop wise addition of dilute aqueous dispersion of clay in PIC solution as shown in scheme 3.2. at different mmol/meq of iron/clay (50, 70, 90, 100 and 110) and the BET surface area was measured. Maximum BET surface area of $269\text{ m}^2\text{ g}^{-1}$ was observed for batches with 90 mmol/meq of iron/clay. So this ratio was standardised for our further experiments.

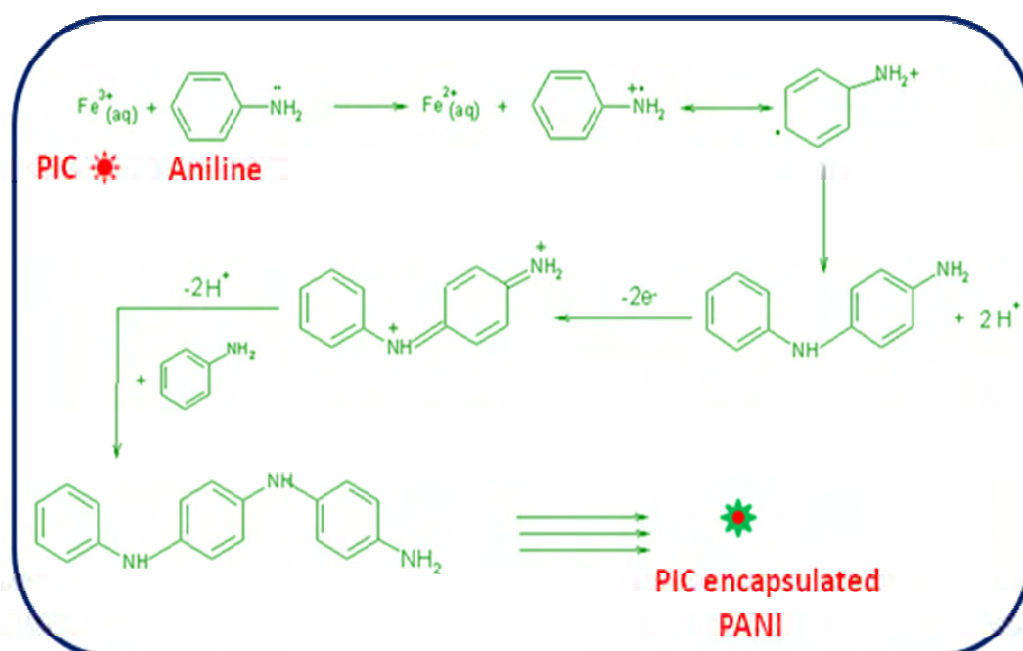
3.3.1.3. Preparation of electromagnetic Polyaniline-polyhydroxy iron - clay composite (PPIC)

Nanostructured electro-magnetic PPIC was prepared by the emulsion polymerization of aniline in presence of aqueous dispersion of PHIC using APS as oxidative radical initiator and the formation of PPIC nanocomposite is shown in scheme 3.2.



Scheme 3.2. Preparation of PPIC

Experiments were performed with different ratio of aniline: PHIC and the details are shown in Table 3.3. The emeraldine green salt formed was isolated by precipitation, filtration and purified by washing several times with water and finally with methanol. Dried under vacuum for 16 h at 50 °C. An interesting observation made during the reaction was the formation of conductive PANI in the absence of APS. When aniline was added to PHIC, the reaction medium changes its color from copper brown to emeraldine green, revealing the formation of PANI in its conductive emeraldine state. Here, the polymerization of aniline to emeraldine salt of PANI is taking place through the oxidative polymerization induced by the $\text{Fe}^{2+}/\text{Fe}^{3+}$ redox couple present in PIC. The mechanism for the same is shown in scheme 3.3. Similar observations were made by Apesteguy and coworkers (Apesteguy *et al.*, 2004), during the preparation of PANI- Fe_3O_4 nanocomposite in presence of Fe (II) and Fe (III) salt without any external oxidant.



Scheme 3.3. Redox Property of $\text{Fe}^{2+}/\text{Fe}^{3+}$ exploited for the polymerization of aniline

Composites prepared in absence of APS exhibited low molecular weight while those prepared in presence of APS exhibited molecular weight in the range of 21,000 da. MALDI-TOF spectrum of a representative PPIC is shown in Figure 3.3.

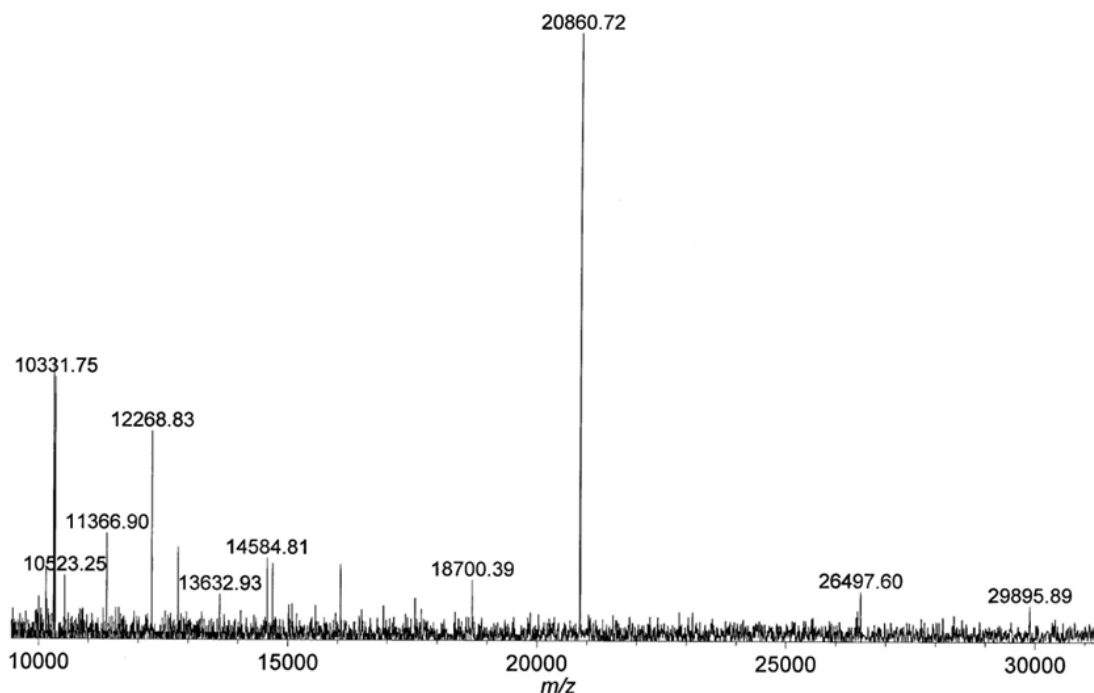
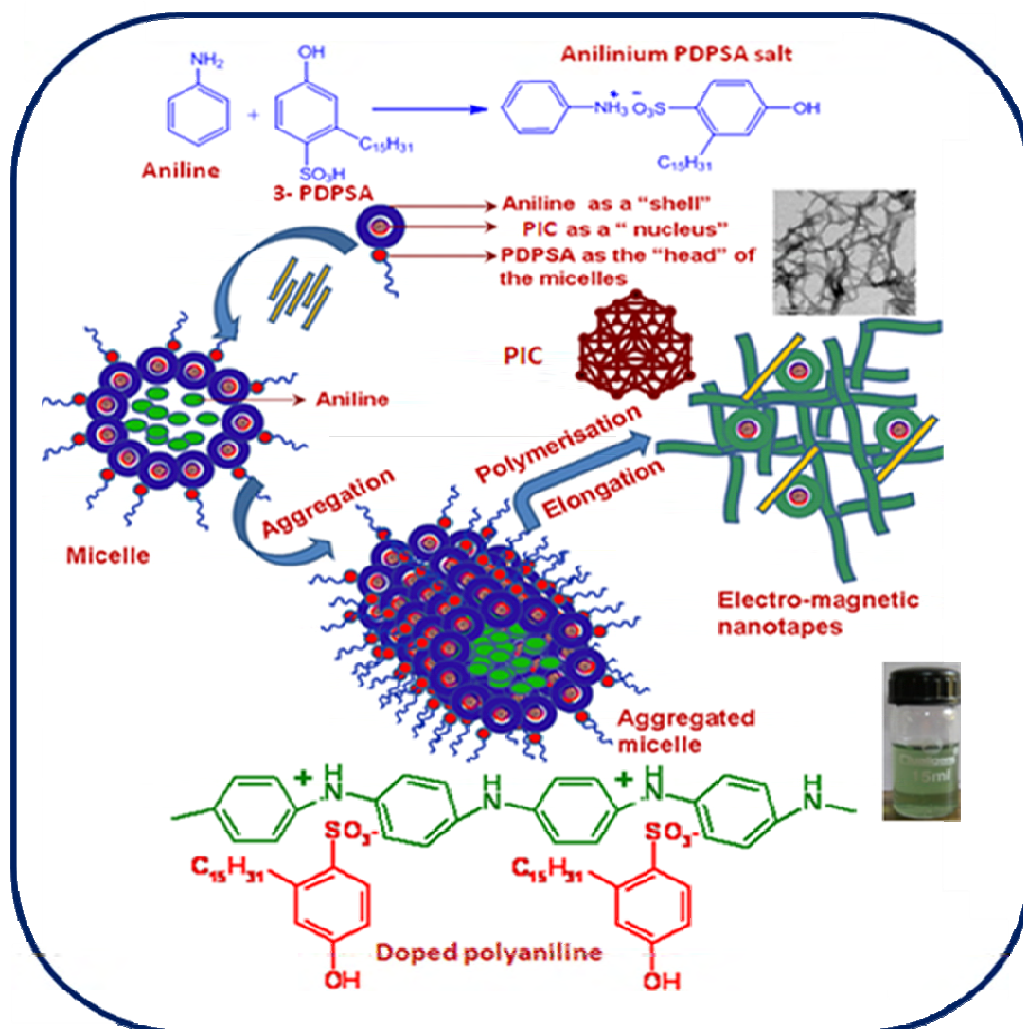


Figure 3.3. MALDI -TOF spectrum of PPIC1

3.3.1.4. Preparation of water dispersible electro-magnetic Polyaniline-polyhydroxy iron - clay composite (PPICSA)

Water dispersible electromagnetic PPICSA was prepared by conducting the above experiment in presence of the amphiphilic dopant, PDPSA and is shown in scheme 3.4. When aniline was added to PHIC mixture containing PDPSA, complex formation occurs due to acid-base type reaction between $-SO_3H$ group of PDPSA and $-NH_2$ group in aniline. Further anilinium-PDPSA complex could self-assemble over the PIC nanoparticles to form spherical micellar structures and then transforms into cylindrical micelle. Upon addition of APS under sonication, polymerization takes place on the surface of the PIC intercalated clay particles.

The polymerized product was found to be dispersible in water and is shown in the scheme 3.4.



Scheme 3.4. Preparation of water dispersible PPIC in presence of PDPSA

PPIC prepared in presence of the amphiphilic dopant was also found to be dispersible in almost all organic solvents. The presence of iron in the PPIC and PPICSA were further confirmed by atomic absorption spectroscopy and that of carbon, nitrogen and sulphur content by CHN elemental analysis and are given in Table 3.1. The observed values were found to be in close agreement with the calculated values.

Table 3.1. Details of elemental analysis

Sample	Calculated					Observed				
	C	H	N	Fe	S	C	H	N	Fe	S
PANI	57.28	3.6	11.13	0	-	52.36	5.34	10.37	0	-
PANICN	51	3.2	9.9	0	-	47.97	5	9.47	0	-
PPC	56	4.79	10.9	10	-	52.53	5.13	10.35	7	-
PPIC1	51	3	9.8	2	-	48.6	3.8	10	1	-
PPIC2	51.5	3.2	10	4	-	49	3	10.3	3	-
PPIC3	52	3.5	10.2	6	-	50	3.2	10.8	5	-
PPIC4	52.5	3.8	10.6	8	-	50.6	3	10.1	7	-
PPIC5	53	4.2	11	10	-	52	4	10	8	-
PPICSA1	48.4	5.3	6.98	4	2.59	43	5.04	6	4.2	2.09
PPICSA2	47	4.8	7.7	4	1.58	44	5	7.7	4	1.3
PPICSA3	46	4.65	8.23	4	1.07	47	4.45	7.9	4.1	0.97
PPICSA4	45.4	4.48	8.53	4	0.5	40	4.18	8	3.8	0.4
PPICSA5	45	4.38	8.7	4	0.02	41	4.08	8.1	3.6	0.012

Figure 3.4. represents the EDS spectra of PPIC and PPICSA. PPIC exhibited signals corresponding to the elements like aluminum, silicon, oxygen, iron etc and hence confirmed the presence of clay layers and iron in the nanocomposite. In PPICSA, in addition to the above peaks, a peak corresponding to sulphur was observed which further confirms the presence of dopant sulphite anion.

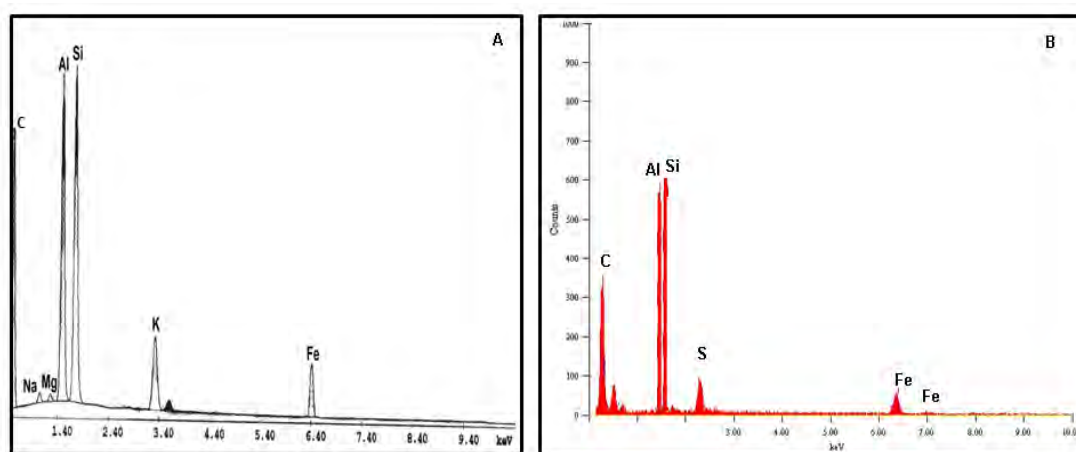


Figure 3.4. EDS spectrum of (A) PPIC and (B) PPICSA

3.3.2. Particle Size Measurements

Particle size measurements of PPIC and PPICSA were done using dynamic light scattering technique and the histograms of representative PPIC and PPICSA are given the Figure 3.5. PPIC exhibited particles size in the micrometer range approaching to 1100 nm (PDI- 0.8) while PPICSA showed in the range of 50- 150 nm (PDI- 0.5). Lower PDI of PPICSA suggests its uniform particle size when compared to PPIC. Thus the result reveals the role of PDPSA in reducing the inter particle interaction and thereby controlling the particle size.

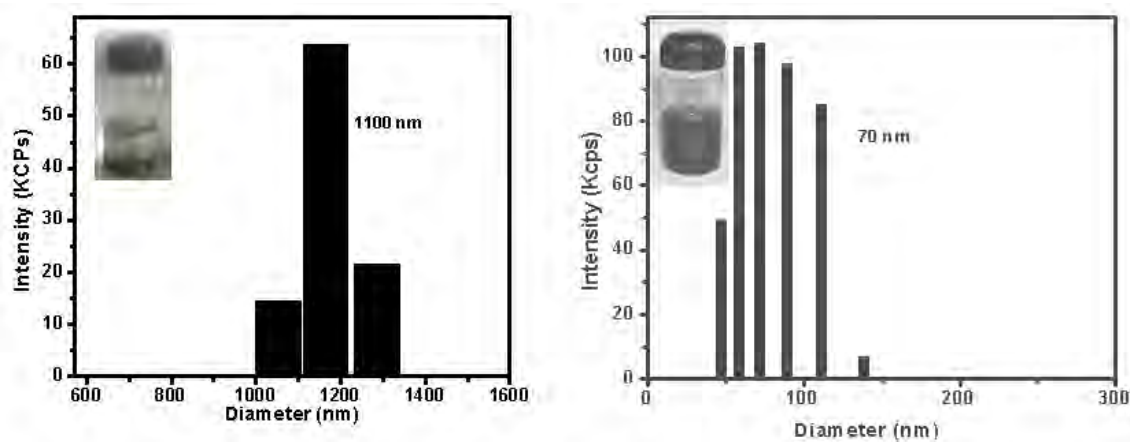


Figure 3.5. DLS histograms showing the size distribution of (A) PPICSA (B) PPIC

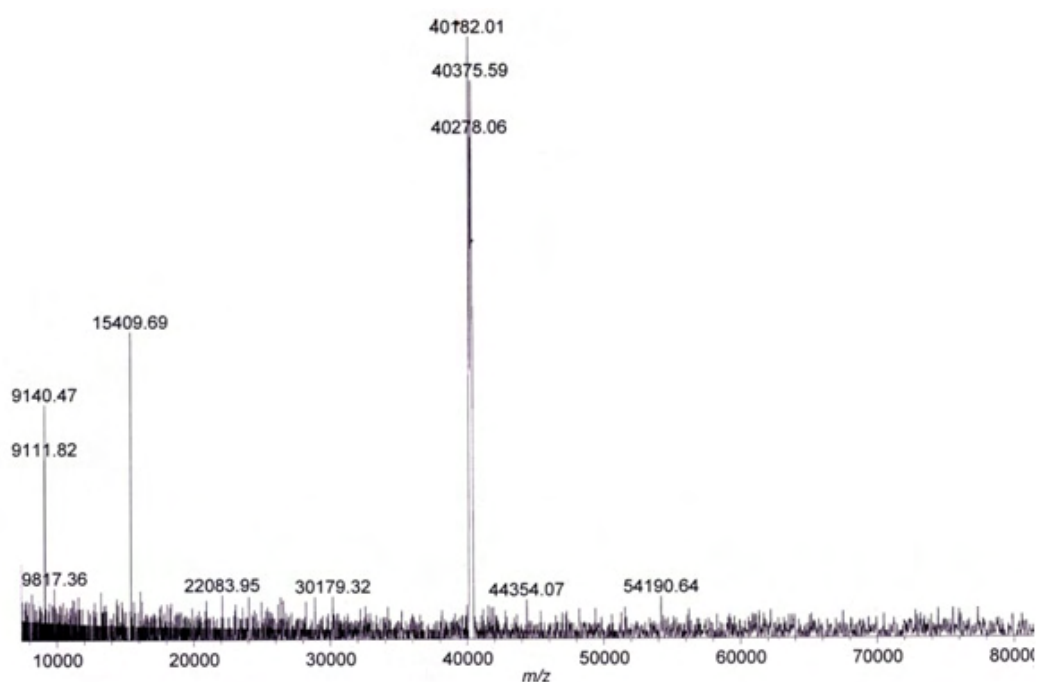


Figure 3.6. Molecular weight determination of PPICSA using MALDI-TOF

Molecular weight of PPICSA was measured using MALDI-TOF and was found to be in the range of 40,000 da, which is higher than the value measured for PPIC. This reveals the higher extent of polymerization for anilinium- PDPSA to PPICSA.

3.3.3. Structural Characterization.

3.3.3.1. UV- vis spectroscopy

Protonic state of the electro-magnetic composites was studied by UV-vis spectroscopy. The UV- vis spectra of PANI, PANICN, PPIC and PPICSA are shown in Figure 3.7. PANI exhibited three absorption peaks in the region (i) ~ 340 nm ($\pi - \pi^*$ transition), (ii) ~ 420 nm (polaron band to π^* transition) and (iii) ~ 700 nm (π - polaron band transition) (Ruokolainen *et al.*, 2000, Lv *et al.*, 2005). The peak observed for PANI at 700 nm, showed a red shift to 780 nm with a free carrier tail in PANICN. This is due to the delocalization of electrons in the polaron band promoted by an extended conformation of the PANI chains inside the clay

galleries. The free carrier tail is shifted to 790 nm and 800 nm in PPIC and PPICSA, respectively.

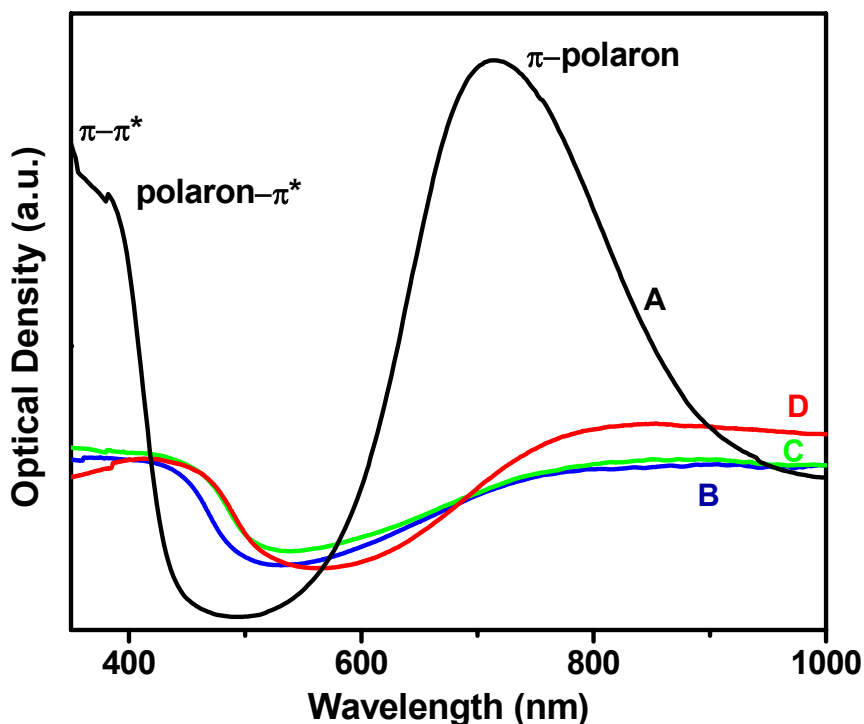


Figure 3.7. UV- vis spectra of (A) PANI, (B) PANICN, (C) PPIC and (D) PPICSA

The broad absorption peak observed at ~ 420 nm in PANICN, PPIC and PPICSA is due to merging of the two peaks - 340 nm and 430 nm (Xia Y *et al.*, 1995), revealing a high degree of doping of PANI in these composites (Han *et al.*, 2002). The red shift observed for the peak at 420 nm in PPIC and PPICSA, compared to PANI and PANICN, is due to the interaction between metal ions and PANI chains, which decreases the energy for the π - π^* transition. The ratio of absorbance of the peaks (π - polaron) / (π - π^*) is seen to follow the order, PPICSA (1.13) > PPIC (1.08) > PANICN (1.0) > PANI (0.893), suggesting more effective delocalization in PPICSA (Stejskal *et al.*, 2005).

3.3.3.2. FT-IR spectroscopy

Formation of electro-magnetic nanocomposite and interaction existing among the moieties were studied using FT-IR spectroscopy. The FT-IR spectra of PPICSA, PPIC, PHIC, PANI and Na⁺ cloisite is shown in Figure 3.8.

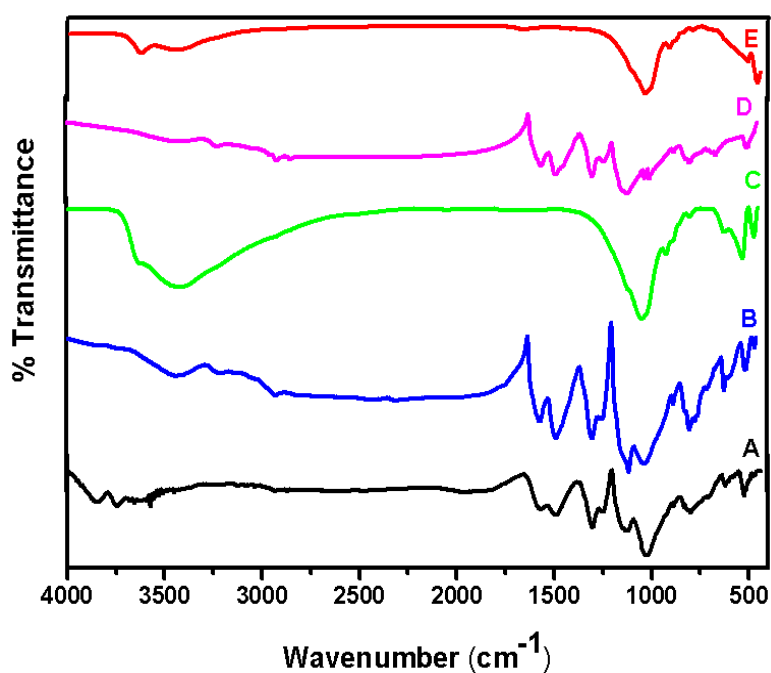


Figure 3.8. FT-IR Spectra of (A) PPICSA, (B) PPIC, (C) PHIC, (D) PANI and (E) Na⁺ Cloisite.

The characteristic bands corresponding to Na⁺ cloisite clay are 1030 cm⁻¹ (Si-O-Si)_{str}, 911 cm⁻¹ (Al-OH)_{str} and 525 cm⁻¹ (Si-O-Al)_{str} (Stubican *et al.*,1961, Kanatzidis *et al.*,1990, He *et al.*,2004). PHIC exhibited an additional peak to Na⁺ cloisite at 590 cm⁻¹, corresponding to Fe-O_{str}. The absorption peak around 1574 and 1490 cm⁻¹ observed in PANI, PPIC and PPICSA are attributed to the C=C_{str} of quinoid and benzenoid, respectively (Chen *et al.*,1995). The (C=C)_{str} deformation of the quinoid in PANI shifts from 1566 to 1554 cm⁻¹ and that of the benzenoid ring from 1498 to 1486 cm⁻¹, indicating a longer effective delocalization in PPIC and PPICSA (Lee *et al.*,2006, Alan *et al.*,1995, Cao *et al.*,1986). The peak at 1295

and 3257 cm^{-1} were assigned to the C–N stretching vibration of the secondary aromatic amine and N–H stretching modes of PANI, respectively (do Nascimento *et al.*, 2004). The bands at 1040 and 506 cm^{-1} observed in PPICSA can be assigned to the absorption of the sulphite anions. The peak at 1298 cm^{-1} observed in PANI is shifted to 1302 cm^{-1} in the composites. Also the peak observed at 590 cm^{-1} (Fe–O) in PHIC, is shifted to 594 cm^{-1} in the PPIC and PPICSA. The shift observed can be due to the interaction between the lone pair of electrons present in the nitrogen atom of the PANI chain and the 3d orbitals of the Fe atom to form a coordinate bond (Tandon *et al.*, 2006). The peak at 1030 cm^{-1} in clay corresponding to the Si–O–Si_{str} shifts to 1020 cm^{-1} in both PPIC and PPICSA due to the hydrogen bonding between PANI chains and the basal surface of clay and the polyhydroxy iron cation (Sudha *et al.*, 2007). All these peak shifts observed in PPIC and PPICSA when compared to the characteristic peaks of clay (Si–O–Si), PIC (Fe–O), and PANI (C=C and C–N) suggest the existence of hydrogen bond interaction among these moieties.

3.3.4. X-ray diffraction studies

The wide-angle X-ray diffraction patterns of Na⁺ Cloisite, PHIC, PPIC and PPICSA are shown in Figure 3.9. and the details of their d- spacings with diffraction angles are listed in Table 3.2. Generally, all the patterns were made up of two distinct types of reflections: general and basal. The general reflections are called the (hk) bands, and are asymmetrical lines (Warren *et al.*, 1941). Such reflections are caused by the structure of the smectite layer themselves, and are independent of external condition. The basal reflections (hkl), on the other hand

have symmetrical peaks, whose positions vary with the nature of the intercalating species, the amount of water and so forth.

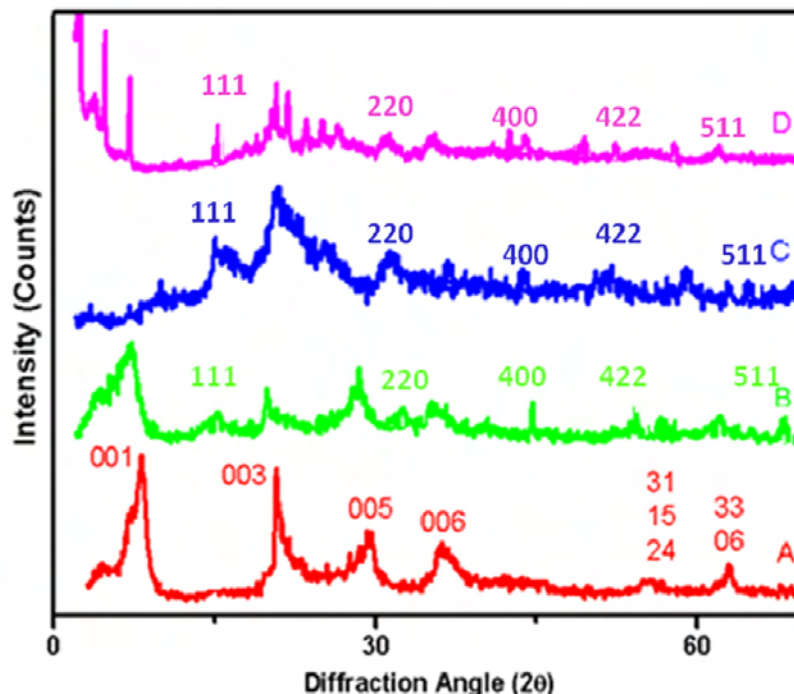


Figure 3.9. XRD diffractogram of (A) Na⁺ Cloisite, (B) PHIC, (C) PPIC and (D) PPICSA

The diffraction pattern of clay (Figure 3.9. A) showed reflections at $2\theta = 7.2^\circ$ (d_{001}), 18.7° (d_{003}), 21.9° (d_{004}), 28.6° (d_{005}), 34.9° (d_{007}), 54.2° (d_{31} , d_{15} , d_{24}) and 61.8° (d_{33} , d_{06}). The basal reflection peak at $2\theta = 7.2^\circ$ with d-spacing 12.1 Å corresponds to the d_{001} basal spacing of the clay. After intercalation of the PIC in clay (PHIC), the d_{001} reflection shifts to a lower angle with a d-spacing of 15 Å with an enhancement in the interlayer distance of 5.5 Å. This increased distance is equal to the dimension of the hydrated PIC. The diffractogram exhibited additional reflections at $2\theta = 15^\circ$ (111), 31° (220), 44.6° (400) 54.3° (422) 55° (422) and 65.1° (511) which are the characteristic peaks of the crystalline spinel structure of PIC (Rightor *et al.*, 1991). The diffractogram of PPIC (Figure 3.9. C) showed silent reflection for d_{001} peak of clay, confirming an exfoliated state of

nanoclay layers. PPICSA (Figure 3.9. D) exhibited more intense extra peaks in the region of $2\theta = 19^\circ$ revealing more ordered crystalline PANI layers in PPICSA composite compared to PPIC. Moreover PPICSA exhibited sharp reflection below $2\theta = 5^\circ$ revealing the presence of self assembled PANI-PDPSA nanostructure in PPICSA and details for the appearance of the same is explained in chapter 2. In PPIC, the characteristic reflections were observed at $2\theta = 29.6^\circ$ (3.01 Å), 35.29° (2.54 Å), 43.25° (2.09 Å), 54.1° (1.69 Å), 61.97° (1.49 Å). In PPICSA, the peaks were observed at $2\theta = 30.1^\circ$ (2.97 Å), 35.42° (2.5 Å), 44.8° (2 Å), 62.1° (1.5 Å). The small discrepancy observed in the d-values of PPIC and PPICSAs, compared to that of PIC may be due to the partially collapsed phase of PIC in the presence of clay and the protonated PANI chains. Thus, it is reasonable to believe that spinel structure of PIC present in PPIC, similar to that of Fe_3O_4 is responsible for the ferromagnetic properties exhibited by the composite (Long *et al.*, 2005).

Table 3.2. Details of XRD studies

Sample	Diffraction Angle 2θ (degrees)	d- spacing Å
Clay	7.2,19.8, 21.9, 28.6, 34.9, 54.2, 61.8	12.1, 4.8, 4, 3.1, 2.6, 1.7, 1.4
PHIC	5.8,19.7,28.4, 30.1, 36, 44.6, 54.3,61.8, 65.1	15.2, 4.5, 3.1, 2.97, 2.5,2,1.7,1.5,1.4
Fe_3O_4	30.1, 35.42, 43.20,53.48, 57.94	2.97, 2.5, 2.09, 2.53, 2.97.
PPIC	29.6, 35.29, 43.25, 54.1, 61.97	3.01, 2.54, 2.09, 1.6, 1.69,1.49
PPICSA	30.1 , 35.42 , 44.8, 62.1	2.97, 2.5, 2, 1.5

3.3.5. Morphology

Morphology of the PPIC and PPICSA nanocomposites was studied using PLM, SEM and TEM. The PLM picture (Figure 3.10.) of drop-casted PPIC showed aggregated fibrillar morphology while PPICSA exhibited well segregated distinct nanofibrils.

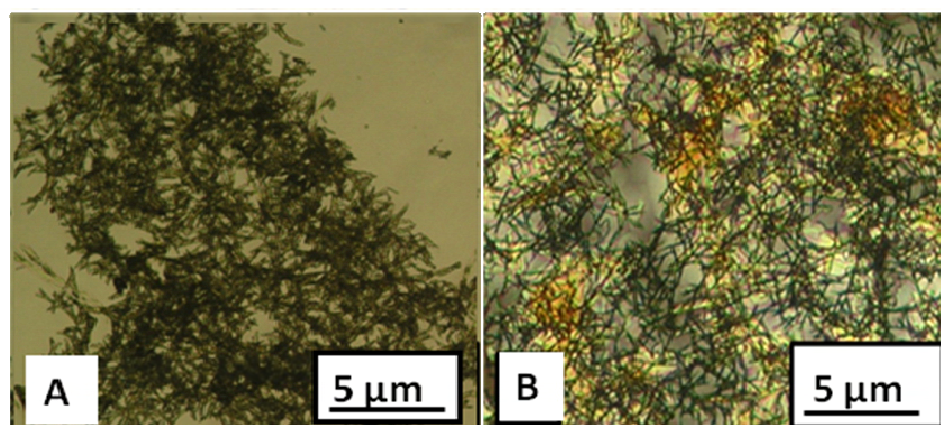


Figure 3.10. PLM images of (A) PPIC (B) PPICSA

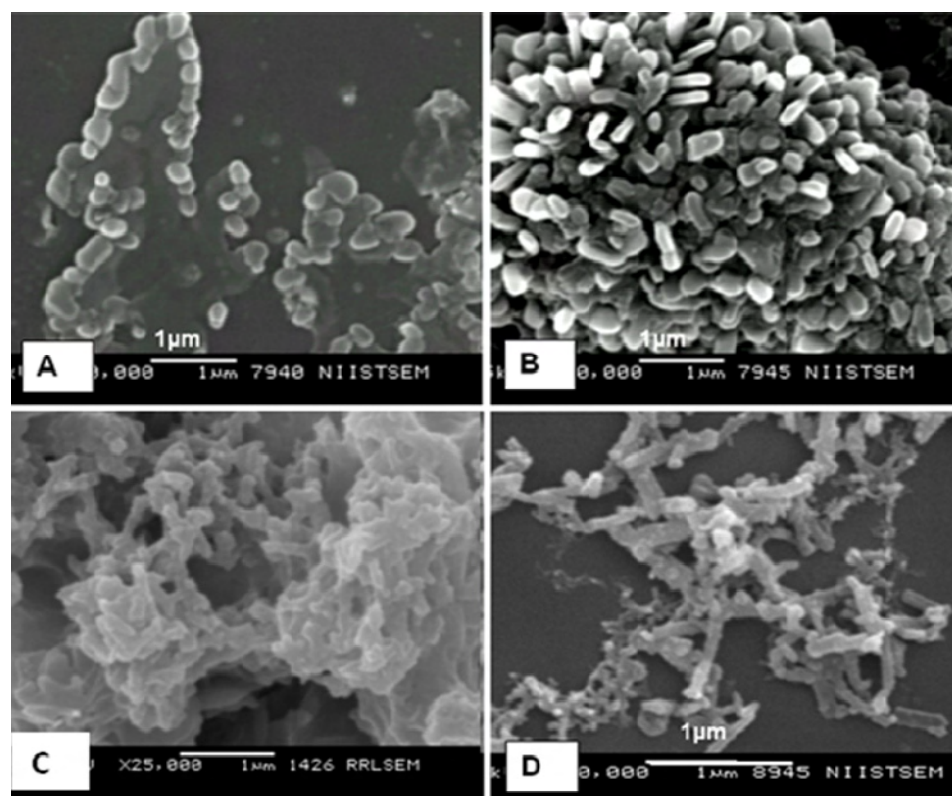


Figure 3.11. SEM images of (A, B) PPC (C) PPIC (D) PPICSA

The SEM pictures of polyaniline polyhydroxy iron cation (PPC) prepared under two different ratios of PIC/aniline (5:95 and 10:90) are shown in Figure 3.11. The micrograph showed chain of nano/micro spherical particles having spherical morphology at lower concentration of PIC (Figure 3.11. A) and capsule like morphology (Figure 3.11. B) with increased amount of PIC. Here, the anilinium ion present in the system is adsorbed on the surface of the charged PIC ions through a static interaction (Li *et al.*, 2006). The redox couple Fe^{+2}/Fe^{+3} present in PIC is endowed with high electron density and can therefore act as a catalyst cum template during the polymerization of aniline and it forms a magnetic core inside the conducting PANI shell. These nano/micro spheres containing magnetic core of PIC and conducting shell of PANI can self-assemble to form PPIC fibres. PPICSA exhibited tape like morphology having diameter below 200 nm and extending to several micrometer length. The observed highly ordered nanotapes of PPICSA can be ascribed due to the formation of self-assembled structure arising from the PANI-dopant interaction.

SEM observations were further strengthened by the studies made from TEM. TEM images of PPIC and PPICSA taken under two different resolutions are shown in Figure 3.12. PPIC exhibited agglomerated fiber like morphology engulfed over the exfoliated clay layers while PPICSA exhibited highly uniform nanotapes having width below 100 nm and several micrometers length. In both PPIC and PPICSA, the dark region observed might be due to the self-assembled magnetic PIC and clay particles, and the light region corresponds to the PANI chains present in the composites. This contrast in the image might be arising from the difference in the electron penetrability when it passes through the

inorganic and organic moieties present in the PPIC and PPICSA. Clay layers are not visible since self assembled nanotapes of the PANI are circumventing clay and iron particles.

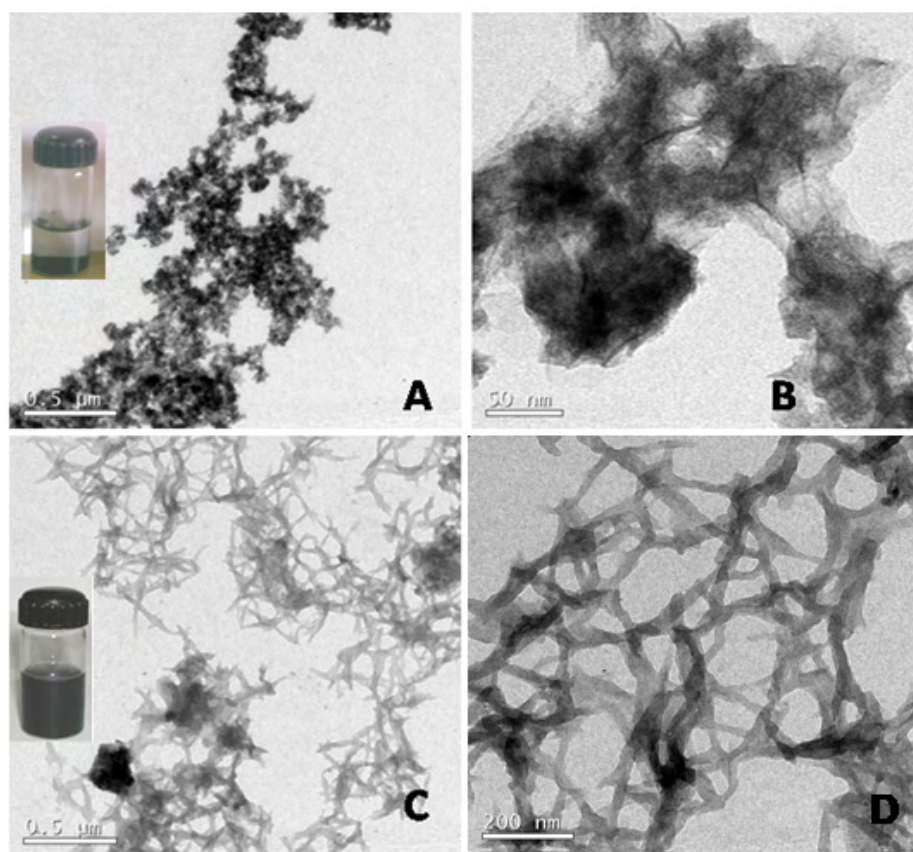


Figure 3.12. TEM images of electro-magnetic composites synthesized with inset showing its dispersion in water (A, B) PPIC and (C, D) PPICSA

A plausible mechanism for the formation of magnetic PIC entrapped conducting nanotape of PPICSA can be explained as shown in scheme 3.4. When anilinium-PDPSA comes in contact with the highly charged iron species, it will adhere to the surface of the iron particles via ion-dipolar interaction to form a shell and hence act as a capping agent and will stabilize the self-assembled keggin iron particles from aggregation. Due to the presence of hydrophobic and hydrophilic group in the anilinium- PDPSA, it forms micellar template by a

combination of many noncovalent interactions (Sudha *et al.*, 2007). It is well accepted that the formed micelles are spherical in shape due to their lowest surface energies. The addition of aniline induces self organization of the micelle and would result in cylindrical micellar template (Zhang *et al.*, 2003). It is reported that organic salts that contain a hydrophobic part and possess a charge opposite to that of the surfactant molecule are highly efficient in promoting a structural transition in micelles. These cylindrical micelles can imbibe aniline species and may act as a structure-directing agent during polymerization. Upon the addition of APS, polymerization proceeds with the formation of electro-magnetic tapes by the process of elongation and flattening as shown in the scheme 3.4. This is supported by the observation made by other researchers (Hassan *et al.*, 2004).

3.3.6. Conductivity measurements

The room temperature electrical conductivity (σ_{dc}) of electro-magnetic polymer composites was measured using a four-probe conductivity meter and the details of the measurement are given in Table 3.3. Bulk PANI exhibited conductivity of $3 \times 10^{-2} \text{ S cm}^{-1}$. Effect of PHIC concentration on the electrical conductivity of PPIC was studied. It was observed that on increasing the amount of PHIC in the nanocomposite, conductivity initially decreases, then increase and finally decrease. The initial decrease might be due to the neutralization of charges of PANI in presence of charged iron particles. Further increase can be explained as: in the disordered electro-magnetic system like PPIC, the conductivity depends on two aspects: microscopic conductivity, which depends

upon the doping level, conjugation length or chain length and the macroscopic conductivity which depends on some external factors like compactness of the sample, orientation of the micro particles, etc (Chen *et al.*, 2003).

Table 3.3. Details of electrical properties of PPIC

Sample	PHIC: Aniline	Conductivity
		(S cm ⁻¹)
PANI	0:100	3.0 x10 ⁻²
PPIC1	2: 98	1.2 x10 ⁻²
PPIC2	4: 96	3.5 x10 ⁻¹
PPIC3	6: 94	5.0 x10 ⁻¹
PPIC4	8: 92	1.0
PPIC5	10:90	1.1
PPIC6	12:88	8.0 x10 ⁻¹
PPIC7	14:86	2.0 x10 ⁻¹

In PPICs, the intrinsic microscopic conductivities are more or less equal, because of the PANI being polymerized in identical conditions. On the other hand, as the PHIC content in the composites was increased, the compactness increases. During the polymerization process, oligomeric species of aniline is adsorbed on the magnetite surface and the crystalline boundaries will become the primary nucleation centers and can act as template during polymerization to form PANI chains on their surface. As a result, the weak links between the grains are increasingly improved and the coupling through the grain boundaries becomes

stronger and hence the conductivity increased. For higher PHIC content (> 10 wt %), the decrease in conductivity may be due to partial blockage of conduction path by the excess PIC nanoparticles and the insulative clay present in PPICs.

Effect of dopant concentration on the conductivity of PPICSA was studied and the details are shown in Table 3.4. It was observed to follow the order, PPICSA5 (0.072 S cm^{-1}) > PPICSA4 (0.3 S cm^{-1}) > PPICSA3 (0.6 S cm^{-1}) > PPICSA2 (1 S cm^{-1}) > PPICSA1 (1.8 S cm^{-1}) suggesting a decrease in conductivity with decrease in PDPSA concentration. The conductivity (σ) is equal to the product of carrier mobility (μ), charge (Q) and charge density (n) as in $\sigma = \mu Qn$. With the decrease in the dopant concentration, the charge density decreases and thereby decreases the conductivity.

Table 3.4. Details of electrical properties of PPICSA

Sample	Aniline : PDPSA	Conductivity (S cm^{-1})
PANISA	1:0.1	7×10^{-2}
PPICSA1	1:0.1	1.8
PPICSA2	1:0.05	1
PPICSA3	1:0.025	0.6
PPICSA4	1:0.01	0.3
PPICSA5	1:0.001	7.2×10^{-2}

3.3.7. Magnetic property

Magnetic properties measurement of the conducting polymers can provide important details of charge carrying species and unpaired spins. Generally it is

studied by measuring the variation of magnetic flux density (M) as a function of magnetizing field (H). The magnetic properties of the nanostructured electro-magnetic PANI, PPIC and PPICSA were measured at room temperature using the vibrating sample magnetometer. Magnetic property measurement of PPICs was done with nanocomposites containing PHIC content from 2 to 10% and the details of the results are shown in the Table 3.5. Typical M-H hysteresis loop curve of PPIC is shown in Figure 3.13. Application of magnetic field (H) will align the magnetic moment of the nanoparticle in the field direction, and magnetization (flux density) rises with increasing field until a saturation value is reached, the point "a". At this point, almost all of the magnetic domains are aligned and an additional increase in the magnetizing force will produce very little increase in magnetic flux. When H is reduced to zero, the curve will move from point "a" to "b". At this point, it could be seen that some magnetic flux remains in the material even though the magnetizing force is zero. This is the point of retentivity on the graph and indicates the remanence or level of residual magnetism in the material. (Some of the magnetic domains remain aligned but some have lost their alignment.). As the magnetizing force is reversed, the curve moves to point "c", where the flux has been reduced to zero. This is called the point of coercivity on the curve. The force required to remove the residual magnetism from the material is called the coercive force or coercivity of the material. As the magnetizing force is increased in the negative direction, the material will again become magnetically saturated but in the opposite direction (point "d"). Reducing H to zero brings the curve to point "e." It will have a level of residual magnetism equal to that achieved in the other direction. Increasing H

back in the positive direction will return B to zero. The curve will take a different path from point "f" back to the saturation point where it will complete the loop.

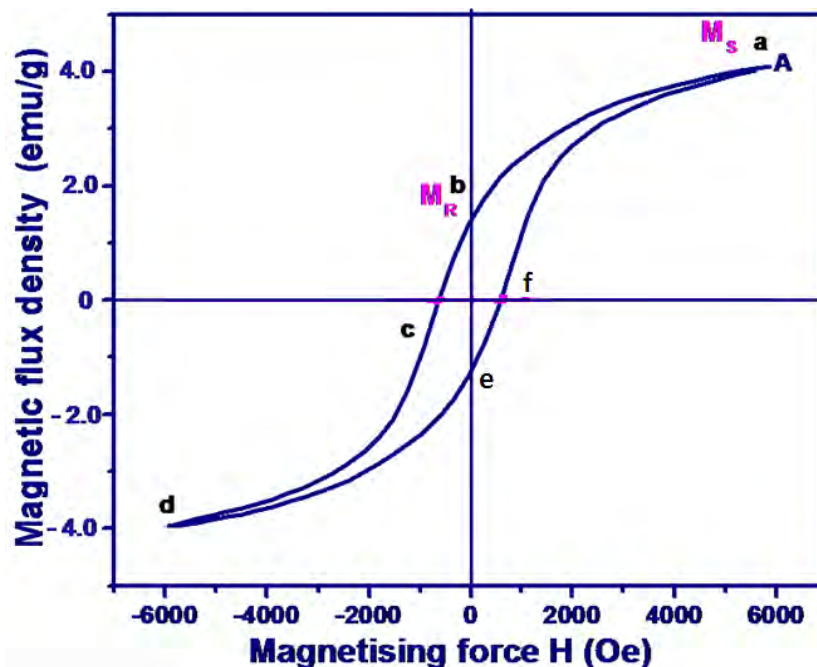


Figure 3.13. Typical M-H curve of PPIC

Table 3.5. Details of magnetic properties of PPIC

Sample	PHIC : Aniline	Saturation magnetization (emu g ⁻¹)	Remnant magnetization (emu g ⁻¹)	Coercive force (H _c)
PANI	0:100	7.3 x10 ⁻³	1 x10 ⁻³	-
PPIC1	2: 98	1	0.1	450
PPIC2	4: 96	2	0.33	563
PPIC3	6: 94	3.5	0.45	583
PPIC4	8: 92	4	0.6	600
PPIC5	10: 90	5.5	0.8	630

PPIC4 exhibited a saturation magnetization (M_s) - 4 emu g⁻¹, coercivity (H_c) - 600 Oe and a retentivity (M_r) - 0.6 emu g⁻¹. The coercivity observed for PPIC is almost similar to that of bulk magnetite (500-800 Oe) (Brown *et al.*, 1963, Craik *et al.* 1981). With increasing amount of PIC from 2 to 10 %, the M_s was observed to increase from 1 to 5.5 emu g⁻¹. The saturation magnetization in the nanoparticles is greatly affected by the surface charge and size effects (Nguyen *et.al.*, 1994, Bidan *et.al.*, 1994). Moreover, the saturation magnetization of the nanocomposites depends on the volume fraction of the magnetic particles. Thus with increasing the amount of PHIC, the volume fraction of magnetic material will increase in the nanocomposite and exhibits an increase in the saturation magnetization. Healing effect may get weakened and leads to the increase in coercivity (Kazantseva *et. al.*, 2004). These materials can be used for the fabrication of EMI shielding materials where the intensity of the interfering electro-magnetic radiation in a low range of frequency.

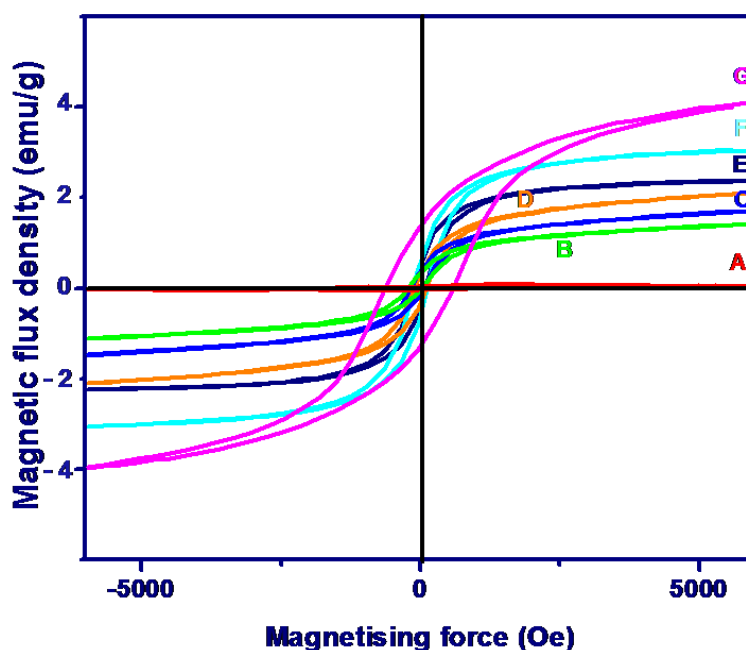


Figure 3.14. M-H curves of (A) PANI, (B) PPICSA1, (C) PPICSA2, (D) PPICSA3, (E) PPICSA4, (F) PPICSA5 and (G) PPIC

M-H hysteresis curves of PPIC4 (8% PHIC content), PANI and PPICSA of various compositions are shown in Figure 3.14. PPIC4 exhibited M_s - 4 emu g^{-1} , H_c - 600 Oe and M_r - 0.6 emu g^{-1} while PANI exhibited M_s - 7.3×10^{-3} emu g^{-1} , H_c - 10.9 Oe and M_r - 206×10^{-6} emu g^{-1} . PPICSA exhibited a lower coercivity below 50 Oe when compared to PPIC. This can be attributed to the smaller particle size of PPICSA. Thus magnetic property measurement gives a direct evidence for the role of dopants in controlling the size of the PPICSA particles. It was observed that the saturation magnetisation showed positive variation with increase in the dopant concentration, which may be due to the hike in the number of charged species.

3.3.8. Thermal Stability

Thermal stability of clay, PANI, PPIC and PPICSA were investigated using thermogravimetry. TG was performed under nitrogen atmosphere to minimize mass increase due to iron oxidation and the result is shown in Figure 3.15.

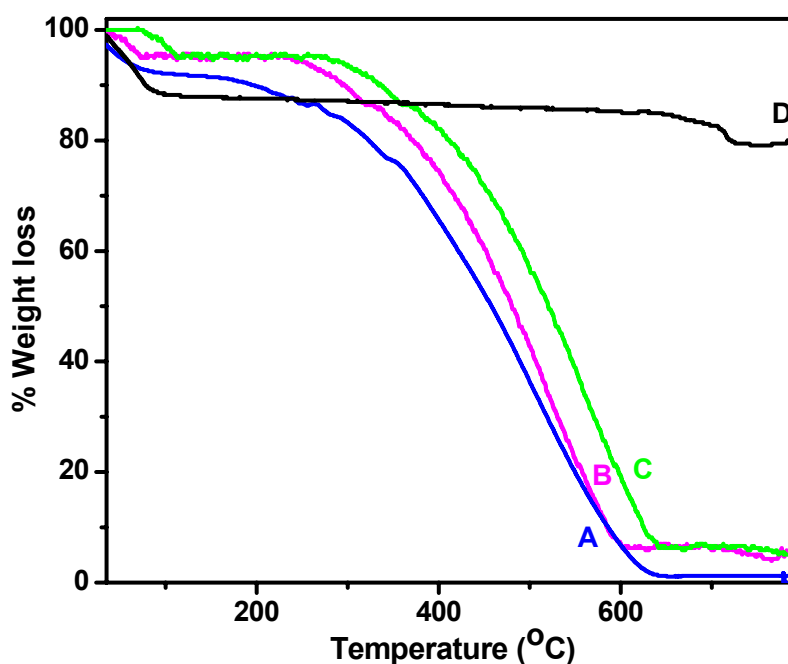


Figure 3.15. TG plot of (A) PANI, (B) PPIC, (C) PPICSA and (D) Clay

TG curve of PANI showed two decomposition stages. The initial weight loss around 80 °C can be ascribed due to the expulsion of water and volatile impurities and the second weight loss starting from 250 °C may be due to the decomposition of the PANI backbone. TG curve of PPIC showed an enhancement in the second stage decomposition temperature to 320 °C and that of PPICSA to 350 °C. The enhanced thermal stability exhibited by the PPIC and PPICSA nanocomposites compared to bulk PANI can be due to the synergetic contribution of insulative clay layers and PIC particles that are present in the former. Thermal stability followed the order: clay > PPICSA > PPIC > PANI.

3.4. Conclusions

In conclusion, nanostructured electro-magnetic polyaniline- polyhydroxy iron-clay composite is prepared by *in-situ* emulsion polymerization of aniline in presence of polyhydroxy iron cation intercalated clay at room temperature. A conceptually new synthetic methodology for water dispersible electro-magnetic nanotapes of PPICSA was developed using the amphiphilic dopant, PDPSA derived from cashew nut shell liquid. This amphiphilic dopant could tune the size of the metal nanoparticle by preventing them from agglomeration and also could act as a micellar template for the formation of nanostructured PANI. Morphology studies revealed that PPIC exhibited nano/micro fibers while PPICSA, nanotapes. These electro-magnetic materials showed excellent electrical conductivity, reasonable magnetic property, good thermal stability and solubility in most of the organic solvents. These attractive properties make them an excellent candidate for high advanced technological applications in the field of EMI shielding materials and chemical sensors. Furthermore, the method described

here offers a simple, low cost and convenient route for fabricating well ordered electro-magnetic nanotapes composed of conducting polymer and other metal keggin ions using various other amphiphilic dopants.

3.5. Experimental Section

For details regarding the materials and preparation methods, see experimental section of chapter 2 and 3.

3.5.1. Materials.

Ferric chloride hexahydrate were purchased from s.d. fine chem limited, Mumbai, India and were used without further purification. Sodium carbonate was purchased from Ranbaxy fine chemicals limited.

3.5.2. Synthesis Procedure.

3.5.2.1. Determination of critical micelle concentration of PDPSA

The amphiphilic dopant, PDPSA was prepared and characterized as per the procedure reported elsewhere. (Sudha et al., 2007)

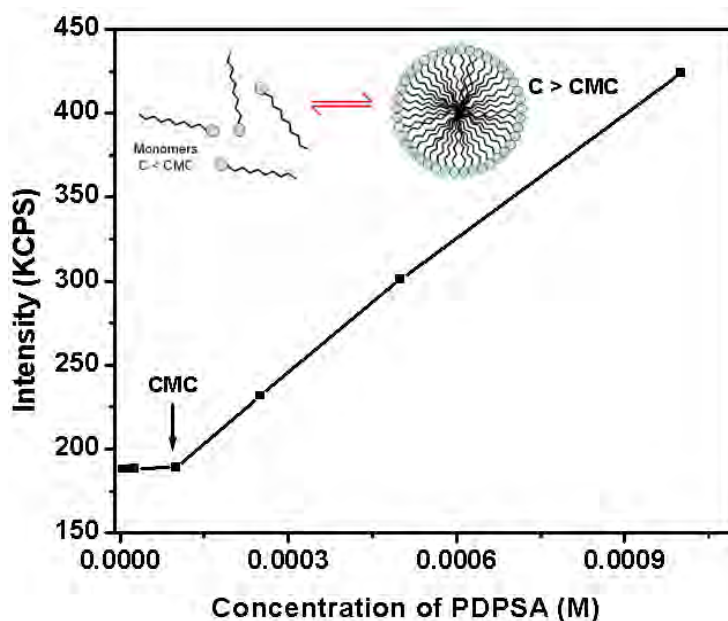


Figure 3.16. Intensity of scattered light against concentration for CMC determination

Solubility of PDPSA in water was studied and was found to form stable emulsion. The critical micelle concentration (CMC) of PDPSA in water was determined by measuring the intensity of scattered light using dynamic light scattering technique with varying concentration of PDPSA ranging from 10^{-5} to 10^{-3} M. Intensity of scattered light versus concentration is shown in Figure 3.16. It was observed that at lower concentration, the intensity of scattered light was similar to that of deionised water. On reaching the concentration of 10^{-4} M, it showed an inflection and on further increase in concentration, exhibited a sharp increase. This concentration was taken as the CMC of PDPSA.

3.5.2.2. Preparation of polyhydroxy iron cation (PIC)

The iron polyhydroxy cation solution was prepared by the hydrolysis of 0.2 M ferric chloride hexahydrate solution with sodium carbonate. The typical procedure is as follows: 0.82 g (0.003 mol) of ferric chloride hexahydrate was dissolved in 15 mL of 0.1 M HCl and stirred vigorously for 20 min at room temperature. 0.32 g (0.003 mol) of anhydrous sodium carbonate powder was added to the stirred solution in small lots. The addition of Na_2CO_3 was controlled in such a way as to prevent precipitation. It was then flushed with nitrogen to facilitate the removal of carbon dioxide that evolved during the hydrolysis and was aged for 1 day at room temperature to allow the growth of the polycation. The hydrolysis condition produced a pH of 1.8. At this pH, highly condensed species of polynuclear keggin iron complexes were present for incorporation into the clay gallery space (Murphy *et.al.*, 1975, Murphy *et.al.*, 1975).

3.5.2.3. Preparation of PIC intercalated clay (PHIC)

Clay (0.125 g) in 12.5 mL of water (1 wt %) was added slowly to a vigorously stirred solution of 11.5 mL of 0.2 M PIC. The ratio of the cation to clay was 90 mmol/ meq for the synthesis. Upon the complete addition of clay to the hydrolyzed Fe³⁺ solution, the reaction mixture was stirred for an additional 2 h. The product was washed to remove excess salt by subsequent centrifugation and decantation. The resulting material was then dried in a vacuum oven at 80 °C for 1 day and ground into powder.

3.5.2.4. Preparation of polyaniline-polyhydroxy iron-clay composites (PPIC)

Clay (0.125 g) in 12.5 mL of water (1 wt %) was added slowly to a vigorously stirred solution of 11.5 mL of PIC (0.2M). It was stirred for 0.5 h and 2.5 g (0.026 mol) of aniline in 100 mL of water was added. Then pH of the solution was adjusted to 2 by the drop wise addition of conc. HCl. Sonicated for 0.5 h, and polymerized by the addition of 6.84 g (0.03 mol) of 1.25 M APS. After the addition of APS, polymerization was continued for 6 h to achieve high molecular weight PANI species. The green emeraldine salt of PPIC formed was isolated by precipitation from methyl alcohol. It was then filtered, washed a number of times with distilled water and finally with methanol. The product was dried under vacuum at 80 °C for 1 day. Nanostructured conductive materials with different aniline/PHIC ratios were prepared, and their abbreviations and details are given in Table 3.4. Solubility of PPIC in many solvents like CHCl₃, NMP, DMAc, and DMF was checked, and was found to be partially soluble. Polyaniline- and polyaniline-clay composites without PIC were also prepared, as

reported in chapter 2 (experimental section) and were designated as PANI and PANICN, respectively.

3.5.2.5. Preparation of PPIC- PDPSA (PPICSA).

Typical procedure for the preparation of PPICSA is as follows. PIC (11.5 mL, 0.2 M) was added to stirred solution of PDPSA (10^{-3} M, 25 mL). Aqueous suspension of clay (0.125 g, 1 wt %) was added to the vigorously stirred solution of PIC-PDPSA. The ratio of the iron/ clay was taken as 90 mmol/meq. Upon the complete addition of clay to the PIC, the reaction mixture was ultrasonicated for 2 h. Aniline (2.5 g) in 25 mL of water was then added and continued ultrasonication for another 0.5 h. Aniline: PDPSA mole ratio was kept to be 1:0.1. Aqueous solution of APS (6.1 g in 60 mL water, 0.1 M) was then added to the above mixture and the resulting solution was stirred for another 5 min to ensure complete mixing. The reaction was kept for 24 h without agitation at room temperature. Finally the product was precipitated from methanol, washed with deionized water until the filtrate become colourless and dried under vacuum at 60 - 80 °C for 12 h. Sample was designated as PPICSA5. Similarly experiments were carried out with varying the ratio of aniline: PDPSA as 1:0.001, 1:0.01, 1:0.025 and 1:0.05 and were designated as PPICSA1, PPICSA2, PPICSA3 and PPICSA4, respectively.

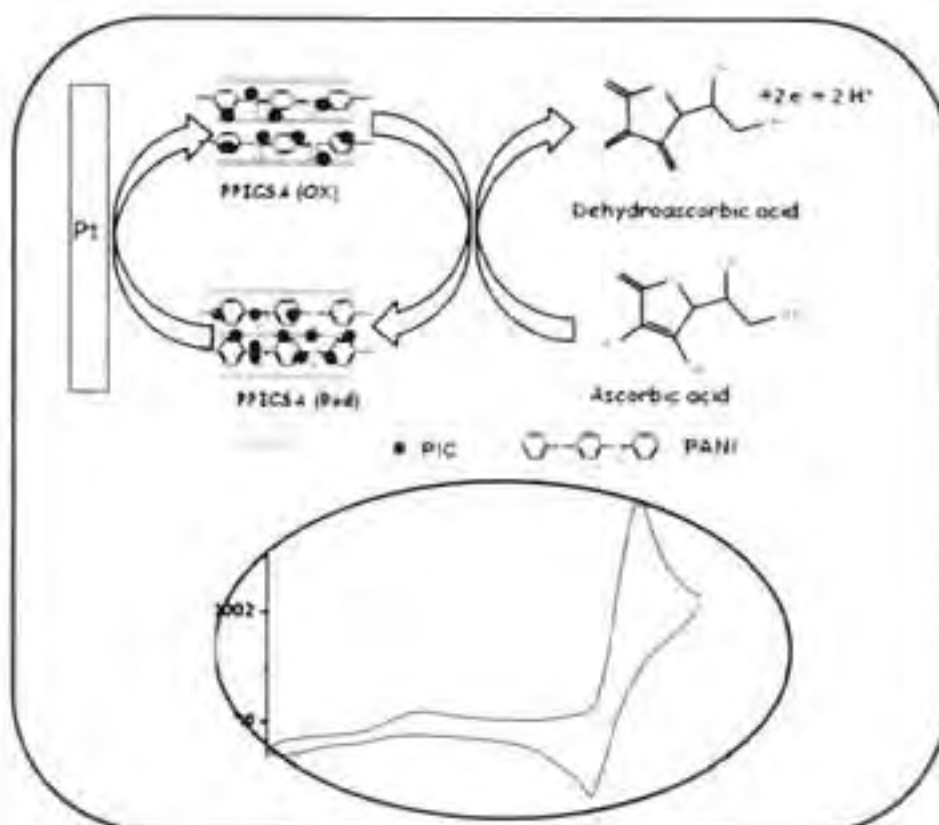
3.5.3. Description of Experimental Techniques.

Molecular weight of the samples were measured using MALDI - TOF mass spectrometer (AXIMA CFR, Shimadzu) equipped with a nitrogen laser emitting at 337 nm and α -cyano-4-hydroxy cinnamic acid as the matrix. Atomic absorption spectroscopy was done using Perkin Elmer model A Analyst 100 flame atomic

absorption spectrometer (Perkin Elmer Life and Analytical Sciences, Shelton, CT, USA). Elemental analysis was performed using Perkin Elmer elemental analyzer. PLM photographs were taken in an Olympus BX 51 microscope after drop casting the solution of sample in a clean dry glass plate. Transmission electroscopy was performed in a FEI, TEC NAI 30G2 S-TWIN microscope with an accelerating voltage of 100 KV. For TEM, SEM and PLM measurements, the sample solutions were prepared in aqueous dispersion under ultrasonic vibrator. For TEM, the solution is deposited on a Formvar coated copper grid and dried in vacuum at room temperature before observation. Surface area measurements were carried out in a Perkin-Elmer Shell sorptometer using nitrogen as the adsorbate at liquid N₂ temperature. DSC scans were performed using Dupont DSC 2010 differential scanning calorimeter attached to Thermal Analyst 2100 data solution under nitrogen atmosphere at a heating rate of 10 °C/min. Magnetic property measurements were made with a vibrating sample magnetometer (VSM). Powder samples were used to collect the hysteresis behaviour of nanoparticles at room temperature. The basis of the method is that a flux change is induced when a vibrating magnetic sample is placed within a uniform magnetic field. The detection coils measure a voltage, which is compared with the voltage of the reference sample. The difference between the two voltages is proportional to the sample's magnetic moment.

Chapter - 4

Development of Amperometric Sensor Based on Nanostructured Polyaniline-Polyhydroxy Iron Cation - Clay Composite Modified Pt Electrode for Ascorbic Acid



4.1. Abstract

Nanostructured polyaniline-polyhydroxy iron cation - clay composite modified platinum electrode has been developed as a novel sensor for ascorbic acid (AA). The performance characteristics of the electrode were studied with respect to response time, sensitivity, operational stability and storage life. The apparent surface concentration of PPICSA at PPICSA/Pt electrode and apparent surface electron transfer rate constant were calculated. Common possible interferences of the sample matrices were tested and the results revealed that the present electrode exhibited high selectivity towards AA. Detection limit of AA was found to be 10^{-2} M to 10^{-6} M. To the best of our knowledge, this is the first report on the amperometric sensor based on PPICSA/Pt electrode for the estimation of AA. Moreover, this unique low cost and user friendly sensor can be used for the analysis of AA present in food, beverages and pharmaceuticals.

4.2. Introduction

Nanostructured electrically conducting polymers immobilised with redox material have attracted considerable research attention due to their unusual commercial exploitation to sensors. They have emerged as promising candidates for high-performance transducer applications since they possess unique properties that are associated with high surface area and high surface-to-volume ratio (Huang *et al.*, 2004, Liu *et al.*, 2003, Wanekaya *et al.*, 2006, Huang *et al.*, 2007, Hatchett *et al.*, 2008, Kros *et al.*, 2002, Wang *et al.*, 2006, Wang *et al.*, 2004). They can exhibit excellent sensitivity via enhanced interaction between CP and the analytes. These nanostructured materials permit rapid adsorption/desorption kinetics for analytes, leading to fast response/recovery time and

increased signal intensity through variation of charge transport behaviour. Polyaniline, polypyrrole and other CPs as well as their derivatives have been reported to be used for constructing various electrochemical sensors (Huang *et al.*, 2004, Ramanaviciusa *et al.*, 2006, Malinauskas *et al.*, 2004, Partridge *et al.*, 2000). Among them, PANI has been widely employed due to its good stability, conductivity, pH and redox sensitivity (Krutovtsev *et al.*, 1992, Agbor *et al.*, 1995, Laranjeira *et al.*, 1997).

L-Ascorbic acid, better known as vitamin C, present in body fluids and also in cerebral fluids is one of the most important biological compound that take part in several significant biological processes, such as immune response, wound healing, and therapeutic purposes. It is a powerful anti-oxidant present in food and beverages, and is also a marker chemical in evaluating food deterioration and product quality. Furthermore, AA has been an object of increasing interest in the cosmetic industry for antiaging treatments (Dumas *et al.*, 1996, Pinnel *et al.*, 1985). In view of these several functionalities, estimation of AA has attracted great deal of attention in biomedical engineering, food and pharmaceutical industries (Aoki *et al.*, 1992). Presently, many analytical techniques like titrimetry, spectrophotometry, fluorimetry, chromatography, etc are used for its analysis (Barakat *et al.*, 1973, Lau M. *et al.*, 1987, Karayannis *et al.*, 1987, Huang *et al.*, 1995, Mall *et al.*, 1987). Generally these methods provide reproducible results with high sensitivity and good selectivity. However, all these analytical techniques require sophisticated instruments and chemical manipulation of sample before the measurement, which may be time consuming and inconvenient. Compared to other techniques, electrochemical analysis has the

advantages of simplicity, accuracy, reproducibility, specificity for various chemical species and is adaptable to even small sample volumes (Uchiyama *et al.*, 1992, Matsumoto *et al.*, 1993).

Literature showed that the catalytic oxidation of AA has been carried out at many mediator-modified electrodes. (Doherty *et al.*, 1995, Yu *et al.*, 1996, Facci *et al.*, 1982, Ueda *et al.*, 1982) Matos *et al.* measured AA in beers, soda, natural juices and commercial vitamin C tablets with a palladium-modified gold electrode (Matos *et al.*, 1998). Aoki *et al.* fabricated a micro multi-band electrode and measured its response to AA (Aoki *et al.*, 1992). Abdullin *et al.* have studied the oxidation of AA at prussian blue modified electrode (Abdullin *et al.*, 2002). Razmi *et al.* have studied the amperometric determination of AA at cadmium pentacyanonitrosyl ferrate film modified glassy carbon electrode (Razmi *et al.*, 2008). Among the various mediator modified electrodes, polymer modified electrodes have been widely used for the immobilization of mediators or enzymes (Ye *et al.*, 1989, Dong *et al.*, 1988, Wheeler *et al.*, 1989, Kang *et al.*, 1992, Tatsuma *et al.*, 1992). Usually, these electrodes exhibited a good stability and catalytic effects that results from their three-dimensional mediator distribution.

PPICSA is receiving importance as a modifier for Pt electrode since it is expected to exhibit excellent sensor efficiency arising from its nanodimension, electrical conductivity, redox property, environmental stability and improved economical efficiency. The presence of nanoclay is expected to facilitate the heterogeneous transportation of electrons between the analyte and the electrode surface and can also stabilize the functional materials from agglomeration (Mousty *et al.*, 2004). PIC is of great importance for their catalytic and sensor

applications due to the easily accessible $\text{Fe}^{2+}/\text{Fe}^{3+}$ redox couple and large number of unpaired electrons. Similar to PANI, the high spin PIC entity present in PPICSA can provide a favourable micro-environment for the direct transfer of electrons for the analyte with the electrode and thereby catalyse the electron transfer activity resulting in an increase in response current (Cao *et al.*, 2003). The nanostructured modifier PPICSA can contribute many unique properties such as large surface area, higher activity, excellent conformation stability, and better contact between analyte and the electrode (Katz *et al.*, 2004, Rossi. *et al.*, 2004). Thus, the PPICSA nanoparticle can provide an ideal remedy to the usually contradictory issues like minimum diffusion limitations, maximum surface area and high effective modifier loading apart from the redox chemistry of $\text{Fe}^{2+}/\text{Fe}^{3+}$ which can be explored for the oxidation of AA. When AA is added to the solution, it catalyses the electro-chemical reduction of Fe^{3+} moiety and increases the peak current proportionally to the increase in concentration of AA (Filho *et al.*, 2000).

The present work envisages the performance of PPICSA as a modifier for Pt electrode in an amperometric sensor for AA. Here, we are exploiting the catalytic efficiency and redox property of $\text{Fe}^{2+}/\text{Fe}^{3+}$ system, conductivity of nanostructured conducting PANI and enhanced electron transfer rate process imparted by nanoclay layers towards the AA assay. The performance characteristics of the electrode was studied with respect to surface concentration of PPICSA at the electrode, surface electron transfer rate, response time, sensitivity, operational stability and storage life. Common possible interference of the sample matrices were also tested for confirming the electrode's selectivity for AA.

4.3. Results and Discussion

4.3.1. Preparation and properties of PPICSA

Preparation and properties of nanostructured PPICSA is reported in the experimental section of chapter 3. PPICSA exhibits a simple redox chemistry of $\text{Fe}^{2+}/\text{Fe}^{3+}$ which was explored for the electrochemical assay of AA.

4.3.2. Electrochemical characteristics of PPICSA modified Pt electrode

Cyclic voltammogram of PPICSA was recorded in the potential range of -0.5 to 1 V starting from 0 V at a scan rate of 100 mVs^{-1} and is displayed in Figure. 4.1.

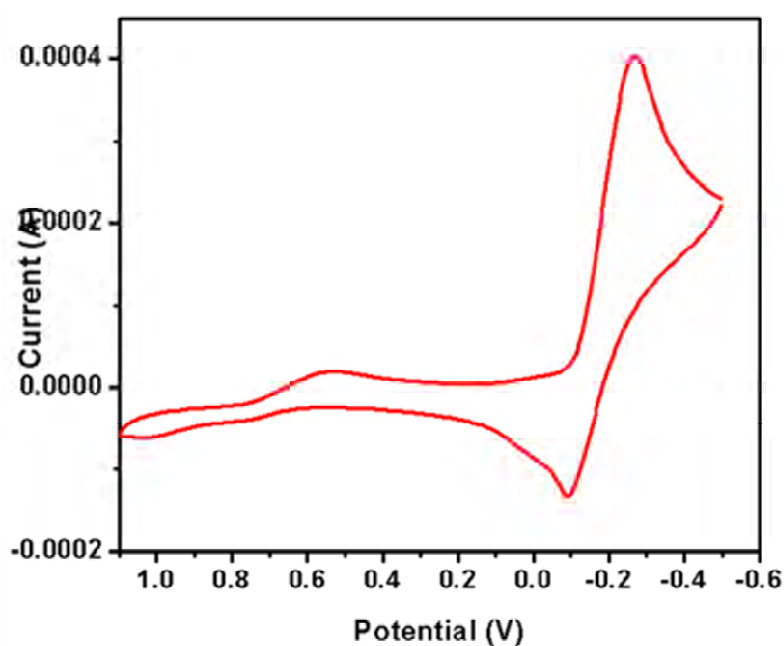


Figure 4.1. A typical cyclic voltammogram of PPICSA at Pt electrode

It exhibited two prominent peaks at 0.6 V and -0.32 V. Literature shows that polyaniline generally exhibits peaks around 0.8 V - 0.6 V and 0.2 V - 0 V corresponding to the conversion from pernigraniline to emeraldine state and emeraldine to leucoemeraldine state, respectively (Pruneanu *et al.*,1999). The broad peak at 0.6 V observed for PPICSA pertains to the oxidation of PPICSA

from pernigraniline to emeraldine state and the broadness indicates more sluggish charge transfer during the oxidation process (Pruneanu *et al.*, 1999). The sharp peak at - 0.32 V corresponds to the reduction of PPICSA, preferably $\text{Fe}^{3+}/\text{Fe}^{2+}$ couple. The sharpness reveals its high rate of electron transfer. Surface electron transfer rate constant and surface concentration of the PPICSA modified Pt electrode was evaluated by performing experiments in different scan rate ranging from 20 - 200 mVs^{-1} . Effect of the potential scan rate (v) on the peak reduction current (i_p) is shown in Figure. 4.2. As expected, the peak current increases with increase in scan rate. The difference between anodic potential (E_{p_a}) and cathodic potential (E_{p_c}) was observed to be 73 mV when the scan rate is 20 mV s^{-1} . With increase in the scan rate, the E_{p_c} shifts more towards the negative direction and E_{p_a} towards the positive direction resulting in an increased ΔE_p i.e., the peaks depart from each other with increase in scan rate. The increase in ΔE_p as a function of scan rate shows that the electron transfer reaction at the electrode/solution interface is reversible (Nalini *et al.*, 2000).

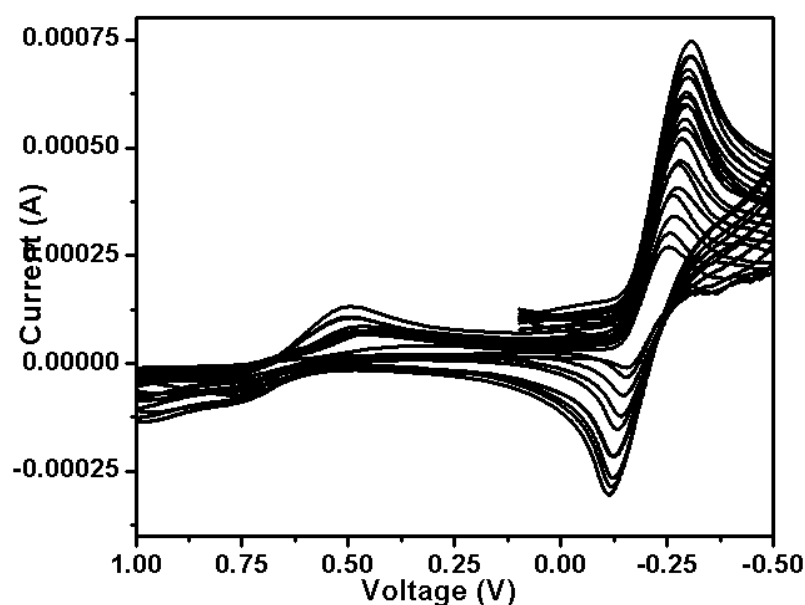


Figure 4.2. Cyclic voltammogram of PPICSA as a function of scan rate at Pt electrode

Charge transfer coefficient ' α '; was calculated as 0.6 from the equation

$$\Delta E_p = (RT / \alpha nF) [\ln v_1 - \ln v_2] \quad (1)$$

Where F is the Faraday's constant and ' n ' is the number of electrons transferred.

Introducing the ' α ' value in the Laviron equation (2) (Laviron *et al.*, 1977).

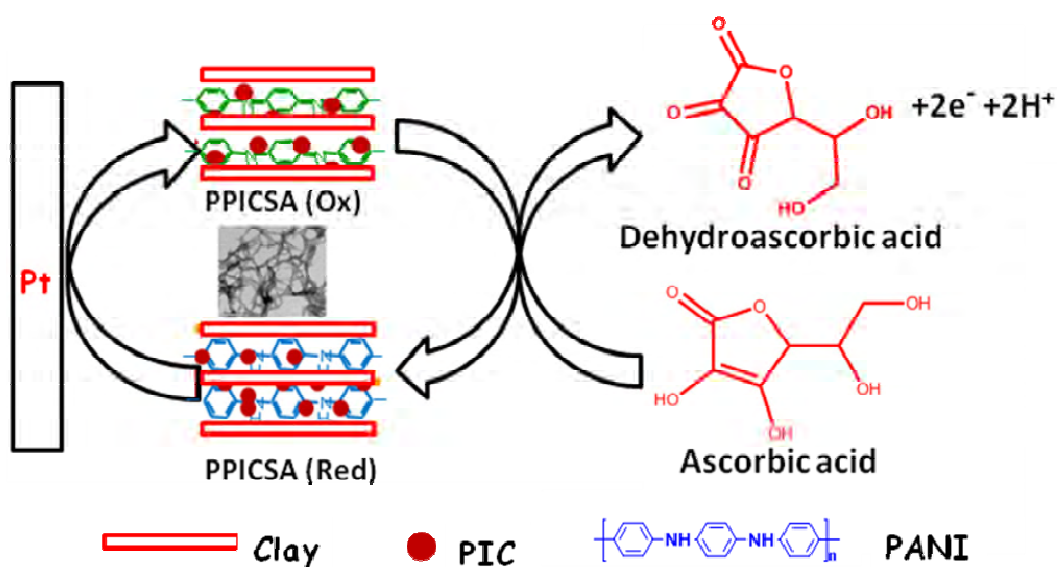
$$\log K^0_s = \alpha \log (1-\alpha) + (1-\alpha) \log (\alpha) - \log (RT / nFv) - \alpha (1-\alpha) \times nF\Delta E_p / (2.3 RT) \quad (2)$$

an apparent surface electron transfer rate constant $K^0_s = 0.12 \text{ s}^{-1}$ was estimated.

The surface concentration Q_r of PPICSA was determined by integrating the area under the cathodic peak. From the equation $I_p = n^2 F^2 \Gamma A v / 4RT$ and $Q_r = nFA\Gamma$, where n is the number of electrons, A the working electrode area (0.0707 cm^2), v scan rate (20 mVs^{-1}) and other parameters have their usual meanings, the surface concentration was calculated to be $6.9 \times 10^{-8} \text{ mol cm}^{-2}$ which is far greater than the reported value (Xu *et al.*, 1998 Kumar *et al.*, 2007).

4. 3.3. Estimation of AA

The schematic representation of the proposed electrode and its electrochemical reaction with AA is shown in scheme 4.1.



Scheme 4.1. Sequence of events that occur in PPICSA mediated AA sensor

The oxidation of AA at the bare electrode is irreversible and occurs at a high over potential of 0.4 V. The non reproducibility of the electrode response is due to the slow electron-transfer kinetics, presumably due to the fouling of the electrode surface by the oxidation product of AA at the bare electrode. Real analyte solutions, however, often contain a plenty of oxidizable species other than ascorbate, which can also be oxidized anodically at a relatively high electrode potential. Thus, the anodic current, concerned with electro-oxidation of these substances, can exceed anodic current response, concerned with electro-oxidation of ascorbate. So, it seems to be of considerably great importance to create electro-catalytically active electrode surface that could enable to lower the electro-oxidation potential of ascorbate up to an appropriate level. The oxidation of AA at the Pt/PPICSA electrode occurs at a lower potential of -0.32 V with a hike in the reduction current intensity. The negative shift of oxidation potential with increase in oxidation current of AA may be due to the favourable electrostatic attraction between the cationic PPICSA and anionic AA. Such an interaction would lead to the increase in reactivity of AA within the electrode. The significant variation in the voltammetric response of AA with PPICSA/Pt confirms the sensitivity of AA. The increase in current density is due to the enhanced transportation of electrons between Pt and AA, mediated by electromagnetic PPICSA. The effect of the potential scan rate (v) on the peak reduction current (i_p) has been investigated in the range 20- 200 mVs^{-1} . The plot of dependence of the catalytic peak current (i_p) on the square root of the scan rates showed linearity with a correlation coefficient of 0.965 and is shown in Figure 4.3.

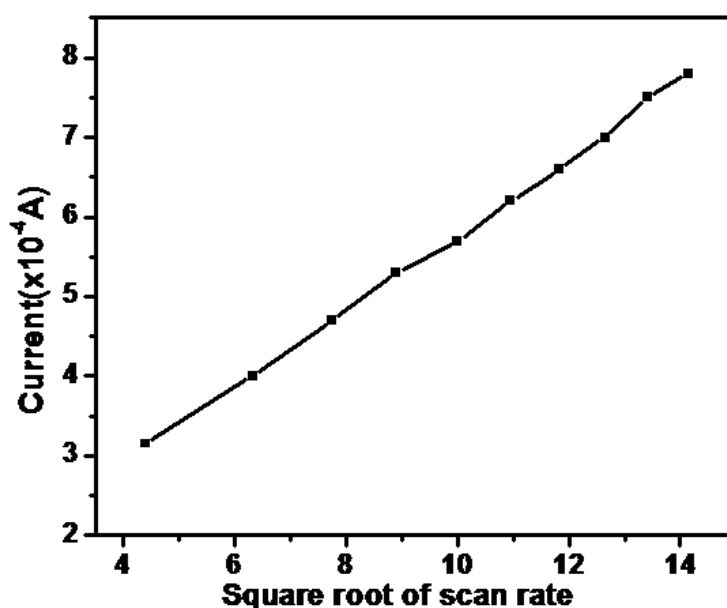


Figure 4.3. Linear relation of square root of scan rate with current

According to Fick's law, this can be concluded as diffusion controlled reaction rather than surface process (Huang *et al.*, 2007). Theoretically, electrochemical reaction of the analyte at the conducting polymer is complex and is associated with three processes:

- (i) diffusion of the analyte to the CP.
- (ii) reaction between the CP and the analyte and
- (iii) transfer of the charge within the CP

If the combination of relative rates of (ii) and (iii) exceeds the rate of (i), then the electrochemical reaction occurs at the analyte-CP interface and is a diffusion controlled process. This will result in acceleration in current intensity at a relatively low overvoltage. The same observation made by us further substantiate that the reaction of AA at PPICSA/Pt interface is diffusion controlled process. The number of electron-proton transfer taking place in aq. PPICSA/Pt electrode interface during AA oxidation is evaluated by plotting ΔE_p Vs $\ln v$ and is shown in Figure 4.4.

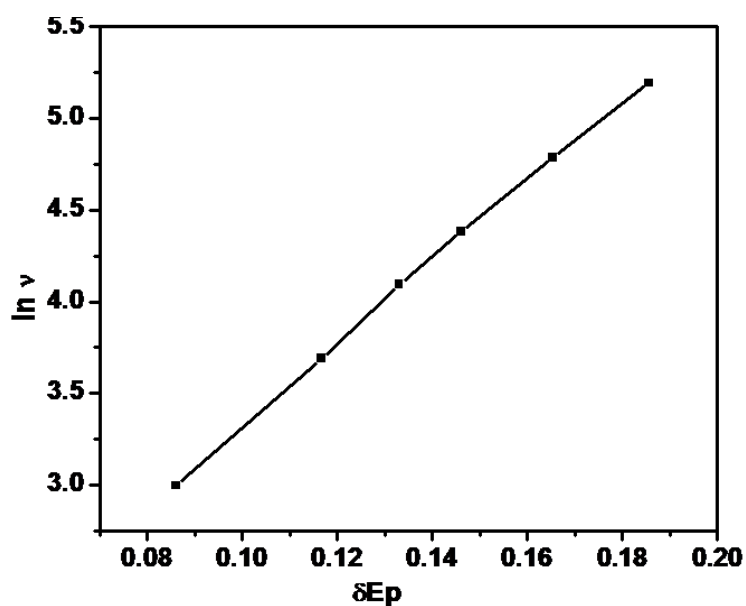


Figure 4.4. Logarithm of scan rate as a function of ΔE_p showing a straight line. Slope of the curve is measured as 22 mV which indicates that the oxidation is a two electron, two proton transfer process (Xu *et al.*, 1998, Castro *et al.*, 2001). Charge transfer coefficient and surface electron transfer constant was calculated as $\alpha = 0.5$ and $K_s = 0.55 \text{ s}^{-1}$, respectively. The addition of AA to PPICSA results in an increase in current at -0.32 V. Experiments were performed with increasing concentration of 1 mM AA from 100 – 700 μL . Linearity of the amperometric response of AA was checked by plotting current against concentration and is shown in Figure 4.5. which gave a straight line with a correlation coefficient of 0.998. Sensitivity of the electrode was checked by injecting known amount of AA and back calculating its concentration from the linear curve. Triplicate experiments were performed for checking the reproducibility of the results. Sensitivity was observed with a minimum relative standard deviation of 1-2 %. Such sensitivity may be ascribed due to the huge surface area, which would load more AA and would be advantageous to the transfer of the electron to the electrode.

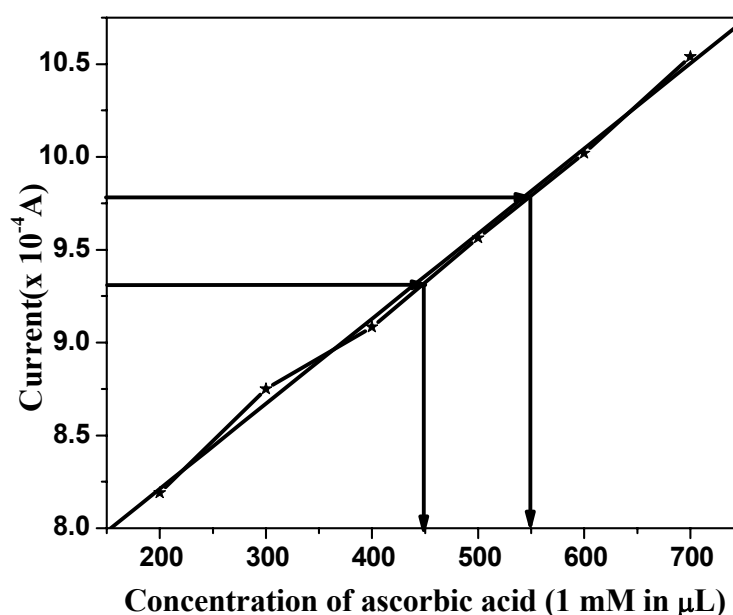


Figure 4.5. Variation in current intensity as a function of concentration of AA (1 mM) at PPICSA/Pt electrode

Response time was observed to be less than 15 seconds, proving the high catalytic efficiency of the PPICSA. In general the nanostructured PPICSA transduces as well as amplifies the signal and increases the electrode's sensitivity to AA assay. For determining the detection limit, cyclic voltammogram of AA at varying concentration ranging from 10^{-8} M to 0.1 M was done and the linearity of current response against concentration was obtained between 10^{-2} to 10^{-6} M. Therefore detection limit was determined to be 10^{-2} to 10^{-6} M.

4.3.4. Operational stability and shelf life

The electrode current showed stability during the continuous scanning between the potentials 1 V and -0.5 V for 50 cycles (Figure 4.6.) revealing that the electroactive species is highly active and its activity do not lose even after 50 cycles. Also when this modified electrode was swept in AA solution for a long time, no pollution phenomenon was observed. Thus, it is promising for further developing these sensors due to its easy-fabrication and stability.

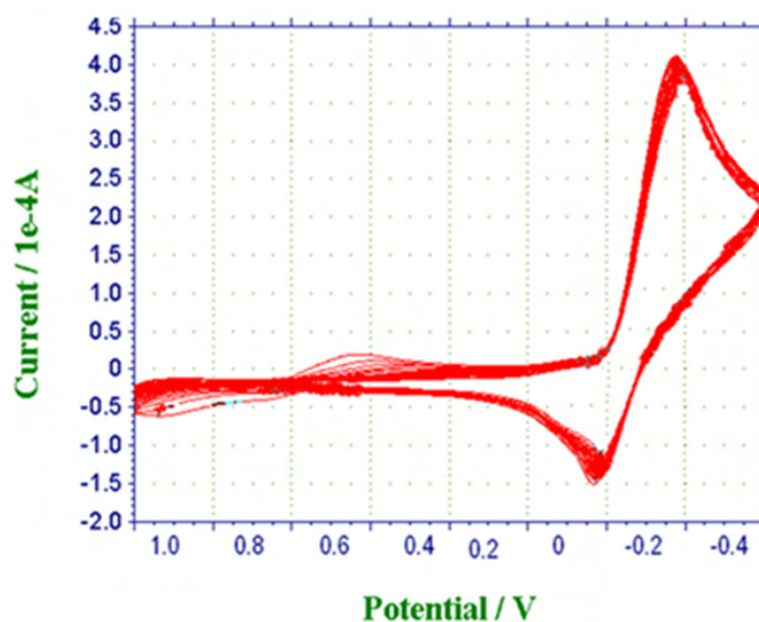


Figure 4.6. Electrochemical study of AA at PPICSA/Pt electrode for 50 cycles showing its reasonably good operational stability

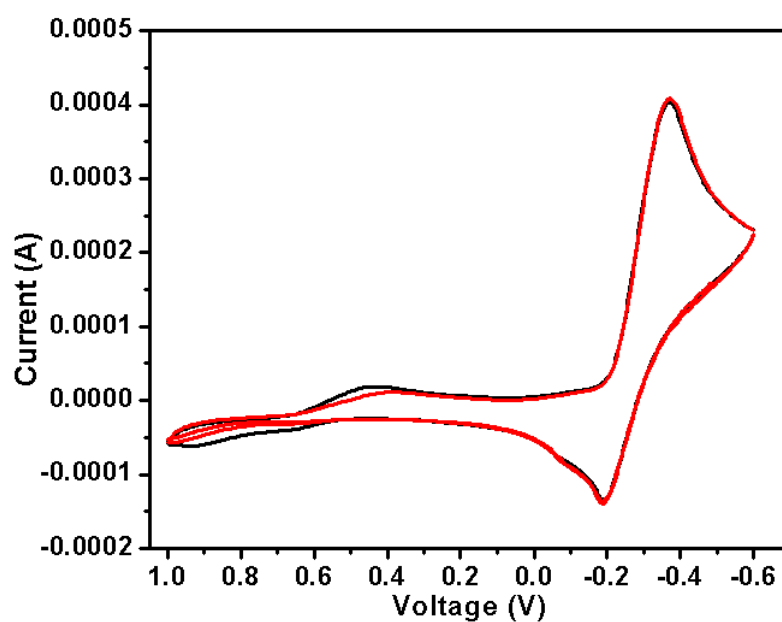


Figure 4.7. Cyclic voltammogram of PPICSA demonstrating its excellent storage stability

The electrochemical storage stability (shelf life) of the PPICSA/Pt electrode was a matter of investigation. The reproducibility of the results was tested by repeating the electrochemical process at various intervals of time within a month and comparing the intensity of the oxidation peak obtained with that of the initial

stage. All the trials resulted in the oxidation of AA at -0.32 V with least decrease in the background current (Figure. 4.7). These results substantiate the suitability of the PPICSA modified Pt electrode sensor to practical applications of the AA assay.

4.3.5. Effect of interference on the determination of AA

To evaluate the selectivity of the aq. PPICSA/Pt sensor, the effect of common potentially interfering compounds (organic acids, antioxidants and sugars) on AA were investigated and is shown in Figure 4.8.

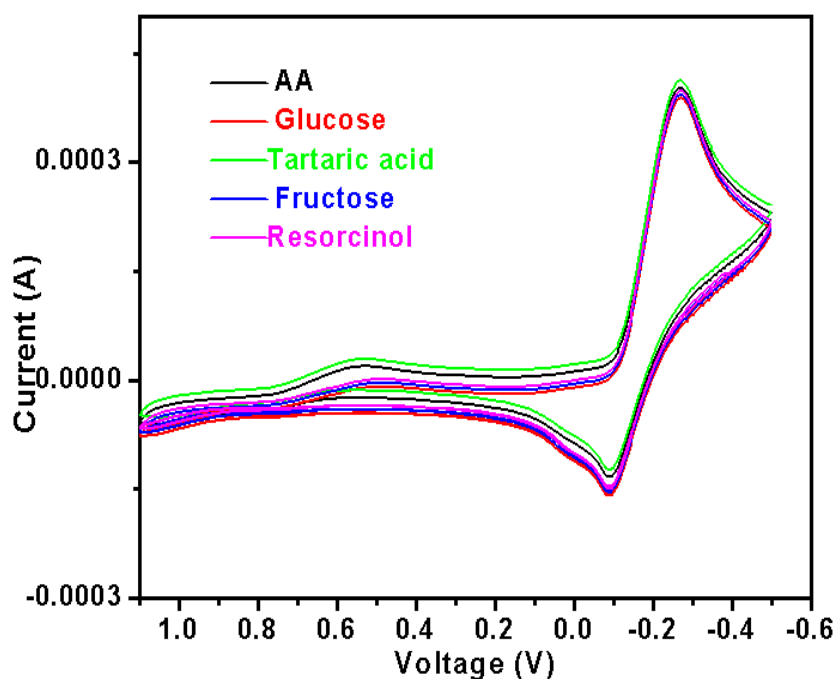


Figure 4.8. Effect of various possible interference towards the estimation of AA

Concentration higher than those of the natural levels expected in the food samples were tested by measuring the AA content of a 1 mM stock solution in presence of the potential interference like glucose, fructose, resorcinol and tartaric acid. Table 4.1. summarizes the percentage signal recovery of 1 mM AA in the presence of mM concentration of various interference. The average signal

recovery ranged from 95-102 %, indicating that the tested species do not cause much interference and thereby demonstrating the specificity and selectivity of the PPICSA sensor to AA over many interfering compounds.

Table 4.1. Recovery of AA in the presence of some possible interference at PPICSA/Pt electrode

Additive	Concentration (mM)	AA concentration (mM)	Current Intensity (mA)		Signal recovery (%)
			Before addition	After addition	
Glucose	1	1	0.4	0.38	95
Fructose	1	1	0.4	0.385	96.3
Tartaric acid	1	1	0.4	0.41	102
Resorcinol	1	1	0.4	0.39	97.5

4.4. Conclusions

In conclusion, we have developed a novel amperometric sensor based on aqueous PPICSA modified Pt electrode and studied its applicability for the assay of AA. Lower noise, better stability, good reproducibility and fast response time open wide possibility for its use in the field of sensors. The electrode exhibited excellent sensitivity, detection limit, good selectivity and antifouling properties. All these results suggest that this aq. PPICSA/Pt electrode will be a prospectable low cost and efficient amperometric sensor which can make promising and outstanding contribution in the food -beverage- medical industries.

4.5. Experimental Section

4.5.1. Materials and Methods

For the details about materials and preparation methods, see experimental section of chapter 2 and 3. Ascorbic acid, glucose, fructose, tartaric acid and resorcinol were purchased from Ranbaxy fine chemicals limited. All chemicals were of analytical grade and were used without further purification. Fresh sample solutions were used for each experiment.

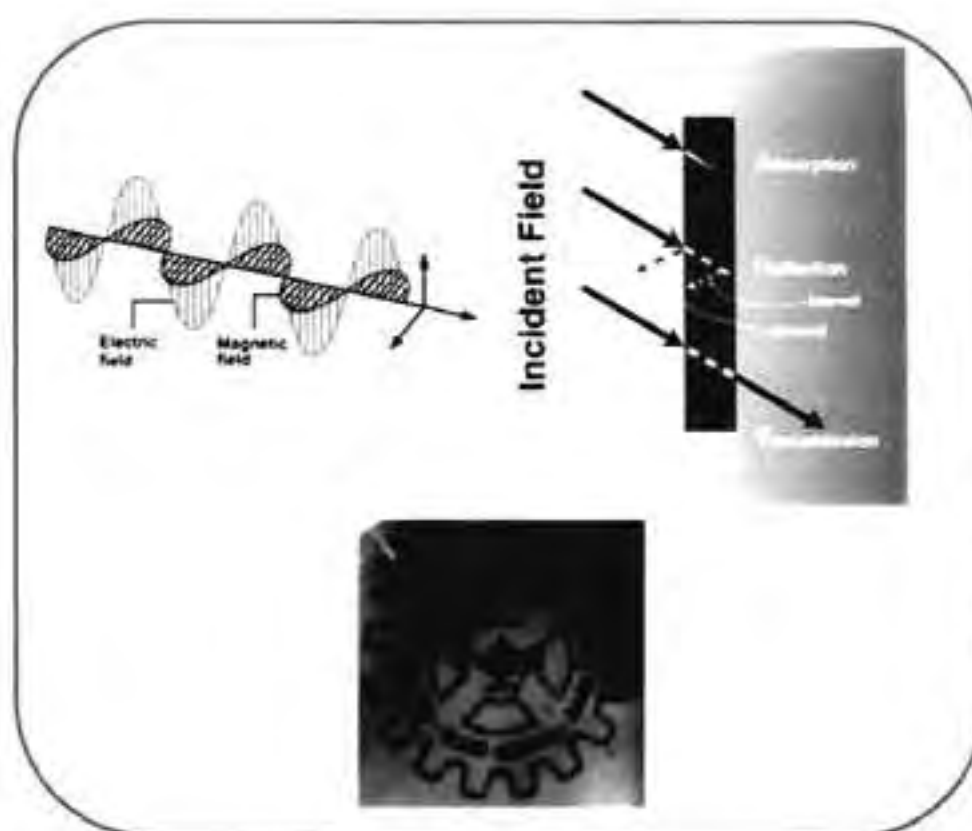
4.5.2. Preparation of PPICSA modified Pt electrode

Preparation of PPICSA is discussed in the experimental section of chapter-3. Cyclic voltammetric studies of PPICSA were performed in an Electrochemical CH Analyser. Experiments were done at ambient temperature in a one-compartment electrochemical cell with a three electrode system. Saturated Ag/AgCl electrode is used as the reference electrode and platinum wire with 0.5 mm diameter and 50 mm length were used as the auxiliary electrode. Pt electrode was modified by dipping in aqueous PPICSA dispersion (0.2M) and was used as the working electrode. Pt electrode was dipped in 50 % HNO₃ overnight and washed thoroughly before use. It was polished to a mirror finish using alumina powder (0.05 μ m) and washed with double distilled water. All the experiments were carried out at 25 \pm 5 °C. Experiments were performed with 10 mL 0.2 M PPICSA aqueous solution. Before performing the experiments, the solution was purged with nitrogen gas for 10 minutes. Cyclic voltammogram of PPICSA was performed between -0.5 V to 1 V starting from 0 V at particular scan rate. After the current achieved a steady state, cyclic voltammogram was recorded by adding aliquots of AA into the cell. For the electrochemical studies

involving estimation of AA, storage stability, operational stability and interference studies, fresh solutions were prepared.

Chapter - 5

- Preparation of Electro-Magnetic Blends of Polyaniline-Polyhydroxy Iron Cation- Clay with Polycarbonate and its Property Evaluation



5.1. Abstract

Electro-magnetic interference shielding material was developed from the composite of nanostructured polyaniline- polyhydroxy iron- clay and polycarbonate through solution blending process. The onset of percolation threshold concentration has been manifested from the morphological studies in combination with electrical conductivity measurements. Temperature dependent electrical conduction mechanism in the blend was found to follow 3D-VRH model. The interaction between the host matrix and nanofiller was studied by rheological property measurement and FT-IR spectroscopy. Blends were further characterized for EMI shielding efficiency and thermo-mechanical properties. All these measurements suggest that these transparent composite films can be used for the fabrication of EMI shielding/ electrostatic dissipation material for encapsulation of electronic devices and as electrostatic material for high technological applications.

5.2. Introduction

Nanostructured multifunctional electro-magnetic materials have attracted a great deal of attention for their potential applications in various fields such as electromagnetic interference (EMI) shielding, antistatic coatings, chemical sensors, transducers, and corrosion protection coatings (Li *et al.*, 2006, Sudha *et al.*, 2009). EMI shielding essentially depends on the conductivity and magnetic property of the materials for various applications. It is known that the conducting material can effectively shield electric component of an electromagnetic waves whereas, only magnetic materials can shield effectively the magnetic component of an electromagnetic waves. Thus materials having dual property of conductivity and magnetic properties are most suitable for EMI

shielding applications. High thermo-mechanical properties are also expected for electromagnetic materials for high technological applications. Moreover, according to the electromagnetic wave percolation theory, if the dimension of the conductive filler is in nanometer regime and retains a high aspect ratio, it easily forms a conductive network at low concentration of the filler with high mechanical strength. Thus the preparation of PPICSA is important since it is a novel guest-host system consisting of exfoliated/intercalated nano clay layers having high aspect ratio, dispersed in nanomagnets encapsulated conducting PANI and is comprised of electric, magnetic and thermo mechanical property in a unique material system. But the problem with these materials is its cost and low processability. To make EMI shielding products viable, composites have been fabricated by blending them with compatible and mechanically sound conventional polymers (Cao *et al.*, 1992, Pud *et al.*, 2003). The conventional polymer, poly(bisphenol A carbonate) (PC) is receiving great attraction for the fabrication of composite for high technological applications because of its excellent processability, transparency, mechanical properties, good adhesion to other materials, good dimensional and thermal stability (Jeevananda *et al.*, 2001). Electrically conductive composites of PC with conducting polymers like PANI and PPy are interesting since it can exhibit low percolation threshold concentration arising from hydrogen bonding interaction between these polymers (Wang *et al.*, 1990, Roy *et al.*, 1998, Lee *et al.*, 2000).

Several strategies were reported for blending conducting polymers with conventional polymers which include solution blending and melt blending. Apart from these, our group (Sudha *et al.*, 2010) have used a one step surfactant

micelle induced emulsion polymerization strategy for the preparation of conductive composite of polyaniline-clay nanocomposite –polystyrene (PS) using the amphiphilic dopant, PDPSA. There are many reports on the use of functionalized protonic acids to dope PANI EB to make it processable (Cao *et al.*, 1993). These functionalized acids having long alkyl chains can increase the solubility of PPICSA in common organic solvents and can induce compatibility through plasticization with other polymer matrices (Heeger *et al.*, 1993).

The EMI attenuation offered by a shield may depend on three mechanisms: the reflection of the wave from the shield, the absorption of the wave as it passes through the shield and the multiple reflections of the waves at various surfaces or interfaces within the shield. The multiple reflections, however, requires the presence of large surface areas (e.g. a porous or foam material) or interface areas (e.g. composite materials containing fillers that have large surface area) in the shield. Thus the composite prepared with PPICSA and PC is expected to be a perfect candidate as an EMI shielding material, since they can shield the electromagnetic wave through all the three mechanisms.

Thus the objective of the present work is to prepare composite films of nanostructured electro-magnetic PPICSA in PC matrix through solution blending process. The prepared blends were characterized for electrical conductivity, percolation threshold concentration, rheological property, morphology, EMI shielding efficiency and thermo-mechanical properties.

5.3. Results and Discussions

Nanostructured electro-magnetic PPICSA was prepared by the oxidative emulsion polymerization of anilinium salt of PDPSA as reported in the experimental section of chapter 3.

Electro-magnetic PPPC composites were prepared with varying ratio of PPICSA to PC. The PPPC composites with 5, 10, 15, 20, 25 and 30 wt % of PPICSA in the composites were designated as PPPC1, PPPC2, PPPC3, PPPC4, PPPC5 and PPPC6, respectively. Visual inspection of the PPPC blends showed transparent film of emeraldine green color whose color intensity increased with the concentration of PPICSA. A representative film of PPPC is shown in Figure 5. 1.



Figure 5.1. Transparent green film of PPPC blend

5.3.1. FT-IR spectroscopy

Most of the peaks of PC and PPPC in FT-IR spectra overlap as shown in Figure 5.2. The band at 1770 cm^{-1} in the spectrum of PC shifted to a lower frequency by about 8 cm^{-1} in PPPC and was seen to bifurcate confirming the hydrogen bonding interaction between -NH of polyaniline and -C=O of PC as represented in the scheme 5.1. (Cao *et al.*, 1993).

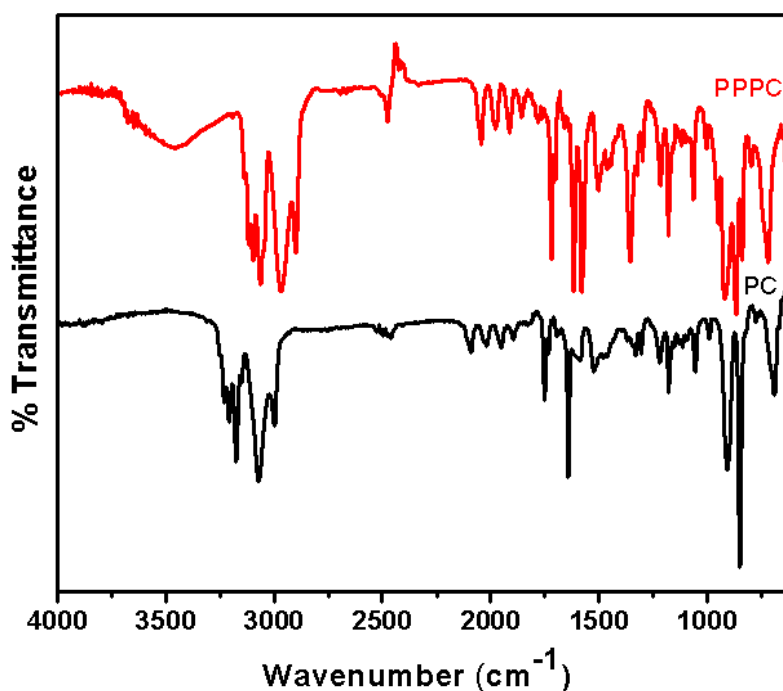
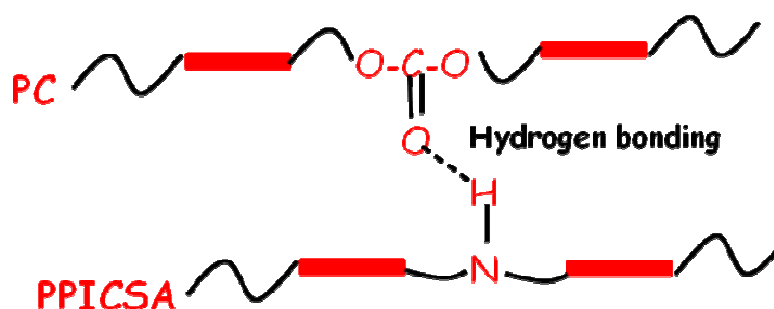


Figure 5.2. FT-IR spectra of PC and PPPC



Scheme 5.1. Schematic representation of hydrogen bonding between PC and PPICSA

5.3.2. Electrical Conductivity and conduction mechanism

Electrical conductivity is the most sensitive method to monitor the continuity of the conductive filler phase within the host matrix. The low value of percolation threshold is an important criterion in the preparation of the conductive blend of polyaniline and insulating polymer as to minimize processing problems and depletion of the mechanical properties of the host-insulating polymer. Table 5.1. summarizes the conductivity values corresponding

to the various composition of the blend. PC is an insulative polymer having conductivity in the range of 10^{-12} S/cm. It was observed that the electrical conductivity can be controlled in a wide range by changing the amount of conducting PPICSA. Electrical conductivity of PPPC showed values 5×10^{-9} , 2.1×10^{-3} , 2.3×10^{-3} , 2.4×10^{-3} , 2.5×10^{-3} and 2.7×10^{-3} S cm^{-1} by the addition of 5, 10, 15, 20, 25 and 30 wt % PPICSA, respectively. Such an unpredictable enhancement in electrical conductivity at 10 wt% PPICSA could be explained by the formation of percolated structure of PPICSA in PPPC. The particular concentration at which there is sharp increase in conductivity can be termed as percolation threshold concentration (Yan *et al.*, 2005). This can be taken as the point where the material changes from insulating phase to conducting. At the threshold concentration, the isolated conducting PPICSA in the PC matrix is bridged by a conducting channel of PPICSA, forming an interconnected network, which results in the abrupt increase in conductivity and thus generating continuous conducting paths. On further increasing the PPICSA concentration, the conductivity channels become wider and the conductivity further increases even though the increase is marginal. Onset of percolation is further strengthened by the morphological observation under PLM, SEM and AFM and is described in the morphology characterization section.

In order to study the electronic transport behavior of the material, the conductivity of the materials as a function of temperature was measured over the range of 303-393 K and is shown in Figure 5.3. The conductivity initially increased with increase in temperature and then decreased which is characteristic to a semiconductor.

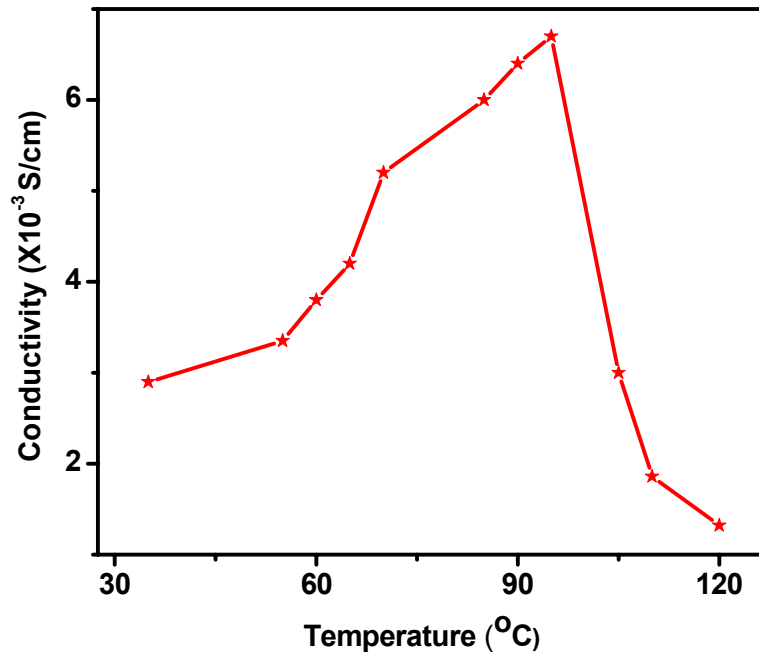


Figure 5.3. Temperature dependant conductivity of PPPC6 blend

According to Arrhenius equation,

$$\sigma = \sigma_0 \exp\left[-\left(\frac{E}{kT}\right)\right] \text{----- (1)}$$

Where E is the thermal activation energy during polaron conduction and σ_0 is a parameter depending on the semiconductor nature. Arrhenius plot of the measured conductivity (σ vs. $1/T$) was made and was observed to be deviating from the straight line and therefore deviates from Arrhenius equation which is typical for simple semiconductors. But it has been observed that the data is fitting to variable range hopping model (VRH) of localized polarons at low temperature according to the equation (2)

$$\rho(T) = \rho_0 \exp(T_0/T)^m \text{----- (2)}$$

Where ρ_0 is the pre- exponential factor and T_0 , the Mott characteristic temperature (Mott, 1978). This can be obtained from the slope of $\ln \rho(T)$ Vs T^{-m} plot.

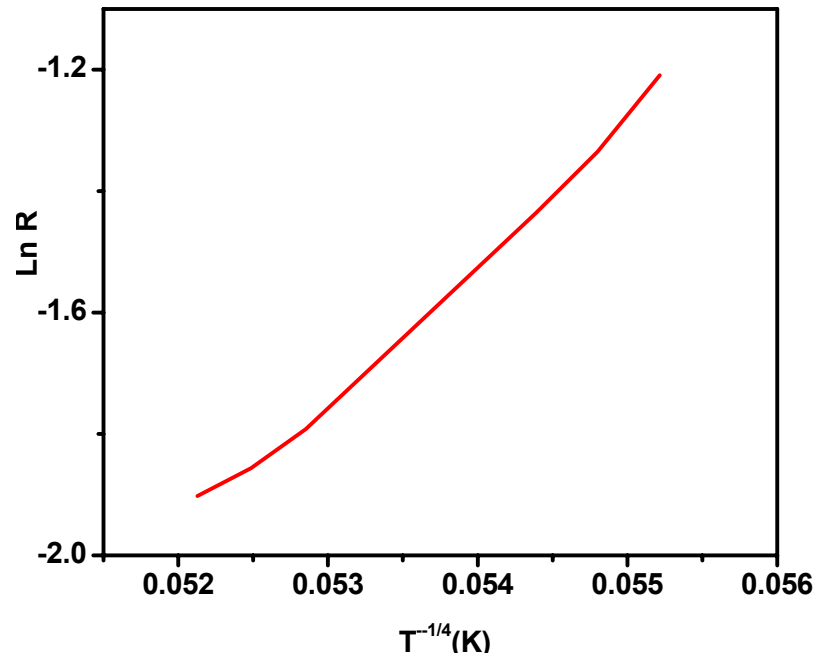


Figure 5.4. 3D VRH curve of PPPC6 blend

The value of the exponent 'm' depends critically on the nature of hopping process. The exponent $m = 1/4$, $1/3$ and $1/2$ for 3D, 2D and 1D hopping, respectively. In order to obtain the exponent m with more accuracy, a plot was made with $\ln \rho$ Vs T^{-m} with m value $1/4$, $1/3$ and $1/2$ and the best fit was obtained for $m = 1/4$ and the plot of $\ln \rho$ Vs $T^{-1/4}$ is given in Figure 5.4. The plot exhibited linearity and therefore followed 3D-VRH model. T_0 values derived from the slope was found to be 226 K.

5.3.3. Morphology of PPPC

Morphology of PPPCs was studied using PLM, SEM and AFM for monitoring the onset of percolation threshold concentration and also checking the compatibility of PPICSA with PC. Figure 5.5 shows the PLM micrographs of PPPC composite films taken with different weight ratios of PPICSA in PPPC at a magnification of 20X.

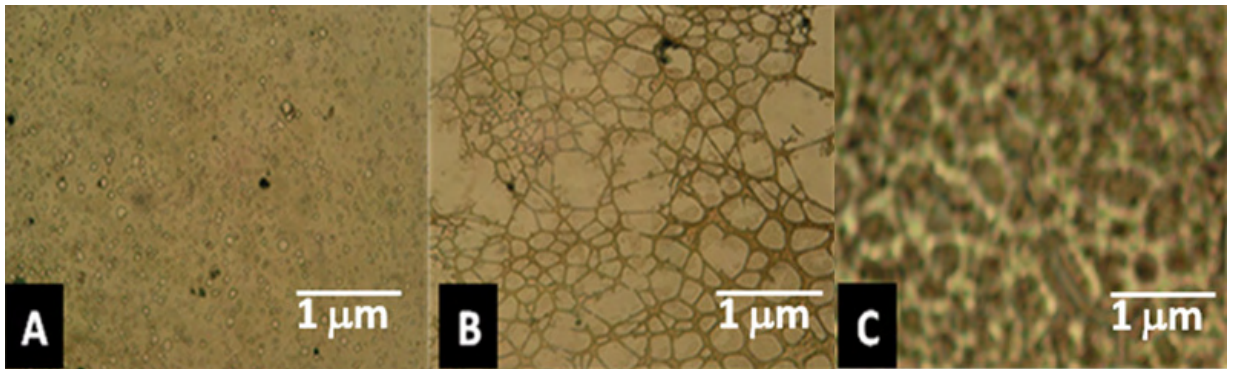


Figure 5.5. Polarized light micrographs of PPC blends with (A) 5 wt% PPICSA, (B) 10 wt% PPICSA and (C) 15 wt% PPICSA showing the percolation network formation

The PLM picture of PPC with 5 wt % loading of PPICSA is given in Figure 5.5. A. In the micrograph, the dispersed phase of PPICSA appears to exist as isolated globules which are mostly surrounded by the insulating matrix. On increasing the weight percentage of PPICSA in the composite, the dispersed PPICSA in PC matrix also increases and at 10 wt% loading of PPICSA, it exhibited a percolated structure (Figure 5.5.B). On further increase in PPICSA, thick network structure was observed (Figure 5.5.C) which tends to form organized aggregates of fibrillar morphology. Further the onset of percolated threshold concentration (PTC) formation of PPICSA in PPC blend was further studied by observation under SEM and AFM.

Figure 5.6. represents the SEM and AFM micrographs of PPC containing 10 wt % PPICSA. The observation made was complimentary to that obtained from PLM. Interconnected network formation could be observed in both SEM and AFM. Bright portion in the SEM micrograph indicated the presence of electromagnetic filler and black portion, the matrix polymer.

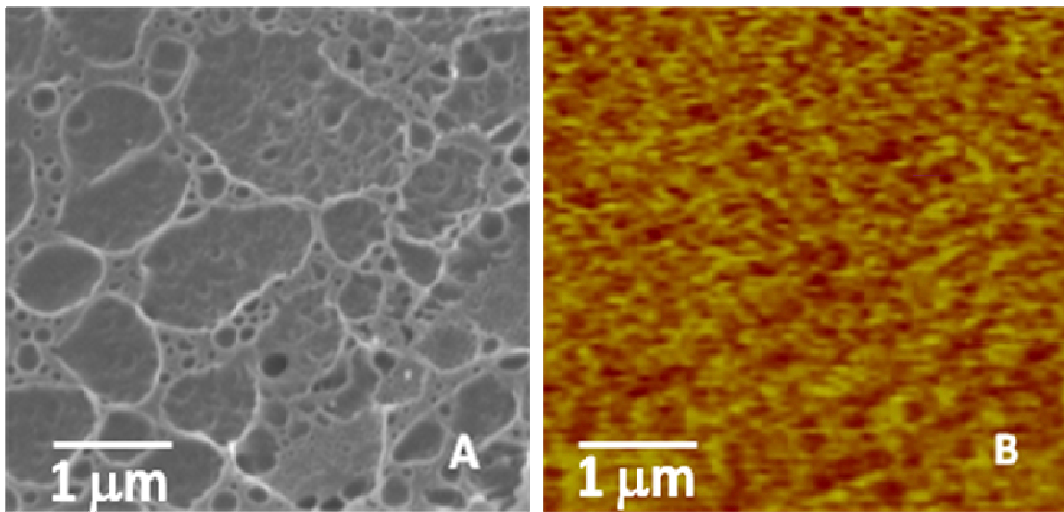


Figure 5.6. SEM and AFM figures of PPC blend at percolation threshold concentration

5.3.4. Rheological Properties

The presence of exfoliated nanoclay and the interaction between the conductive filler host matrix were manifested from the rheological property measurements. The dynamic oscillatory measurements of the conductive blends were carried out under angular frequency sweep. Loss modulus (G'') and storage modulus (G') were measured as a function of frequency at 170 °C under angular sweep of 1-100 rad /s at 5% strain and is shown in Figure 5.7. The G' is related to the ability of the material to store energy when an oscillatory force is applied to the specimen and the G'' is related to the ability to dissipate the energy. These properties were measured to examine the degree of filler- host matrix interaction in the conductive film. Solid like behavior ($G' > G''$) could be observed from the dynamic oscillatory responses. The G' value of PC and PPC measured at 10 rad/s are 10.9 KPa and 15 KPa, respectively. PPC exhibited enhanced storage modulus when compared to PC which may be attributed to the interaction between the PPICSA and PC. It was observed from the plot that PPC

showed a frequency of 2.06 rad/s for the intersection of G' and G'' while neat PC showed an obviously higher value of 4.56 rad/s. This may be due to the dramatic exfoliation of clay into nanometer scale and also due to the interaction between the nano clay layers and the primary particles contributing to shear thinning as reported by Acierno and coworkers (Fillipone *et al.*, 2008).

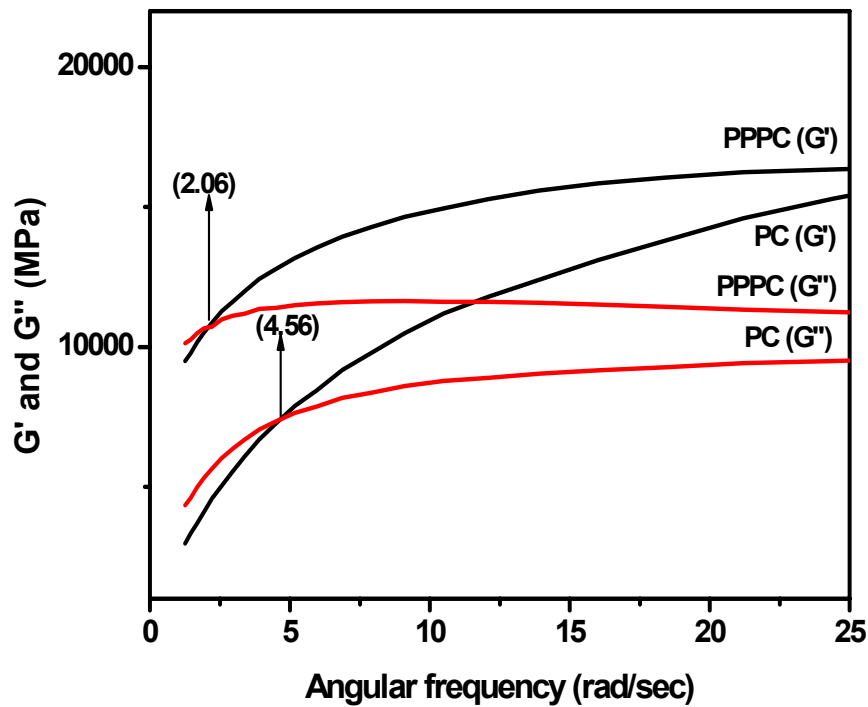


Figure 5.7. Plot of storage modulus and loss modulus vs. angular frequency

5.3.5. Thermal Stability

Thermal stability of PPC and PC were studied by thermogravimetry and is shown in Figure 5. 8. Both PPC and PC showed a small weight loss below 100 °C presumably caused by the loss of solvent and low molecular weight volatile impurities. The second stage weight loss occurs at 411°C in PC corresponding to the decomposition of the polymer. In PPC, the decomposition temperature was observed at 422 °C. The higher decomposition temperature observed for PPC compared to PC can be due to the hydrogen bonding interaction existing

between PPICSA and PC and also due to presence of nanoclay particles with high aspect ratio which may hinder the degradation process by providing a barrier to preclude evaporation of small molecules generated during the thermal decomposition process. According to Zanetti and coworkers (Zanetti *et al.*, 2007), the barrier effect of the clay increases during volatilization because of the reassembly of the silicate layers on the polymer surface during the thermal decomposition.

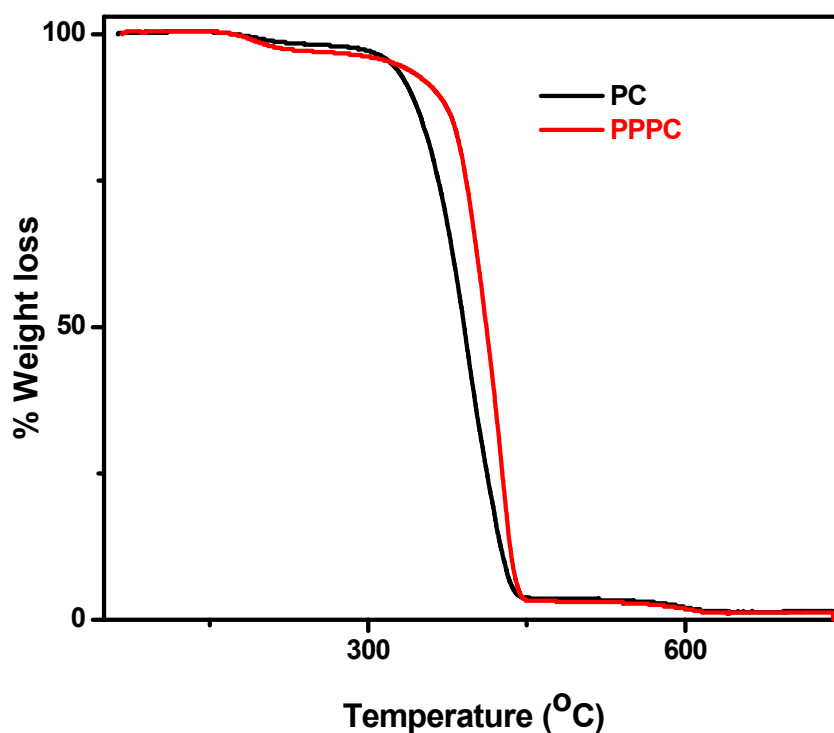


Figure 5.8. TG plots of PC and PPPC blends

Thermal phase transition temperature of PC and PPPC were studied by differential scanning calorimetry and is shown in Figure 5.9. PC exhibited an endothermic peak at 145 °C which corresponds to its glass transition temperature (T_g) and another around 418 °C corresponding to the decomposition of PPPC, while DSC curve of PPPC showed T_g at 110 °C and

decomposition at 426 °C. The results were found to be in agreement with the TG data.

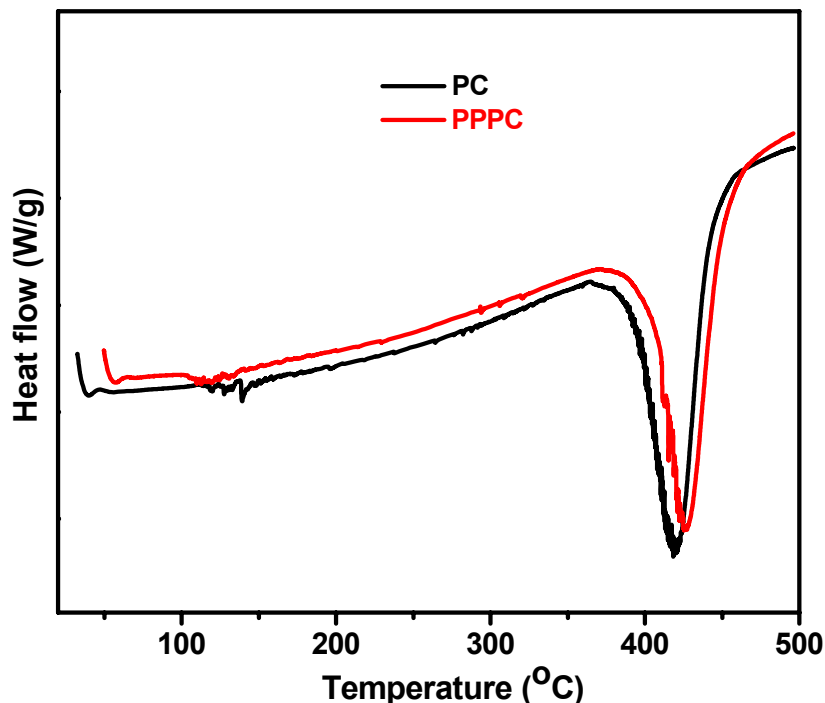


Figure 5.9. DSC plots of PC and PPPC blends

5.3.6. Mechanical testing

Mechanical properties of the PPPC blends were measured with uniform size strips of their films as per the ASTM standard procedure. Effect of amount of conductive filler on the ultimate tensile strength was measured and is shown in Table 5.1. PC showed ultimate tensile strength (UTS) of 17 MPa and elongation at break at 230%. Generally, the ultimate tensile strength and elongation at break decreased by the addition of conductive fillers indicating that the conductive components are slightly incompatible with the PC matrix despite the nature of the counter ion used for the protonation. But the UTS and elongation at break of these PPPC films showed positive variation in presence of the PPICSA. It exhibited UTS and elongation at break of 17.18 (232%), 18.1 (232%), 18.2 (235%), 18.5 (236%), 18.7(236%) and 18.7 (236%), respectively. The higher

value observed for nanocomposites is due to the presence of exfoliated nano clay having high aspect ratio and also due to the excellent compatibility induced by the amphiphilic dopant (Guilherme *et al.*, 2001).

Table 5.1. Electrical Conductivity and mechanical property of PPC blends

Sample	PPICSA/PC (% weight ratio)	Electrical Conductivity (S/cm)	Tensile strength (Mpa)	Elongation at break (%)
PC	0:100	5×10^{-12}	17	230
PPPC1	5:95	5×10^{-9}	17.18	232
PPPC2	10:90	2.1×10^{-3}	18.1	232
PPPC3	15:85	2.3×10^{-3}	18.2	235
PPPC4	20:80	2.4×10^{-3}	18.5	236
PPPC5	25:75	2.5×10^{-3}	18.7	236
PPPC6	30:70	2.5×10^{-3}	18.7	236

5.3.7. EMI shielding

EMI SE of the conductive films was measured as per the standard procedure (Wang *et al.*, 2005). EMI SE can be taken as the ratio of the field strength of the electro-magnetic wave before and after attenuation. It was observed that as the amount of filler loading was increased, SE also increased. When irradiated with electromagnetic radiation of 8.5 GHz, the SE of conductive films were measured to have values: 24 dB (5% PPICSA), 28 dB (10%), 30 dB (15%) and 30 dB (30%), respectively and the details are summarized in Table

5.2. The conductive films containing PPICSA can attenuate electromagnetic radiation by three mechanisms of absorption, reflection and multiple reflections. Absorption loss is caused by the energy loss under the action between magnetic and electric dipole present in the shielding material and the electromagnetic field. Reflection due to the magnetic polyhydroxy iron species and the multiple reflection loss due to the presence of porous/multiple layered clay present in the shielding material which contribute large surface/interface area for multiple reflections. Higher the SE value, the less energy passes through the sample.

Table 5.2. EMI SE details of PPPC blends

Sample	PPICSA/PC (% weight ratio)	EMI SE (dB)
PC	0:100	-
PPPC1	5:95	24
PPPC2	10:90	28
PPPC3	15:85	30
PPPC6	30:70	30

5.4. Conclusion

We have successfully developed electromagnetic interference shielding material from the conductive composite of PC and nanostructured electromagnetic PPICSA. The onset of percolation threshold concentration was manifested from the studies made from electrical conductivity and morphology. Temperature dependant electrical conduction mechanism in PPPC was found to

be following 3D variable range hopping. The superior rheological properties exhibited by conductive blends containing clay nanocomposites can be explained due to the presence of the nanoclay primary particles and the strong interfacial interactions between the doped PPICSA and clay platelets present on the former. EMI SE and thermo mechanical measurements suggest that these materials can be used as a prospectable candidate for the encapsulation of electronic devices for high technological applications

5.5. Experimental Section

5.5.1. Materials and Methods.

Preparation and properties of PPICSA is given in chapter 3. Polycarbonate was purchased from GE plastics, India. ($M_w \sim 50,000$ g/mol, $T_g = 150$ °C). Chloroform (A.R. grade) is purchased from s.d fine chemical and was used without further purification.

5.5.2. Preparation of electro-magnetic blends of PPICSA/PC (PPPC)

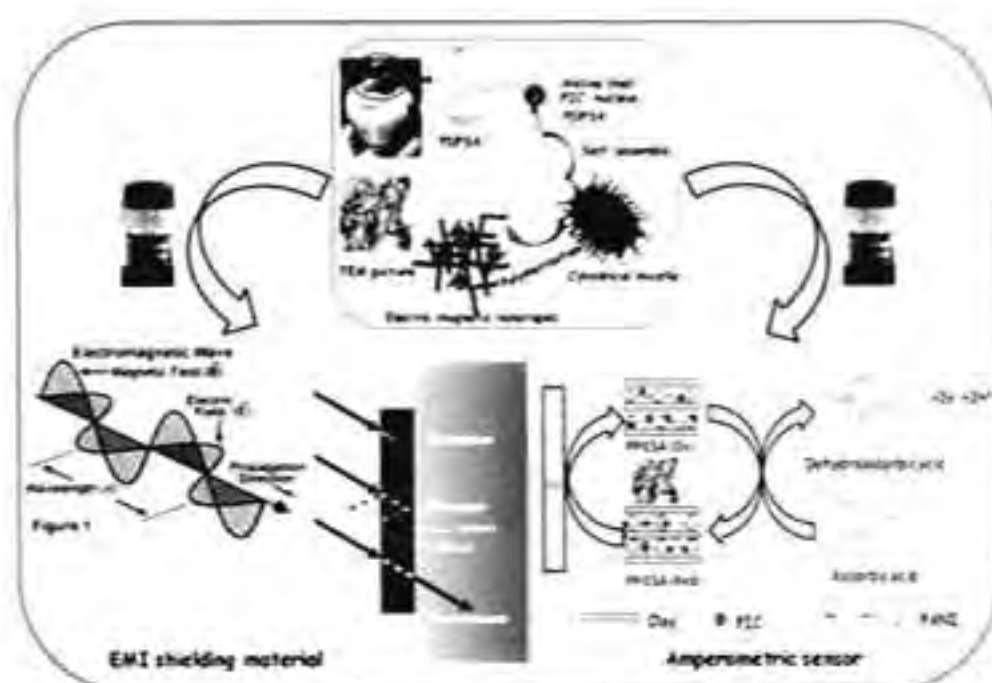
PPICSA was prepared as per the procedure reported in chapter 3. Electrically conductive blends of PPPC were prepared via solution blending. Stock solutions of PPICSA (5% wt/vol) and PC (5% wt/vol) in chloroform were prepared separately. The PC solution and the PPICSA solution were mixed at different proportions and blended by subjecting to mechanical stirring for 2 h. Films were casted on a glass plate from solution and dried under slow evaporation and finally under vacuum for 48 h.

5.5.3. Description of experimental Techniques

Atomic force microscopy (AFM) images were recorded under ambient conditions using Ntegra multimode Nanoscope IV operating in the tapping mode

regime. Micro fabricated silicon cantilever tips (MPP-11100-10) with a resonance frequency of 284-299 kHz and a spring constant of 20-80 Nm⁻¹ were used. The scan rate varied from 0.5 to 1.5 Hz. SEM and PLM experiments were performed with films casted from chloroform solution and the details of the instrumentation is same as explained in chapter 3. Rheological properties of the conductive blends were measured using Modulated Compact Rheometre-150 Physica (Germany) in dynamic oscillatory mode at 170 °C (frequency range 0.001–1000 rad/s). In all the rheological tests the parallel plate sensor with a diameter of 50 mm and a gap size of 0.25 mm were used. Tensile tests of the PC and PPICSA composites were conducted using dumb-bell shaped samples of width 4 mm and thickness in the range 1.5-2 mm. The measurements were carried out in an Instron universal testing machine. HTE-5KN Load cell is used and calibration done as per the ASTM procedure D 638 at a cross head speed of 2 mm/min at room temperature. EMI SE measurements were carried out with Schwartz EMI receiver with anechoic chamber using wave power receiving set up consisting of pyramidal horned antenna. The SE was measured using an X-band wave guide as a sample holder by noting the power with and without the samples by placing them near to the surface of the antenna. Samples having a thickness of 2 mm were used during measurement.

Summary, Conclusions and Future Perspective



Summary and Conclusion

Development of nanostructured electro-magnetic polymer composites from inorganic- organic hybrid guest-host systems invokes new interests and opportunities in high technological areas. They are receiving considerable attention for their potential applications in various fields such as electro-magnetic interference shielding, antistatic coatings, chemical sensors, magnetic recorders, catalysis, corrosion protection coating, and electro chromic devices and so forth since they exhibit electrical conductivity, magnetic property, excellent thermo-mechanical properties and processability in a unique system. Physical morphology, size etc. of the composite are very important for defining their properties such as electrical conductivity, magnetic behaviour, catalytic effects, microwave absorption etc. Hence to exploit the full potential of the technological application of these materials, it is important to make a systematic study for addressing all these problems.

Development of polyaniline- clay nanocomposite was receiving importance since it could exhibit excellent electrical conductivity with superior thermo-mechanical properties with low loading of PANI. Effect of structure and functionality of amphiphilic dopant on the physical morphology, electrical conductivity, thermal stability of PANIs and PANICNs were investigated by preparing them using six structurally different amphiphilic dopants like DBSA, pTSA, PDPSA, NSA, CSA and SA. Studies revealed that the rigidity and functionality of the dopant has got profound influence on the electrical conductivity, morphology, thermal stability and phase transition temperature of

PANIs and PANICNs. The difference in morphology observed in PANIs and PANICNs were due to the change in functionality of the dopant and the modes of self assembling arising from the combination of various non-covalent interactions like inter-molecular hydrogen bonding, ion-dipole interaction, electrostatic layer by layer stacking and inter-plane phenyl-phenyl stacking among the PANI chains, PANI- dopant and PANI- clay surfaces. Thermal stability of PANICN was observed to be higher than doped PANIs due to the presence of insulative nanoclay layers in the former. Studies also showed that the amphiphilic dopant PDPSA derived from renewable resource is a low cost intercalating agent-cum-dopant which can be successfully used as structure directing agent for the preparation of micro/nanostructured PANICNs with controlled morphology. The prospects of the direct application of these nanocomposites were developing electrically conductive composites by blending with other conventional polymers for mitigation of electric charge/EMI shielding materials.

The main challenge of the present research programme was to prepare water dispersible environmentally stable electro-magnetic materials and to design the structure which will have the greatest effect on the magnetic, conducting and thermo-mechanical properties with processability which are desired for these materials in advanced electro-magnetic applications. With this perspective, a conceptually new synthetic methodology was developed for the preparation of water dispersible electromagnetic polyaniline-polyhydroxy iron cation-clay nanocomposite (PPICSA) by polymerization of aniline in the aqueous

dispersion of polyhydroxy iron intercalated clay in presence of PDPSA at room temperature. This amphiphilic dopant could tune the size of the metal nanoparticle by preventing them from agglomeration and also could act as a micellar template for the formation of nanostructured PANI. These electro-magnetic materials showed nanodimension, excellent electrical conductivity, reasonable magnetic property, good thermal stability and solubility in most of the organic solvents. These attractive properties make them an excellent candidate for high advanced technological applications in the field of EMI shielding materials and chemical sensors. Hence, we made investigation for evaluating its efficiency as a platinum electrode modifier in amperometric sensor for the analysis of ascorbic acid and also developed polycarbonate-PPICSA blend for studying its characterisations as an EMI shielding material.

PPICSA is receiving importance as a modifier for Pt electrode in the respect that it is expected to exhibit excellent sensor efficiency arising from its nanodimension, electrical conductivity, redox property, environmental stability and improved economical efficiency. Moreover, the presence of nanoclay is expected to facilitate the heterogeneous transportation of electrons between the analyte and the electrode surface. Nanostructured PPICSA modified platinum electrode has been developed as an amperometric sensor for ascorbic acid. The performance characteristics of the electrode were studied with respect to response time, sensitivity, operational stability and storage life. This material could contribute many unique properties such as large surface area, higher activity and better contact between analyte and the electrode. Common possible

interferences of the sample matrices were tested and the results revealed that the present electrode exhibited high selectivity towards AA. Moreover, this unique low cost and user friendly sensor can be used for the analysis of AA present in food, beverages and pharmaceuticals.

Nanostructured electro-magnetic PPICSA would attract a great deal of attention as EMI shielding material since they possess dual property of conductivity and magnetic property endowed with thermo-mechanical stability and processability. Electromagnetic interference shielding materials based on PPICSA and polycarbonate were developed by solution blending technique. The blends exhibited low percolation threshold concentration, excellent thermo-mechanical stability and EMI shielding efficiency 20-40 dB when using electromagnetic radiation of 8 GHz. All these property evaluation suggest that these transparent composite films can be used for the fabrication of EMI shielding/ electrostatic dissipation material for the encapsulation of electronic devices and as electrostatic material for high technological applications.

Future Perspectives

From the above mentioned studies it can be proposed that this novel strategy adopted for the preparation of PPICSA allows the formation of electromagnetic nanofibers/tapes through a soft template approach and its capability in retaining the properties of the material is challenging for high advanced technological applications. Furthermore, this method is a simple, low cost and convenient route and can be used for fabricating well ordered electro-

magnetic composites composed of various other conducting polymers with other metal nanoparticles. Multiple role of the low cost amphiphilic dopant 3- PDPSA investigated in the present study can be proposed for controlling the size, shape of other metal nanoparticles and also dopant and structure –directing agent for various other conducting polymers.

The unique low cost and user friendly PPIC modified platinum electrode based amperometric sensor can be used for the analysis of ascorbic acid present in food, beverages and pharmaceuticals. The process for the development of EMI shielding material from the blend of PC and PPICSA can be exploited for other commodity polymers like polypropylene, polystyrene etc.

Furthermore, the method described here offers a simple and convenient route for fabricating well dispersed multifunctional polymeric nanocomposites composed of other conducting polymers and metals/metal oxides like silver, TiO₂, CuO, etc. The improvement in the conductivity, magnetic property, thermo-mechanical stability and better dispersability for making them suitable for various technological applications should be the goal of the future.

List of Publications

Papers Published in International Journals

1. Facile green strategy for micro/nano structured conducting polyaniline-clay nanocomposite (PANICN) via template polymerization using amphiphilic dopant, 3-pentadecyl phenol 4- sulphonic acid. Sudha, J. D.; **Reena, V. L.**; Pavithran, C. *J. Polym. Sci. Part B. Polym. Phy.* 45, **2007**, 2664-2673.
2. Structure – directing effect of renewable resource based amphiphilic dopants on the formation of conducting polyaniline-clay nanocomposite. Janardhanan D. Sudha, **Viswan L. Reena.** *Macromol. Symp.* 254, **2007**, 274-283
3. Development of electromagnetic shielding materials from the conductive blends of polyaniline and polyaniline-clay nanocomposite-EVA: Preparation and properties. Sudha, J. D.; Sivakala, S.; Prasanth, R.; **Reena, V. L.**; Radhakrishnan Nair, P. *Comp. Sci. Tech.* 69, **2009**, 358-364.
4. Role of amphiphilic dopants on the formation and properties of electrically conducting polyaniline-clay nanocomposite. **Viswan L. Reena**, Janardhanan D. Sudha, Chorappan Pavithran. *J. Appl. Polym. Sci.* 113, **2009**, 4066-4076.
5. Nanostructured electro-magnetic functional materials from inorganic organic hybrid guest- host system of polyaniline-clay-magnetite composite. **Reena, V. L.**; Sudha, J. D.; Pavithran, C. *J. Phys. Chem. B.* 114, **2010**, 2578-2585.
6. Bio based self-assembly approach for the preparation of polyaniline –keggin iron –clay electromagnetic nanotapes. **Reena, V. L.**; Sudha, J. D. (communicated)
7. Development of novel amperometric sensor based on nanostructured electro-magnetic polyaniline- polyhydroxy iron cation - clay composite modified Pt electrode for ascorbic acid. **Reena, V. L.**; Sudha J. D. (communicated)

8. Development of electromagnetic shielding materials from the composite of nanostructured polyaniline- polyhydroxy iron-clay and polycarbonate. **Reena, V. L.**; Sudha J. D. (communicated)
9. Water dispersible nanostructured electro-magnetic polyaniline laponite hybrid material. Sudha, J. D.; Sivakala, S.; **Reena, V. L.**; Andrij Pich and Hans-Juergen P. Adler (manuscript under preparation)
10. Nanostructured electro-optic polyaniline-titanate cation-clay composites for photocatalytic applications. Ramakrishnan, R.; **Reena, V. L.**; Sivakala, S.; Sudha, J. D. (manuscript under preparation)

Papers Presented at Conferences

1. Development of novel amperometric sensor based on nanostructured polyaniline- polyhydroxy iron cation- clay composite modified platinum electrode for ascorbic acid. **Reena, V. L.**; Sudha J. D.; Pavithran, C. "*International Conference on Recent trends in Materials Science and Technology*", **2010** October 29-31.
2. Bio based approach for the preparation of electromagnetic nanotapes of polyaniline -keggin iron -clay nanocomposite. **Reena, V. L.**; Sudha, J. D.; Pavithran, C. "*Indian Science congress*", **2010**, January 3-7.
3. Multifunctionalised nanostructured electromagnetic materials from inorganic organic hybrid guest- host system of polyaniline-clay- magnetite. **Reena, V. L.**; Pavithran, C.; Sudha, J. D. "*MACRO*" **2009**, March 9-11.
4. Biosensor based on nanostructured electrically conducting polyaniline clay composite (PANICN)/ Eupatorium peroxidase for analyzing phenolic antioxidants. (Selected for the best poster award) **Reena, V. L.**; Sudha, J. D.; Soly Cheriyan, Emilia Abraham, T. "*Indian Analytical Science Congress*" **2008**, November 21-23.

List of publications

5. Tuning the morphology of electrically conducting polyaniline -clay nanocomposite using amphiphilic dopants. **Reena, V. L.**; Sudha, J. D.; Pavithran, C. *“International conference on advanced materials and composites”*, Thiruvananthapuram, India, **2007**, October 24-26.

6. Structure directing effect of amphiphilic dopants on the morphology of novel self- assembled nano/micro structured conducting polyaniline- clay nanocomposites (PANICNs) Sudha, J. D.; **Reena, V. L.**; Prabhakar Rao, P.; Pavithran C.; Pillai, C. K. S. Poster presented at *“National conference on electron microscopy”*, Thiruvananthapuram, India, **2006**, April 19-21.

Bibliography and References

- Abdelaziz, R.; Yang, D. Highly conductive polyaniline nanofibers. *J. Mater. Lett.* 62, **2008**, 4311-4314.
- Abdullin, I. F.; Turova, E. N.; Ziyatdinova, G. K.; Budnikov, G. K. Potentiometric determination of ascorbic acid: Estimation of its contribution to the total antioxidant capacity of plant materials. *J. Anal. Chem.* 57, **2002**, 353–355.
- Adams, P. N.; Devasagayam, P.; Pomfret, S. J.; Abell, L.; Monkman, A. A new acid-processing route to polyaniline films which exhibit metallic conductivity and electrical transport strongly dependent upon intrachain molecular dynamics. *J. Phys. Condens. Matter.* 10, **1998**, 8293-8304.
- Agbor, N. E.; Petty, M. C.; Monkman, A. P. Polyaniline thin films for gas sensing. *Sens. Actuat. B.* B28, **1995**, 173-179.
- Alan, G. M.; Arthur, J. E. Secondary doping in polyaniline, *Synth. Met.* 69, **1995**, 85-92.
- Alexandre, M.; Dubois. P. Polymer-layered silicate nanocomposites: Preparation, properties and uses of a new class of materials. *Mater. Sci. Eng. R.* 28, **2000**, 1–63.
- Aoki, A.; Matsue, T.; Uchida, I. Multichannel electrochemical detection with a microelectrode array in flowing streams. *Anal. Chem.* 64, **1992**, 44-49.
- Aphesteguy, J. C.; Jacobo, S. E. Composite of polyaniline containing iron oxides. *Physica B.* 354, **2004**, 224-227.
- Aphesteguy, J.C.; Jacobo, S. E. Synthesis of a soluble polyaniline–ferrite composite: Magnetic and electric properties. *J. Mater. Sci.* 42, **2007**, 7062-7068.
- Arias-Marin, E.; Romero, J.; Ledezma-Perez, A. S.; Kniajansky, S. Enzymatic mediated polymerization of functional aniline derivatives in nonaqueous media. *Polym. Bull.* 37, **1996**, 581–587.

- Armes, S. P.; Gottesfeld, S.; Beery, J. G.; Garzon, F.; Agnew, S. F. Conducting polymer-colloidal silica composites. *Polymer*. 32, **1991**, 2325-2330.
- Atkins, M. P.; Mitchell, I. V. In Pillared Layered Structures; Elsevier Applied Science: London, **1990**.
- Barakat, M. Z.; Shehab, S. K.; Darnish, N.; El-Zoheivy, A. A new titrimetric method for the determination of ascorbic acid. *Anal. Biochem*, 53, **1973**, 245-251.
- Barros, R. A.; Azevedo, W. M.; Aguiar, F. M. Photo-induced polymerization of polyaniline. *Mater. Charact.* 50, **2003**, 131-134.
- Bates, F. S.; Fredrickson, G. H. Block Copolymers—Designer soft materials. *Physics Today*, 52, **1999**, 32-36.
- Beecroft, L. L.; Ober, C. K. Nanocomposite materials for optical applications. *Chem. Mater.* 9, **1999**, 1302-1317.
- Berkovsky, B. M.; Medvedev, V. F.; Karkov, M. S. Magnetic fluids: engineering application. *Oxford University Press: New York*. **1993**.
- Beyer, G. Nanocomposites a new class of flame retardants for polymers. *Plast. Addit. Compound.* 4, **2002**, 22-27.
- Bidan, G.; Jarjayes, O.; Fruchart, J. M.; Hannecart, E. New nanocomposites based on "tailor dressed" magnetic particles in a polypyrrole matrix. *Adv. Mater.* 6, **1994**, 152-155.
- Bradley, S. M.; Kydd, R. A. Comparison of the species formed upon base hydrolyses of gallium (III) and iron (III) aqueous solutions: the possibility of existence of an $[\text{FeO}_4\text{Fe}_{12}(\text{OH})_{24}(\text{H}_2\text{O})_{12}]^{7+}$ polyoxocation. *J. Chem. Soc., Dalton Trans.* **1993**, 2407-2413.
- Brindley, G. W.; Moll, W. F. Complexes of natural and synthetic Ca-Montmorillonites

- with fatty acids (clay-organic studies-IX). *Am. Mineral.* 50, **1965**, 1355-1370.
- Brindley, G. W.; Semples, R. E. Preparation and properties of some hydroxy-aluminum beidellites. *Clay Miner.* 12, **1977**, 229-237.
- Brown, W. F. Thermal fluctuations of a single-domain particle. *Phys. Rev.* 130, **1963**, 1677-1686.
- Campos, M.; Bello, J. B. Mechanism of conduction in doped polyaniline. *J. Phys. D. Appl. Phys.* 30, **1997**, 1531-1535.
- Cao, G.; Garcia, M. E.; Aleala, M.; Burgess, L. F.; Mallouk, T.E. Chiral molecular recognition in intercalated zirconium phosphate. *J. Am. Chem. Soc.* 114, **1992**, 7574-7575.
- Cao, D.; He P.; Hu, N. Electrochemical biosensors utilizing electron transfer immobilized on Fe₃O₄ nanoparticles. *Analyst.* 128, **2003**, 1268-1274.
- Cao, Y.; Li, S.; Xue, Z.; Guo, D. Spectroscopic and electrical characterization of some aniline oligomers and polyaniline. *Synth. Met.* 16, **1986**, 305-315.
- Cao, M.; Liu, T.; Gao, S.; Sun, G.; Wu, X.; Hu, C.; Wang, Z. L. Single-crystal dendritic micro-pines of magnetic α -Fe₂O₃: Large-scale synthesis, formation mechanism, and properties. *Angew. Chem. Int. Ed.* 44, **2005**, 4197-4201.
- Cao, Y.; Paul, S.; Heeger, A. J. Counter-ion induced processability of conducting polyaniline and of conducting polyblends of polyaniline in bulk polymers. *Synth. Met.* 48, **1992**, 91-97.
- Cao, Y.; Smith, P.; Heeger, A. J. Counter-ion induced processability of conducting polyaniline. *Synth. Met.* 57, **1993**, 3514-3519.
- Carswell, A. D. W.; O'Rear, E. A.; Grady, B. P. Adsorbed surfactants as templates for the synthesis of morphologically controlled polyaniline and polypyrrole

- nanostructures on flat surfaces: from spheres to wires to flat films. *J. Am. Chem. Soc.* 125, **2003**, 14793-14800.
- Caruso, F. Nano engineering of particle surfaces. *Adv. Mater.* 13, **2001**, 11-22.
- Castro, S. S. L.; Balbo, V. R. ; Barbeira, P. J. S.; Stradiotto, N. R. Flow injection amperometric detection of ascorbic acid using a prussian blue film-modified electrode. *Talanta* 55, **2001**, 249-254.
- Chan, H. S. O.; Nag, S. C.; Ho, P. K. Polyanilines doped with phosphonic acids: Their preparation and characterization. *Macromolecules.* 27, **1994**, 2159-2164.
- Chen, S. A.; Hwang, G. W. Water-soluble self-acid-doped conducting polyaniline: Structure and properties. *J. Am. Chem. Soc.* 117, **1995**, 10055-10062.
- Chen, S. A.; Lee, H. T. Structure and properties of poly(acrylic acid)-doped polyaniline. *Macromolecules* . 28, **1995**, 2858-2866.
- Chen, A.; Wang, H.; Zhao, B.; Li, X. The preparation of polypyrrole-Fe₃O₄ nanocomposites by the use of common ion effect. *Synth. Met.* 139, **2003**, 411-415.
- Cho, M. S.; Choi, H. J.; Ahn, W. S. Enhanced Electro rheology of conducting polyaniline confined in MCM-41 channels. *Langmuir.* 20, **2004**, 202-207.
- Cho, M. S.; Park, S. Y.; Hwang, J. Y.; Choi, H. J. Synthesis and electrical properties of polymer composites with polyaniline nanoparticles. *Mater. Sci. Eng. C.* 24, **2004**, 15-18.
- Choi, J.; Sauer, G.; Goring, P.; Nielsch, K.; Wehrspohn, R. B.; Gosele, U. Monodisperse metal nanowire arrays on Si by integration of template synthesis with silicon technology. *J. Mater. Chem.* 13, **2003**, 1100-1103.
- Choi, J.; Sauer, G.; Nielsch, K.; Wehrspohn, R. B.; Gosele, U. Hexagonally arranged

- monodisperse silver nanowires with adjustable diameter and high aspect ratio. *Chem Mater.* 15, **2003**, 776–779.
- Cornell, R.; Schwertmann, U. *The Iron Oxides. VCH Verlagsgesellschaft: Weinheim, Germany, 1996.*
- Craik, D. J. *Magnetic Oxides, Part 2; Wiley: New York, 1981*, 703.
- Dauginet-De Pra, L.; Demoustier-Champagne, S. Investigation of the electronic structure and spectro electro chemical properties of conductive polymer nanotube arrays. *Polymer*, 46, **2005**, 1583-1594.
- Delvaux, M.; Duchet, J.; Stavaux, P. Y.; Legras, R.; Demoustier-Champagne, S. Chemical and electrochemical synthesis of polyaniline micro- and nano-tubules. *Synth. Met.* 113, **2000**, 275–280.
- Demoustier-Champagne, S.; Duchet, J.; Legras, R. Chemical and electrochemical synthesis of polypyrrole nanotubules. *Synth. Met.* 101, **1999**, 20–21.
- Deore, B. A.; Yu, I.; Freund, M. S. A. Switchable self-doped polyaniline: Interconversion between self-doped and non-self-doped forms. *J. Am. Chem. Soc.* 126, **2004**, 52-53.
- Diaz A. F., Logan J. A. Electroactive polyaniline films. *J Electroanal. Chem.* 111, **1980**, 111–114.
- Ding, X.; Han, D.; Wang, Z.; Xu, X.; Niu, L.; Zhang, Q. Micelle-assisted synthesis of polyaniline/magnetite nanorods by in situ self-assembly process. *J. Col. Interf. Sci.* 320, **2008**, 341–345.
- Ding, H.; Liu, X. M.; Wan, M.; Fu, S. Y. Electromagnetic functionalized cage-like polyaniline composite nanostructures. *J. Phys. Chem. B.* 112, **2008**, 9289-9294.
- Doherty, A. P.; Stanley M. A.; Vos, J. G. Electrocatalytic oxidation of ascorbic acid.

- Analyst.* 120, **1995**, 2371-2376.
- Dong, B.; Lu, N.; Zelsmann, M.; Kehagias, N.; Fuchs, H.; Torres, C. M. S. ; Chi, L. Fabrication of high-density, large-area conducting-polymer nanostructures. *Adv. Funct. Mater.* 16, **2006**, 1937-1942.
- Dong, S.; Sun Z.; Lu, Z. A new kind of chemical sensor based on conducting polymer film. *J. Chem. Soc. Chem. Commun.* **1988**, 993-995.
- Drelinkiewicz, A.; Hasik, M.; Choczynski, M. Preparation and properties of polyaniline containing palladium *Mater. Res. Bull.* 33, **1998**, 739-762.
- Dumas, M.; Chaudagne, C.; Bonte, F.; Meybeck, A.; Acad C. Age-related response of fibroblasts to L-ascorbic acid: Study of type I and III collagen synthesis. *Sci. III.* 319, **1996**, 1127-1132.
- Epstein, A. J.; Blatchford, J. W.; Kim, K.; Lin, L. B.; Gustafson, T. L.; Coplin, K. A. Long lived neutral solitons in pernigraniline base. *Mol. Cryst. Liq. Cryst.* 256, **1994**, 399-406
- Epstein, A. J.; Ginder, J. M.; Zhuo, F.; Woo, H. S.; Tanner, D. B.; Richter, A. F.; Angelopoulos, M.; Huang, W. S.; Alan, G. M. Structural phase transitions in (TMTSF)₂X and related compounds. *Synth. Met.* 13, **1987**, 63-69.
- Esteban, P. O.; Leger, J. M.; Lamy, C.; Genies, E. Electrocatalytic oxidation of methanol on platinum dispersed in polyaniline conducting polymers. *J. Appl. Electrochem.* 19, **1989**, 462-464.
- Facci J.; Murray, R. W. Binding of pentachloroiridite to plasma polymerized vinylpyridine films and electrocatalytic oxidation of ascorbic acid. *Anal. Chem.*, 54, **1982**, 772-777.
- Filho O. F.; Vieira I. C. L-Ascorbic acid determination in pharmaceutical formulations

- using a biosensor based on carbon paste modified with crude extract of zucchini (*Cucurbita pepo*). *J. Braz. Chem. Soc.* 11, **2000**, 412-418.
- Filippone, G.; Dintcheva, N.; Acierno D., La Mantia, F. P. The role of organoclay in promoting co-continuous morphology in high-density poly (ethylene)/poly (amide) 6 blends. *Polymer.* 49, **2008**, 1312-1315.
- Fripiat, J. J.; Internal surface of clays and constrained chemical reactions. *Clays. Clay. Miner.* 34, **1986**, 501-506.
- Gajewski, K. I.; Gilberr, M. H.; Liotta, D. *In Advances in Molecular Modeling.* J.A.I. Press. Greenerick, CT, **1990**, Vol. 2.
- Gangopadhyay, R.; De, A. Conducting polymer nanocomposites: A brief overview. *Chem. Mater.* 12, **2000**, 608-623.
- Gangopadhyay, R.; De, A. I. Polypyrrole–ferric oxide conducting nanocomposites: Synthesis and characterization. *Eur. Polym. J.* 35, **1999**, 1985-1992.
- Genies, E. M.; Boyle, A.; Lapkowski, M.; Tsintavis C. Polyaniline: A historical survey. *Synth Met.* 36, **1990**, 139–82.
- Genies, E. M.; Syed, A. A.; Tsintavis, C. Electrochemical study of polyaniline in aqueous and organic medium, redox and kinetic properties. *Mol. Cryst. Liq. Cryst.* 121, **1985**, 181–186.
- Genies, E. M.; Tsintavis, C. Redox mechanism and electrochemical behavior of polyaniline deposits. *J. Electroanal. Chem.* 195, **1985**, 109–128.
- Goddard, Y. A.; Vold, R. L.; Hoatson, G. L. Deuteron NMR study of polyaniline and polyaniline/clay nanocomposite. *Macromolecules.* 36, **2003**, 1162-1169.
- Guilherme, M. O.; Barra, M. E.; Bluma, G.; Soares, I. H. Mechanical property electrically conductive, melt-processed polyaniline/EVA blends. *J. Appl. Polym.*

- Sci.* 82, **2001**, 114–123.
- Hable, C. T.; Wrighton, M. S. Electrocatalytic oxidation of methanol by assemblies of platinum/tin catalyst particles in a conducting polyaniline matrix. *Langmuir*. 7, **1991**, 1305-1309.
- Han, M. G.; Cho, S. K.; Oh, S. G.; Im, S. S. Preparation and characterization of polyaniline nanoparticles synthesized from DBSA micellar solution. *Synth. Met.* 126, **2002**, 53-60.
- Han, J.; Liu, Y.; Wang, L.; Guo, R. A versatile surfactant-mediated synthetic route to gold/polyaniline derivative core/shell nanocomposites. *J. Polym. Sci. Part A: Polym. Chem.* 48, **2010**, 3903-3912.
- Hassan, P. A.; Sawant, S. N.; Bagkar, N. C.; Yakhmi, J. V. Microstructural changes in SDS micelles induced by hydrotropic salt. *Langmuir* 18, **2004**, 2543-2548.
- Hatchett, D. W.; Josowicz, M. Composites of intrinsically conducting polymers as sensing nanomaterials. *Chem. Rev.* 108, **2008**, 746-769.
- He, H.; Frost, R. L.; Deng, F.; Zhu, J.; Wen, X.; Yuan, P. Conformation of surfactant molecules in the interlayer of montmorillonite studied by ¹³C MAS NMR. *Clays Clay Miner.* 52, **2004**, 350-356.
- Heeger, A. J. The fourth generation of polymeric materials semiconducting and metallic polymers. *Rev. Mod. Phys.* 73, **2001**, 681-700.
- Heeger, A. J. Polyaniline with surfactant counterions: Conducting polymer materials which are processible in the conducting form. *Synth. Met.* 57, **1993**, 3471-3482.
- Hiemenz, P. C. Principles of colloid and surface chemistry. *Marcel Dekker: New York*, **1986**.
- Hirao, T. Conjugated systems composed of transition metals and redox-active π

- conjugated ligands. *Coord. Chem. Rev.* 226, **2002**, 81-91.
- Huang, H.; Cai, R.; Du Y.; Zeng, Y. Flow injection stopped flow spectrofluorimetric kinetic determination of total ascorbic acid based on an enzyme linked coupled reaction. *Anal. Chim. Acta.* 309, **1995**, 271-282.
- Huang, X. J.; Choi, Y. K. Chemical sensors based on nanostructured materials. *Sens. Actuators B.* 122, **2007**, 659-671.
- Huang, W. S.; Humphrey, B. D.; MacDiarmid, A. G. Polyaniline, a novel conducting polymer. Morphology and chemistry of its oxidation and reduction in aqueous electrolytes. *J. Chem. Soc., Faraday Trans.* 82, **1986**, 2385-2400.
- Huang, S. W.; Neoh, K. G.; Kang, E. T.; Han, H. S.; Tan, K.L. Palladium-containing polyaniline and polypyrrole microparticles. *J. Mater. Chem.* 8, **1998**, 1743-1748.
- Huang, C. L.; Partch, R. E.; Matijevic, E. Coating of uniform inorganic particles with polymers: II. Polyaniline on copper oxide. *J. Coll. Interf. Sci.* 170, **1995**, 275-283.
- Huang, J.; Virji, S.; Weiller, B. H.; Kaner, R. B. Nanostructured polyaniline sensors. *Chem. Eur. J.* 10, **2004**, 1314-1319.
- Huang, J.; Virji, S.; Weiller, B. H.; Kaner, R. B. Polyaniline nanofibers: Facile synthesis and chemical sensors. *J. Am. Chem. Soc.* 125, **2003**, 314-322.
- Huang, J.; Wan, M. X. Polyaniline doped with different sulfonic acids by in situ doping polymerization. *J. Polymer Sci.: Part A: Polymer Chem.* 37, **1999**, 1277- 1284.
- Huang, K.; Wan, M. X. Self-assembly polyaniline nanostructures with photoisomerization function. *Chem. Mater.* 14, **2002**, 3486-3492.
- Huang, K.; Wan, M. X. Self-assembly of nanostructured polyaniline doped with azobenzenesulfonic acid. *Synth. Met.* 135-136, **2003**, 173-174.
- Huang, P. F.; Wang, L.; Bai, J. Y.; Wang, H. J.; Zhao, Y. Q.; Fan, S. D. Simultaneous

- electrochemical detection of dopamine and ascorbic acid at a poly(p- toluene sulphonic acid) modified electrode. *Microchim Acta.* 157, **2007**, 41-47.
- Huang, L. M.; Wang, Z. B.; Wang, H. T.; Cheng, X. L.; Mitra, A.; Yan, Y. X. Polyaniline nanowires by electro polymerization from liquid crystalline phases. *J. Mater. Chem.* 12, **2002**, 388-391.
- Huguenin, F.; Ferreira, M.; Zucolotto, V.; Nart, F. C.; Torresi, R. M.; Oliveira, O. N. Molecular-Level Manipulation of V₂O₅/Polyaniline layer-by-layer films to control electrochromogenic and electrochemical properties. *Chem. Mater.* 16, **2004**, 2293-2299.
- Hulteen, J. C.; Martin, C. R. A general template-based method for the preparation of nanomaterials. *J. Mat. Chem.* 7, **1997**, 1075-1087.
- Jackowska, K.; Bieguński, A. T.; Tagowska, M. Hard template synthesis of conducting polymers: A route to achieve nanostructures. *J. Sol. State Electrochem.* 12, **2008**, 437-443.
- Jarjays, O.; Fries, P. H.; Bidan, G. Nanostructured conducting polymer composites — superparamagnetic particles in conducting polymers. *Synth. Met.* 94, **1998**, 99-104.
- Javed, A.; Riaz, U.; Ahmad S. Effect of ferrofluid concentration on electrical and magnetic properties of the Fe₃O₄/PANI nanocomposites. *J. Magn. Magn. Mater.* 314, **2007**, 93-99.
- Jeevananda, T.; Siddaramaiah, V.; Annadurai, Somashekar, R. Studies on SLS doped polyaniline and its blend with PC. *J. Appl. Polym .Sci.* 82, **2001**, 383-388.
- Jia, W.; Segal, E.; Kornemandel, D.; Lamhot, Y.; Narkis, M.; Siegmann, A. Polyaniline-DBSA/organophilic clay nanocomposites: synthesis and characterization. *Synth.*

- Met.* 128, **2002**, 115-120.
- Kanatzidis, M. G.; Bissessur, R.; Degroot, D. C.; Schindler, J. L.; Kannewurf, C. R. New intercalation compounds of conjugated polymers. Encapsulation of polyaniline in molybdenum disulfide. *Chem. Mater.* 5, **1993**, 595-596.
- Kanatzidis, M. G.; Wu, C. G.; Marcy, H. O.; DcGroot, D. C.; Kannewurf, C. R.; Kostikas, A. Intercalation chemistry of conducting polymers: New crystalline microlaminate phases in the polyaniline/FeOCl system. *Adv. Mater.* 2, **1990**, 364-366.
- Kang, Y.; Lee, M. H.; Rhee, S. B. Electrochemical properties of polyaniline doped with poly(styrenesulfonic acid). *Synth. Met.* 52, **1992**, 319-328.
- Karatchevtseva, Z.; Zhang, J.; Hanna, V.; Luca. Electrosynthesis of macroporous polyaniline-V₂O₅ nanocomposites and their unusual magnetic properties. *Chem. Mater.* 18, **2006**, 4908-4916.
- Karayannis M. I.; Farasoglou, D. I. Kinetic-spectrophotometric method for the determination of ascorbic acid in orange juice, parsley and potatoes. *Analyst.* 112, **1987**, 767-770.
- Katz, E.; Willner I.; Wang, J. Electro analytical and bio electro analytical systems based on metal and semi conductive nanoparticles. *Electroanalysis* 16, **2004**, 19-44.
- Kaynak, A. Electromagnetic shielding effectiveness of galvanostatically synthesized Conducting polypyrrole films in the 300–2000 MHz frequency range. *Mater. Res. Bull.* 31, **1996**, 845-852.
- Kazantseva, N. E.; Vilcakova, J.; Kresalek, V.; Saha, P.; Sapurina, I.; Stejskal, J. Magnetic behaviour of composites containing polyaniline-coated manganese-zinc ferrite. *J. Magn. Mater.* 269, **2004**, 30-37.

- Khanna, P. K.; Singh, N.; Charan, S.; Viswanath, A. K. Synthesis of Ag/polyaniline nanocomposite via an in situ photo-redox mechanism. *Mater. Chem. Phys.* **92**, **2005**, 214–219.
- Kim, B. H.; Jung, J. H.; Hong, S. H.; Kim, J. W.; Choi, H. J.; Joo, J. Physical characterization of emulsion intercalated polyaniline–clay nanocomposite. *Curr. Appl. Phys.* **1**, **2001**, 112–115.
- Kim, B. H.; Jung, J. H.; Joo, J.; Epstein, A. J.; Mizoguchi, K.; Kim, J. W.; Choi, H. J. Nanocomposite of polyaniline and Na⁺–montmorillonite clay. *Macromolecules*. **35**, **2002**, 1419–1423.
- Kim, B. H.; Jung, J. H.; Kim, J. W.; Choi, H. J.; Joo, J. Effect of dopant and clay on nanocomposites of polyaniline (PAN) intercalated into Na⁺-montmorillonite (Na⁺-MMT). *Synth. Met* **121**, **2001**, 1311–1312.
- Kim, J. W.; Liu, F.; Choi, H. J.; Hong, S. H.; Joo, J.; Intercalated polypyrrole/Na⁺-montmorillonite nanocomposite via an inverted emulsion pathway method. *Polymer*. **44**, **2003**, 289–293.
- Kim, H. S.; Sohn, B. H.; Lee, W.; Lee, J. K.; Choi, S. J.; Kwon, S. J. Multifunctional layer-by-layer self-assembly of conducting polymers and magnetic nanoparticles. *Thin Solid Films*. **419**, **2002**, 173–177.
- Kobayashi, S.; Uyama, H.; Kimura, S. Enzymatic polymerization. *Chem. Rev.* **101**, **2001**, 3793–3818.
- Kros, A.; Nolte, R. J. M.; Sommerdijk, N. A. J. M. Conducting polymers with confined dimensions: track-etch membranes for amperometric biosensor applications. *Adv. Mater.* **14**, **2002**, 1779–1782.
- Krutovtsev, S. A.; Sorokin, S. I.; Zorin, A. V.; Letuchy, Y. A.; Antonova, O.Y. Polymer

- film-based sensors for ammonia detection. *Sens. Actuat. B.* B7, **1992**, 492-494.
- Ksenofontov, V.; Gaspar, A. B.; Niel, V.; Reiman, S.; Real, J. A.; Gutlich, P. On the nature of the Plateau in two-step dinuclear spin-crossover complexes. *Chem. Eur. J.* 10, **2004**, 1291-1298.
- Kuila, B. K.; Nandi, A. K. Physical, mechanical, and conductivity properties of poly(3-hexylthiophene)-montmorillonite clay nanocomposites produced by the solvent casting method. *Macromolecules.* 37, **2004**, 8577-8584.
- Kuila, B. K.; Nandi, A. K. Structural hierarchy in melt-processed poly (3-hexyl thiophene)-montmorillonite clay nanocomposites: Novel physical, mechanical, optical, and conductivity properties. *Macromolecules.* 110, **2006**, 1621-1631.
- Kulesza, P. J.; Chojak, M.; Miecznikowski, K.; Lewera, A.; Malik, M. M.; Kuhn, A. Polyoxometallates as inorganic templates for monolayers and multilayers of ultrathin polyaniline. *Electrochem. Commun.* 4, **2002**, 510-515.
- Kumar, S. A.; Chen, S. M. Electrocatalytic reduction of oxygen and hydrogen peroxide at poly (p-aminobenzene sulfonic acid)-modified glassy carbon electrodes. *J. Mol. Cat. A: Chem.* 278, **2007**, 244-250.
- Lahav, M.; Weiss, E.; Xu, Q.; Whitesides, G. M. Core-Shell and segmented polymer-metal composite nanostructures. *Nano Lett.* 6, **2006**, 2166-2171.
- LaMer, V. K.; Dinegar, R. H.; Theory, production and mechanism of formation of mono dispersed hydrosols. *J. Am. Chem. Soc.* 72, **1950**, 4847- 4854.
- Laranjeira, J. M. G.; Deazevedo, W. M.; Dearaujo, M. C. U. A conductimetric system based on polyaniline for determination of ammonia in fertilizers. *Anal. Lett.* 30, **1997**, 2189-2209.
- Laska, J.; Pron, A.; Lefrant, S. Phosphoric acid diesters protonated polyaniline

- :Preparation, spectroscopic properties, and processability. *J. Polym Sci A: Polym. Chem.* 33, **1995**, 1437-1445.
- Lau, O. W.; Luk S. F.; Wang, K. S. Determination of ascorbic acid in pharmaceuticals using direct ultraviolet spectrophotometry. *Analyst.* 112, **1987**, 1023-1025.
- Laviron, E. Adsorption, autoinhibition and autocatalysis in polarography and in linear potential sweep voltammetry. *J. Electroanal. Chem.* 52, **1974**, 355-393
- Lee, W.; Du, G.; Long, S. M.; Epstein, A. J.; Shimizu, S.; Saitoh, T. Charge transport properties of fully-sulfonated polyaniline. *Synth. Met.* 84, **1997**, 807-808.
- Lee, W. J.; Kim Y. J.; Kaang, S. Electrical properties of polyaniline/sulfonated polycarbonate blends. *Synth. Met.* 113, **2000**, 237-243.
- Lee, D.; Lee, S. H.; Char, K.; Kim, J. Expansion distribution of basal spacing of the silicate layers in polyaniline/Na⁺-montmorillonite nanocomposites monitored with X-ray diffraction. *Macromol. Rapid Commun.* 21, **2000**, 1136-1139.
- Li, J.; Fang, K.; Qiu, H.; Li, S.; Mao, W. Micromorphology and electrical property of the HCl-doped and DBSA-doped polyanilines. *Synth. Met.* 142, **2004**, 107-111.
- Li, L.; Jiang, J.; Xu, F. Novel polyaniline-LiNi_{0.5}La_{0.02}Fe_{1.98}O₄ nanocomposites prepared via an in situ polymerization. *Eur. Polym. J.* 42, **2006**, 2221-2227.
- Li, L.; Liu, H.; Wang, Y.; Jiang, J.; Xu, F. Preparation and magnetic properties of Zn-Cu-Cr-La ferrite and its nanocomposites with polyaniline. *J. Coll. Interf. Sci.* 321, **2008**, 265-271.
- Li, X. G.; Lu, Q. F.; Huang, M. R. Facile Synthesis and optimization of conductive copolymer nanoparticles and nanocomposite films from aniline with sulfodiphenylamine. *Chem. A. Eur. J.* 12, **2006**, 1349-1359.

- Li L.; Qin, Z.Y.; Liang, X.; Fan, Q.Q.; Lu, Y.Q.; Wu, W.H.; Zhu, M.F. Facile fabrication of uniform core-shell structured carbon nanotube-Polyaniline nanocomposites. *J. Phys. Chem. C.* 113, **2009**, 5502-5507.
- Li, X.; Wan, M.; Wei, Y.; Shen, J.; Chen, Z. Electromagnetic functionalized and core-shell micro/nanostructured polypyrrole composites. *J. Phys. Chem. B.* 110, **2006**, 14623-14626.
- Lim, S. T.; Hyun Y. H.; Choi, H. J.; Jhon, M. S. Synthetic biodegradable aliphatic polyester/montmorillonite nanocomposites. *Chem. Mater.* 14, **2002**, 1839-1844.
- Liu, R.; Duay, J.; Lee, S. B. Redox Exchange Induced MnO₂ Nanoparticle enrichment in Poly(3,4-ethylenedioxythiophene) Nanowires for Electrochemical Energy Storage. *ACS Nano.* 4, **2010**, 4299-4307.
- Liu, Y. J.; Kanatzidis, M. G. Topotactic polymerization of aniline in layered uranyl phosphate. *Inorg. Chem.* 32, **1993**, 2989-2991.
- Liu, R.; Lee, S. B. MnO₂/Poly(3,4-ethylenedioxythiophene) coaxial nanowires by one-step coelectrodeposition for electrochemical energy storage. *J. Am. Chem. Soc.* 130, **2008**, 2942-2943.
- Liu, J.; Lin, Y.; Liang, L.; Voigt, J. A.; Huber, D. L.; Tian, Z. R.; Coker, E.; Mckenzie, B.; Mativetsky, J.; Datars, W. R. Properties of alumina-membrane templated polypyrrole nanostructures. *Solid. State. Commun.* 122, **2002**, 151-154.
- Liu, J.; Lin, Y.; Liang, L.; Voigt, J. A.; Huber, D. L.; Tian, Z. R.; Coker, E.; Mckenzie, B.; Mcdermott, M. J. Templateless assembly of molecularly aligned conductive polymer nanowires: A new approach for oriented nanostructures. *Chem. Eur. J.* 9, **2003**, 604-611.

- Long, Y. Z.; Chen, Z. J.; Duvail, J. L.; Zhang, Z. M.; Wan, M. X. Electrical and magnetic properties of polyaniline/Fe₃O₄ nanostructures. *Physica B.* 370, **2005**, 121-130
- Lv, R.; Zhang, S.; Shi, Q.; Kan, J. Electrochemical synthesis of polyaniline nanoparticles in the presence of magnetic field and erbium chloride. *Synth. Met.* 150, **2005**, 115-122.
- MacDiarmid, A. G. "Synthetic Metals": A novel role for organic polymers (Nobel Lecture). *Angew. Chem.* 40, **2001**, 2581-2590.
- MacDiarmid, A. G. A novel role for organic polymers, Nobel Lecture: "Synthetic metals". *Rev. Mod. Phys.* 73, **2001**, 701-712.
- Malinauskas, A.; Garjonyte, R.; Mazeikiene, R.; Jureviciute, I. Electrochemical response of ascorbic acid at conducting and electrogenerated polymer modified electrodes for electroanalytical applications. *Talanta* 64, **2004**, 121-129.
- Mall N.; Joly, J. P. Determination of ascorbic acid in beers by high-performance liquid chromatography with electrochemical detection. *J. Chromatography.* 405, **1987**, 347-356.
- Martin, C. R. Nanomaterials: A membrane-based synthetic approach. *Science* 266, **1994**, 1961-1966.
- Martin, C. R. Template synthesis of electronically conductive polymer nanostructures. *Acc. Chem. Res.* 28, **1995**, 61-68.
- Martin, C. R. Membrane-based synthesis of nanomaterials. *Chem. Mater.* 8, **1996**, 1739-1746.
- Matos, R. C.; Augelli, M. A.; Pedrotti, J. J.; Lago C. L.; Angnes, L. Amperometric differential determination of ascorbic acid in beverages and vitamin C tablets using a flow cell containing an array of gold microelectrodes modified with

- palladium. *Electroanalysis* 10, **1998**, 887-890.
- Matsumoto, K.; Baeza J. J.; Mottola, H. A. Simultaneous kinetic-based determination of fructose and ascorbate with a rotating bioreactor and amperometric detection: application to the analysis of food samples. *Anal. Chem.* 65, **1993**, 1658-1661.
- Mcdermott, M. Conjugated polymers: Theory synthesis properties and characterization. *J. Chem. Eur. J.* 9, **2003**, 605-611.
- Mehrotra, V.; Giannelis, E. P. Metal-insulator molecular multilayers of electroactive polymers: Intercalation of polyaniline in mica-type layered silicates. *Sol. Stat. Commun.* 77, **1991**, 155-158.
- Mehrotra, V.; Giannelis, E. P. Conducting molecular multilayers: intercalation of conjugated polymers in layered media. *Mater. Res. Soc. Symp. Proc.* 171, **1990**, 39-44.
- Mejias, L.; Reihmann, M. H.; Sepulveda-Boza, S.; Ritter, H. New polymers from natural phenols using horseradish or soybean peroxidase. *Macromol. Biosci.* 2, **2002**, 24-32.
- Mott, N. F. Electrons in glass. *Rev. Mod. Phys.* 50, **1978**, 203-208.
- Mott, N. F.; Davis, E. A. Electronic Processes in Non-Crystalline Materials. *Clarendon Press; Oxford*, 1979.
- Mousty, C. Sensors and biosensors based on clay-modified electrodes new trends. *Appl. Clay Sci.* 27, **2004**, 159- 177.
- Murphy, P. J.; Posner, A. M.; Quirk, J. P. Chemistry of iron in soils ferric hydrolysis products. *Aust. J. Soil Res.* 13, **1975**, 189-201.
- Murphy, P. J.; Posner, A. M.; Quirk, J. P. Gel filtration chromatography of partially neutralized ferric solutions. *J. Coll. Inter. Sci.* 52, **1975**, 229-238.

- Nakajima, H.; Matsubayashi, G. Intercalation and polymerization of 4-anilinoaniline and 4-anilinoanilinium iodide in the VOPO₄ and V₂O₅ interlayer spaces. *J. Mater. Chem.* 5, **1995**, 105-108.
- Nalini B.; Sriman Narayanan, S. Amperometric determination of ascorbic acid based on electrocatalytic oxidation using a ruthenium(III) diphenyldithiocarbamate-modified carbon paste electrode. *Anal. Chim. Acta.* 405, **2000**, 93-97.
- Nascimento, G. M.; Constantino, V. R. L.; Landers, R.; Temperini, M. L. A. Aniline polymerization into montmorillonite clay: A spectroscopic investigation of the intercalated conducting polymer. *Macromolecules* 37, **2004**, 9373-9385.
- Nastase, C.; Nastase, F.; Dumitru, A.; Ionescu, M.; Stamatina, I. Thin film composites of nano carbons-polyaniline obtained by plasma polymerization technique. *Compos. Part A Appl. S.* 36, **2005**, 481-485.
- Nastase, F.; Stamatina, I.; Nastase, C.; Mihaiescu, D.; Moldovan, A. Synthesis and characterization of PANi-SiO₂ and PTh-SiO₂ nanocomposites' thin films by plasma polymerization. *Prog. Solid. State. Chem.* 34, **2006**, 191-199.
- Nazar, L. F.; Zhang, Z.; Zinkweg, D. Insertion of poly(p-phenylenevinylene) in layered MoO₃. *J. Am. Chem. Soc.* 114, **1992**, 6239-6240.
- Nazzari, A. I.; Street, G. B. Pyrrole-styrene graft copolymers. *J. Chem. Soc. Chem. Commun.* 6, **1985**, 375-376.
- Neamtu, I.; Ioanid, A. ; Chiriac, A.; Nita, L.E. ; Ioanid, G.E.; Popescu, M. Polymer - coated ferrite nanocomposites synthesized by plasma polymerization *J. Phys.* 50, **2005**, 1081-1087.
- Neoh, K. G.; Tan, K. K.; Goh, P. L.; Huang, S. W.; Kang, E. T.; Tan, K. L. Electroactive polymer-SiO₂ nanocomposites for metal uptake. *Polymer* 40, **1999**, 887-893.

- Nguyen, T.; Diaz, A. A novel method for the preparation of magnetic nanoparticles in a polypyrrole powder. *Adv. Mater.* 6, **1994**, 858-860.
- Park, S. G.; Park, J. E.; Cho, E. I.; Hwang, J. H.; Ohsaka T. Electrochemical detection of ascorbic acid and serotonin at a boron-doped diamond electrode modified with poly(N,N-dimethylaniline. *Res. Chem. Intermed.* 32, **2006**, 595–601.
- Partch, R.; Gangolli, S. G.; Matijevic, E.; Cai, W.; Arajs, S. Conducting polymer composites : I. Surface-induced polymerization of pyrrole on iron(III) and cerium(IV) oxide particles. *J. Coll. Interf. Sci.* 144, **1991**, 27-35.
- Partridge, A. C.; Jansen, M. L. ; Arnold, W. M. Conducting polymer-based sensors. *Mater. Sci. Eng. C.* 12, **2000**, 37-42.
- Paul, R. K.; Pillai, C. K. S. Melt/solution processable conducting polyaniline with novel sulfonic acid dopants and its thermoplastic blends. *Synth. Met.* 114, **2000**, 27-35.
- Pavlidoua, S.; Papaspyrides, C. D. A review on polymer-layered silicate nanocomposites. *Prog. Polym. Sci.* 33, **2008**, 1119–1198.
- Pinnell, S. R.; Yale, J. Regulation of collagen biosynthesis by ascorbic acid: A review. *Biol. Med.* 58, **1985**, 553-559.
- Plee, D.; Gattineau, Fripiat, L. J. Pillaring processes of smectites with and without tetrahedral substitution. *Clays Clay Miner.* 35, **1987**, 81-88.
- Porter, T. L.; Hagerman, M. E.; Eastman, M. P. Surface and intergallery polymerization reactions of organic monomers on layered silicate hosts. *Recent Res. Dev. Polym. Sci.* 1, **1997**, 1-17.
- Porter, D.; Metcalfe E.; Thomas, M. J. K. Nanocomposite fire retardants—A review. *Fire Mater.* 24, **2000**, 45–52.

- Pruneanu, S.; Veress, E.; Marian, I.; Oniciu, I. Characterization of polyaniline by cyclic voltammetry and UV-vis absorption spectroscopy. *J. Mater. Sci.* 34, **1999**, 2733 – 2739.
- Pud, A.; Ogurtsov, N.; Korzhenko, A.; Shapoval, G. Some aspects of preparation methods and properties of polyaniline blends and composites with organic polymers, *Prog. Polym. Sci.* 28, **2003**, 1701-1753.
- Purnell, J. H.; Mitchell, I. V. In Pillared Layered Structures. *Elsevier Applied Science: London*, **1990**.
- Qi, Z.; Pickup, P. G. High performance conducting polymer supported oxygen reduction catalysts. *Chem. Commun.* 21, **1998**, 2299-2300.
- Rajeshwar, K.; Tacconi, N. R.; Chenthamarakshan, C. R. Semiconductor-based composite materials: preparation; properties, and performance. *Chem. Mater.* 13, **2001**, 2765-2782.
- Raji, K. P.; Veena, V.; Pillai, C. K. S. Melt/solution processable conducting polyaniline: Doping studies with a novel phosphoric acid ester. *Synth. Met.* 104, **1999**, 189-195.
- Ramanaviciusa, A.; Ramanavicienea, A.; Malinauskas, A. Electrochemical sensors based on conducting polymer—polypyrrole. *Electrochim. Acta.* 51, **2006**, 6025-6037.
- Rao, P.S.; Subrahmanya, S.; Sathyanarayana, D. N. Synthesis by inverse emulsion pathway and characterization of conductive polyaniline–poly (ethylene-co-vinyl acetate) blends. *Synth. Met.* 139, **2003**, 397–404.
- Ray, S. S.; Okamoto, M. Polymer/layered silicate nanocomposites: a review from preparation to processing. *Prog. Polym. Sci.* 28, **2003**, 1539–1641.

- Razmi H.; Harasi, M. Voltammetric behavior and amperometric determination of ascorbic acid at cadmium pentacyanonitrosylferrate film modified GC electrode. *Inter. J. Electrochem. Sci.* 3, **2008**, 81-94.
- Reddy, K. R.; Lee, K. P.; Gopalan, A. I. Self-assembly approach for the synthesis of electro-magnetic functionalized Fe₃O₄/polyaniline nanocomposites: Effect of dopant on the properties. *Colloids and Surfaces A: Physicochem. Eng. Aspects* 320, **2008**, 49-56
- Reddy, K. R.; Lee, K. P.; Gopalan, A. I. Novel electrically conductive and ferromagnetic composites of poly (aniline-co-amino naphthalene sulfonic acid) with iron oxide nanoparticles: Synthesis and characterization. *J. Appl. Polym. Sci.* 106, **2007**, 1181-1191.
- Reena, V. L.; Pavithran, C.; Verma, V.; Sudha J. D. Nanostructured multifunctional electromagnetic materials from the guest-host inorganic-organic hybrid ternary system of a polyaniline-clay-polyhydroxy iron composite: Preparation and properties. *J. Phys. Chem. B.* 114, **2010**, 2578-2585.
- Rightor, E. G.; Tzou, M. S.; Pinnavaia, T. J. Iron oxide pillared clay with large gallery height: Synthesis and properties as a Fischer-Tropsch catalyst. *J. Catal.* 130, **1991**, 29-40.
- Rong, J.; Jing, Z.; Li, H.; Sheng, M. Polyethylene nano composites prepared via *in-situ* polymerization. *Macromol. Rapid. Commun.* 22, **2001**, 329-334.
- Rosensweig, R. E. Ferrohydrodynamics. *Cambridge University Press: Cambridge, England.* **1985**.
- Rossi, L.M.; Quach A. D.; Rosenzweig Z. Glucose oxidase- magnetite nanoparticle bioconjugate for glucose sensing. *Anal. Bioanal. Chem.* 380, **2004**, 606-613.

- Roy, R.; Bhattacharyya, A.; Sen, S. K.; Sen, S. Electrically conducting polyaniline and polyaniline PC composite films: preparation, characterization and electrical conductivity measurements. *Phys. Stat. Sol.* 165, **1998**, 245-253.
- Ruokolainen, J.; Eerikainen, H.; Torkkeli, M.; Serimaa, R.; Jussila, M.; Ikkala, O. Comb-shaped supramolecules of emeraldine base form of polyaniline due to coordination with zinc dodecyl benzenesulfonate and their plasticized self-organized structures. *Macromolecules*. 33, **2000**, 9272- 9276.
- Sarno, D. M.; Manohar, S. K.; Mac Diarmid, A. G. Controlled interconversion of semiconducting and metallic forms of polyaniline nanofibers. *Synth. Met.* 148, **2005**, 237-243.
- Sauer, G.; Brehm, G.; Schneider, S.; Nielsch, K.; Wehrspohn, R. B.; Choi, J. Highly ordered monocrystalline silver nanowire arrays. *J. Appl. Phys.* 91, **2002**, 3243–3247.
- Schollhorn, R. Intercalation systems as nanostructured functional materials. *Chem. Mater.* 8,**1996**; 1747-1757.
- Shao, Y.; Jin, Y.; Dong, S. DNA-templated assembly and electro polymerization of aniline on gold surface. *Electrochem. Commun.* 4, **2002**, 773-779.
- Shirakawa, H. The discovery of polyacetylene film—the dawning of an era of conducting polymers. *Rev. Mod. Phys.* 73, **2001**, 713-718.
- Shirakawa, H.; McDiarmid, A.; Heeger, A. Twenty-five years of conducting polymers. *Chem. Commun.* **2003**, 1-4.
- Shklovskii, B. I.; Efros, A. L. Electronic properties of semiconductors. *Berlin: Springer-Verlag*; **1985**.
- Skotheim, T. A.; Elsenbaumer, R. L.; Reynolds, J. R. Handbook of conducting

- polymers. *Marcel Dekker, New York*, **1998**,409.
- Somani, P.; Kale, B. B.; Amalnerkar, D. P. Charge transport mechanism and the effect of poling on the current-voltage characteristics of conducting polyaniline–BaTiO₃ composites. *Synth. Met.* 106, **1999**, 53-58.
- Somani, P. R.; Marimuthu, R.; Mulik, U. P.; Sainkar, S. R.; Amalnerkar, D. P. High piezoresistivity and its origin in conducting polyaniline/TiO₂ composites *Synth. Met.* 106, **1999**, 45-52.
- Stejskal, J. ; Sapurina, I.; Polyaniline: Thin films and colloidal dispersions. *Pure Appl. Chem.* 77, **2005**, 815-826.
- Stubican, V.; Roy, R. Infrared spectra of layer-structure silicates. *J. Am. Ceram. Soc.* 44, **1961**, 625-627.
- Sudha, J. D.; Reena, V. L. Structure – directing effect of renewable resource based amphiphilic dopants on the formation of conducting polyaniline-clay nanocomposite. *Macromol. Symp.* 254, **2007**, 274-283.
- Sudha, J. D.; Reena, V. L.; Pavithran, C. Facile green strategy for micro/nano structured conducting polyaniline-clay nanocomposite via template polymerization using amphiphilic dopant, 3-pentadecyl phenol 4-sulphonic acid. *J. Polym. Sci: Part B: Polym. Phys.* 45, **2007**, 2664-2673.
- Sudha, J. D.; Sasikala, T. S. Studies on the formation of self-assembled nano/microstructured polyaniline–clay nanocomposite (PANICN) using 3-pentadecyl phenyl phosphoric acid (PDPPA) as a novel intercalating agent cum dopant. *Polymer.* 48, **2007**, 338-347.
- Sudha, J. D.; Sivakala, S.; Kamalesh Patel; Radhakrishnan Nair, P. Development of electromagnetic materials from the conductive blends of polystyrene

- polyaniline- clay nanocomposite. *Composites Part A: Appl. Sci. Manufac.* 41, **2010**, 1647-1652.
- Sudha, J. D.; Sivakala, S.; Prasanth, R.; Reena, V. L.; Radhakrishnan Nair, P. Development of electromagnetic shielding materials from the conductive blends of polyaniline and polyaniline-clay nanocomposite-EVA: Preparation and properties. *Comp. Sci. Tech.* 69, **2009**, 358-364.
- Sun, Y.; Ruckenstein, E. Polypyrrole-bearing conductive composite prepared by an inverted emulsion pathway involving nonionic surfactants. *Synth. Met.* 72, **1995**, 261-267.
- Stejskal, J.; Kratochvil, P.; Jenkins, A. D. The formation of polyaniline and the nature of its structures. *Polymer* 37, **1996**, 367-369.
- Taka, T.; Laakso, J.; Levon, K. Conductivity and structure of DBSA-protonated polyaniline. *Sol. Stat. Commun.* 92, **1994**, 393-396.
- Tandon, R. P.; Tripathy, M. R.; Arora, A. K.; Hotchandani, S. Gas and humidity response of iron oxide—Polypyrrole nanocomposites. *Sens. Actuators B.* 114, **2006**, 768-773.
- Tang, B. Z.; Geng, Y.; Lam, J. W. Y.; Jing, B. L.; Wang, X.; Wang, F.; Pakhomov A. B.; Zhang, X. X. Processible nanostructured materials with electrical conductivity and magnetic susceptibility: Preparation and properties of maghemite/polyaniline nanocomposite films. *Chem. Mater.* 11, **1999**, 1581-1589
- Tatsuma, T.; Gondaria M.; Watanabe, T. Peroxidase-incorporated polypyrrole membrane electrodes. *Anal. Chem.* 64, **1992**, 1183-1187.
- Tomlinson, A. A. G. Characterization of pillared layered structures. *J. Porous Mater.* 5, **1998**, 259-274.

- Torsi, L.; Pezzuto, M.; Siciliano, P.; Rella, R.; Sabbatini, L.; Valli, L.; Zambonin, P. G. Conducting polymers doped with metallic inclusions: New materials for gas sensors. *Sens. Actuat. B, Chem.* 48, **1998**, 362-367.
- Treuba, M.; Montero, A.L.; Rieumont. Pyrrole nanoscaled electro polymerization: Effect of the proton. *J. Electrochim. Acta.* 49, **2004**, 4341-4349.
- Uchiyama, S. Catalytic kinetic determination of ultratrace amounts of nitrite with detection by linear scan voltammetry at a DME. *Talanta.* 39, **1992**, 1289-1292.
- Ueda, C.; Tse D. C. S.; Kuwana, T. Stability of catechol modified carbon electrodes for electrocatalysis of dihydronicotinamide adenine dinucleotide and ascorbic acid. *Anal. Chem.* 54, **1982**, 850-856.
- Vaia, R. A.; Ishii, H.; Giannelis, E. P. Synthesis and properties of two dimensional nanostructures by direct intercalation of polymer melts in layered silicates. *Chem. Mater.* 5, **1993**, 1694-1696.
- Vaia, R. A.; Krishnamurthy, R. In Polymer nanocomposite: Synthesis and characterization and modeling. *American Chemical Society: Washington DC.* **2001**, 1.
- Vaia, R. A.; Teukolsky, R. K.; Giannelis, E. P. interlayer structure and molecular environment of alkylammonium layered silicates. *Chem. Mater.* 6, **1994**, 1017-1022.
- Vassilion, J. K.; Ziebarth, R. P.; Disalvo, F. J. Preparation of a novel polymer blend of poly(ethylene oxide) and the inorganic polymer molybdenum selenide (Mo_3Se_3).infin.: infrared absorption of thin films. *Chem. Mater.* 2, **1990**, 738-741.
- Vaughan, D. E.; Burch, W. R. In Catalysis Today; Ed.; *Elsevier Science Publishers: Amsterdam.* Vol II, **1988**, 187.

- Vijay, T. J.; Blake, S.; McPherson, G. L.; Bose, A. Recent developments in materials synthesis in surfactant systems. *Coll. Interf. Sci.* 7, **2002**, 288-295.
- Virji, S. ; Huang, J.; Kaner, R. B. ; Weiller, B. H. polyaniline nanofiber gas sensors: Examination of response mechanisms. *Nano Lett.* 4, **2004**, 491-496.
- Viswan L. Reena, Janardhanan D. Sudha, Chorappan Pavithran. Role of amphiphilic dopants on the shape and properties of electrically conducting polyaniline-clay nanocomposite. *J. Appl. Polym. Sci.* 113, **2009**, 4066–4076.
- Vossmeier, T.; Guse, B.; Besnard, I.; Bauer, R. E.; Mullen, K.; Yasuda, A. Gold nanoparticle/polyphenylene dendrimer composite films: preparation and vapor-sensing properties. *Adv. Mater.* 14, **2002**, 238-242.
- Wan, M. Mechanism of proton doping in polyaniline. *J. Appl. Polym. Sci.* 55, **1995**, 399-405.
- Wan, M.; Li, J. J. Synthesis and electrical–magnetic properties of polyaniline composites. *Polym. Sci.: Part A: Polym. Chem.* 36, **1998**, 2799-2805.
- Wan, M. X.; Wei, Z. X.; Zhang, Z. M.; Zhang, L. J. Studies on nanostructures of conducting polymers via self-assembly method. *Synth. Met.* 135–136, **2003**, 175-176.
- Wan, M.; Zhou, W.; Li, J. Composite of polyaniline containing iron oxides with nanometer size. *Synth. Met.* 78, **1996**, 27-31.
- Wanekaya, A. K.; Chen, W.; Myung, N. V.; Mulchandani, A. Nanowire- based electrochemical biosensors. *Electroanalysis.* 18, **2006**, 533-550.
- Wang, J.; Chan, S.; Carlson, R. R.; Luo, Y.; Ge, G.; Ries, R. S., Heath, J. R. ; Seng, H. R. *Nano Lett.* 4, **2004**, 1693-1697.
- Wang, Y. Y; Jing, X. L. Intrinsically conducting polymers for electromagnetic

- interference shielding. *Polym. Adv. Technol.* 16, **2005**, 344-351.
- Wang, H.; Lin, T.; Kaynak, A. Polypyrrole nanoparticles and dye absorption properties. *Synth. Met.* 151, **2005**, 136-140.
- Wang, J.; Mo, X.; Ge, D.; Tian, Y.; Wang, Z.; Wang, S. Polypyrrole nanostructures formed by electrochemical method on graphite impregnated with paraffin. *Synth. Met.* 156, **2006**, 514-518.
- Wang, Z. H.; Scherr, E. M.; MacDiarmid, A. G.; Epstein, A. J. Transport and EPR studies of polyaniline: a quasi-one-dimensional conductor with three-dimensional "metallic" states. *Phys. Rev. B.* 45, **1992**, 4190- 4202.
- Wang, H. L.; Toppare L.; Fernandez, J. E. Conducting polymer blends: polythiophene and polypyrrole blends with polystyrene and poly (bisphenol A carbonate). *Macromolecules.* 23, **1990**, 1053-1059.
- Wang, C.; Wang, Z.; Li, M. K.; Li, H. L. Well-aligned polyaniline nano-fibril array membrane and its field emission property. *Chem. Phys. Lett.* 341, **2001**, 431-434.
- Wang, J.; Wang, Z.; Wang, S. Electrocatalytic oxidation of ascorbic acid at polypyrrole nanowire modified electrode. *Synth. Met.* 156, **2006**, 610- 613.
- Warren, B. E. X-Ray diffraction in random layer lattices. *Phys. Rev.* 59, **1941**, 693-698.
- Wheeler, B. L.; Caple, G.; Henderson, A.; Francis, J.; Cantrell, K.; Vogel, S.; Grey, S.; Russell, D. Electrochemical amine sensors using carboxylate functionalized polythiophene films. *J. Electrochem. Soc.* 136, **1989**, 2769-2770.
- Wu, C. G.; Degroot, D. C.; Marcy, H. O.; Shindler, J. L.; Kannewurf, C. R.; Liu, Y. J.; Hirpo, W.; Kanatzidis, M. G. Redox intercalative polymerization of aniline in V₂O₅ xerogel. *Chem. Mater.* 8, **1996**, 1992-2004.

- Wu, Q.; Xue, Z.; Qi Z.; Wang, F. Synthesis, characterization and electrochromic properties of a near infrared active conducting polymer of 1,4-di(selenophen-2-yl)-benzene. *Polymer*. 41, **2000**, 2029-2032.
- Xia, Y.; Wiesinger, J. M.; MacDiarmid, A. G.; Epstein, A. J. Camphor sulfonic acid fully doped polyaniline emeraldine salt: conformations in different solvents studied by an ultraviolet/visible/near-infrared spectroscopic method. *Chem. Mater.* 7, **1995**, 443-445.
- Xiong, S.; Wang, Q.; Xia, H. Template synthesis of polyaniline/TiO₂ bilayer microtubes. *Synth. Met.* 146, **2004**, 37-42.
- Xu, P.; Han, X.; Wang, C.; Zhou, D.; Lv, Z.; Wen, A.; Wang, X.; Zhang, B. Synthesis of electromagnetic functionalized nickel/polypyrrole core shell composites. *J. Phys. Chem. B.* 112, **2008**, 10443-10448.
- Xu, L.; Zhang, W.; Ding, Y.; Peng, Y.; Zhang, S.; Yu, W.; Qian, Y. Formation, characterization, and magnetic properties of Fe₃O₄ nanowires encapsulated in carbon microtubes. *J. Phys. Chem. B.* 108, **2004**, 10859-10862.
- Xu, J. J.; Zhou, D. M.; Chen, H. Y. A reagentless hydrogen peroxide biosensor based on the coimmobilization of thionine and horseradish peroxidase by their cross-linking with glutaraldehyde on glassy carbon electrode. *Electroanalysis.* 10, **1998**, 713-716.
- Xuan, S.; Xiang, Y.; Wang, J.; Leung, K. C. F.; Shu, K. Synthesis of Fe₃O₄ @ polyaniline core/shell microspheres with well-defined blackberry-like morphology. *J. Phys. Chem. C.* 112, **2008**, 18804-18809.
- Xue, W.; Fang, K.; Qiu, H.; Li, J.; Mao, W. Electrical and magnetic properties of the Fe₃O₄-polyaniline nanocomposite pellets containing DBSA-doped polyaniline

- and HCl-doped polyaniline with Fe₃O₄ nanoparticles. *Synth. Met.* 156, **2006**, 506-509.
- Yamanaka, S.; Brindley, G. W. Hydroxy-nickel interlayering in montmorillonite by titration method. *Clays Clay Miner.* 26, **1978**, 21-24.
- Yan, Y. L.; Gupta, M. C.; Dudley, K. L.; Lawrence, R. W. A comparative study of EMI shielding properties of carbon nanofiber and multi-walled carbon nanotube filled polymer composites. *J. Nanosci. Nanotechnol.* 5, **2005**, 927-935.
- Yang, C.; Chih, Y.; Cheng, H.; Chen, C. Nanofibers of self-doped polyaniline. *Polymer.* 46, **2005**, 10688-10698.
- Yang, Y. W. C.; Yang, H. C.; Li, G. J.; Li, Y. K. Thermal and anticorrosive properties of polyurethane/ clay nanocomposites. *J. Polym. Res.* 11, **2005**, 275-283.
- Ye, J.; Baldwin, R. P.; Schlager, J. W. LCEC determination of the copper protein ceruloplasmin in human serum at a polyaniline chemically modified electrode. *Electroanalysis.* 1, **1989**, 133-140.
- Yeh, J. M.; Liou, S. J.; Lai, C. Y.; Wu, P. C.; Tsai, T. Y. Enhancement of corrosion protection effect in polyaniline via the formation of polyaniline-clay nanocomposite materials. *Chem. Mater.* 13, **2001**, 1131-1136.
- Yin, H. R.; Jiang, J. S. Synthesis and characterization of γ -Fe₂O₃-polythiophene nanocomposites. *J. Mater. Sci.* 40, **2005**, 3013-3015.
- Yu, A. M.; Sun, D. M.; Gu H. Y.; Chen, H. Y. Catalytic oxidation of ascorbic acid at a polyhistidine modified electrode and its applications to the voltammetric resolution of ascorbic acid and dopamine. *Anal. Lett.* 29, **1996**, 2633-2643.
- Zanetti, S. M.; Pereira M. G. S.; Nono, M. C. A. Soft-chemical derived Bi₂O₃-ZnO-Ta₂O₅ nanopowder and ceramics. *J. Eur. Ceram. Soc.* 27, **2007**, 3647-3649.

- Zhang, Z.; Sui, J.; Zhang, L.; Wan, M.; Wei, Y.; Yu, L. Synthesis of polyaniline with a hollow; octahedral morphology by using a cuprous oxide template. *Adv. Mater.* 17, **2005**, 2854-2857.
- Zhang, L.; Wan, M. X. Self-assembly of polyaniline from nanotubes to hollow microspheres. *Adv. Funct. Mater.* 13, **2003**, 815-820.
- Zhang, L. J.; Wan, M. X. Synthesis and characterization of self-assembled polyaniline nanotubes doped with D-10- camphor sulfonic acid. *Nanotech.* 13, **2002**, 750-755.
- Zhang, L. J.; Wan, M. X. Chiral polyaniline nanotubes synthesized via a self-assembly process. *Thin Sol. Films.* 477, **2005**, 24-29.
- Zhang, H.; Zhu, Y. Significant visible photoactivity and antiphotocorrosion performance of CdS photocatalysts after monolayer polyaniline hybridization. *J. Phys. Chem. C.* 114, **2010**, 5822–5826.
- Zhu, N.; Chang, Z.; He, P.; Fang, Y. Electrochemically fabricated polyaniline nanowire-modified electrode for voltammetric detection of DNA hybridization. *Electrochim. Acta.* 51, **2006**, 3758- 3762.